Analysis of combined conduction and radiation heat transfer in a square enclosure containing an absorbing, emitting and isotropically scattering gray medium

by

Cemal Niyazi Sokmen

A Thesis Submitted to the
Graduate Faculty in Partial Fulfillment of the
Requirements for the Degree of
MASTER OF SCIENCE

Major: Nuclear Engineering

Iowa State University
Ames, Iowa
1986

TABLE OF CONTENTS

LIST OF TABLES

LIST OF FIGURES

I. INTRODUCTION

The analysis of heat transfer involving a participating medium has been receiving considerable amount of interest since the last decade. The applications are numerous and diverse, such as combustion chambers, gaseous nuclear reactors, and plasma generators for nuclear fusion. However, the integral nature of radiation transport, the complex coupling between the radiative properties and temperature, and the dependence of radiation transport on the geometry complicates the analysis of heat transfer problems with radiation.

A great deal of work has been reported on the interaction of radiation and conduction. Most of the work reported in combined conduction and radiation problems involving a participating medium is confined to one-dimensional studies. Several approximate and exact solutions have been reported over the years and the results of these studies are well-documented in radiation heat transfer textbooks [1-3]. However, in two-dimensional problems there are only a few studies. Razzaque formulated the energy and heat flux equations for an absorbing-emitting gray medium contained in a rectangular enclosure and utilized a Galerkin finite element approach to obtain solutions [4]. Ratzel used a P-N approximation to analyze the interaction of radiation and conduction in a rectangular

enclosure containing an absorbing, emitting and isotropically scattering gray medium [5]. Shih and Chen proposed a computationally attractive discretized intensity method for radiation conduction problems [6]. For cylindrical geometry the energy equation and heat flux equations were developed and solved by the Galerkin finite element technique by Fernandes and Francis [7].

Radiative equilibrium problems in rectangular geometry has been solved by many methods. The most common method is probably Hottel's zone method [8]. This method has been modified recently by Larsen to include interaction of radiation with other modes of heat transfer [9]. Fiveland used discrete ordinates to solve the radiative transport equation for a specified temperature distribution in rectangular geometry [10]. The P-N approximation results for radiative equilibrium are reported in [5]. Yuen and Wong [11] and Yuen and Ho [12] present point a collocation solution to the radiative equilibrium in two-dimensional rectangular enclosures. The latter study considers effects of heat generation. The Galerkin finite element solution of the exact energy equations are reported in [4]. Recently Crosbie and Schrenker [13] contributed another exact solution based on a quadrature method.

Several investigators report that the finite element technique is a viable means of analyzing the interaction of

conduction with radiation involving a participating medium [4,14-16]. The numerical solution of integral equations arising in radiative transfer problems has also been addressed [17,18]. The finite element technique is reported to be a viable method for solving integral equations. A general description of the finite element method can be found in [19].

Present work is an extension of the work reported in [4] to include scattering and heat flux boundary conditions. The governing equations are modified to include isotropic scattering, and the effects of scattering albedo, Stark number, wall emissivities and Biot number are investigated. The main assumptions involved in the analysis are that the medium and the surrounding walls of the enclosure are gray, and have uniform constant properties.

The basic complexity introduced in this study over previous studies is the consideration given to more general type boundary conditions, namely convective heat flux boundary conditions. Although the engineering importance of heat flux boundary conditions is apparent, except for a recent one-dimensional study, this problem has not been addressed [20].

II. ANALYSIS OF COMBINED CONDUCTION AND RADIATION

The objective of this analysis is to formulate the governing equations for combined conduction and radiation heat transfer in an absorbing, emitting, and isotropically scattering gray medium contained in a rectangular enclosure of diffuse gray walls. The major assumptions used in the analysis will be stated first. The energy equation and the incident radiation equation will be developed based on these assumptions in Section B. Section C will contain the nondimensional form of the governing equations. The heat flux equations on the surrounding walls will be stated in Section D. Finally, the boundary conditions required will be explained in Section E.

A. Assumptions

An exact analysis of the combined conduction and radiation problem is extremely complex due to the coupling between the temperature field and radiation transfer. The radiative properties of the materials are dependent on the temperature and wavelength of the radiation and the temperature is dependent on the radiative transfer in a nonlinear manner. In order to reduce the exact problem to a more tractable one the following assumptions are made:

- The radiative properties of the medium are independent of wavelength, temperature, and

position, i.e., the medium is gray with constant and uniform absorption and scattering coefficients.

- The scattering is independent of the direction, i.e., the scattering is isotropic.
- The surrounding walls of the enclosure are opaque and their radiative properties are independent of wavelength, temperature, and direction, that is, the surrounding walls are diffusely emitting and reflecting gray walls with constant and uniform emissivities.
- The medium is in local thermodynamic equilibrium; hence Kirchoff's laws are valid, i.e., the absorption and emission coefficients are equal.
- The index of refraction is unity.
- The thermal conductivity of the medium is constant and uniform.
- The medium is stationary, i.e., it does not move due to temperature or external effects.
- The enclosure can be considered two dimensional.
- The system is at steady-state.

Among the above assumptions the first one, namely assuming a gray medium, is the most restrictive assumption. However, this assumption simplifies the analysis of the problem considerably. Unfortunately, real materials are not gray and exhibit rapidly varying radiative properties with

temperature and wavelength [1,2]. Yet the gray medium approximation has been used extensively by many researchers in order to develop computational methods for radiative transfer problems. This is because of the simplicity of this approximation. Furthermore, some engineering materials have absorption bands in certain wavelength regions over which the radiative properties of the material are independent of the wavelength. Therefore, those materials can roughly be considered as a mixture of gray materials [1,2].

The assumption of isotropic scattering is applicable to systems with randomly placed scattering particles, which is a common situation [2]. However, non-isotropic scattering can easily be handled if the phase function for the scattering is independent of the incidence angle provided that the phase function can be approximated accurately.

Non-uniform or temperature dependent properties can also be easily handled with the numerical method used in this study without introducing any additional complexity.

B. Energy Equation

With the above assumptions in mind, the energy equation for a participating gray medium with conduction and radiation as the only modes of heat transfer can be expressed as:

$$\nabla (q^c + q^r) = q''' \tag{1}$$

where q^c and q^r are the conductive and the radiative heat fluxes and q''' is the heat generation rate. Considering a control volume, Eq. (1) states that the net energy leaving the control volume by conduction and radiation is equal to the heat generated in the control volume. The divergence of the conductive heat flux is given by

$$\nabla q^c = -k\nabla^2 T \tag{2}$$

where k is the thermal conductivity and T is the temperature.

In order to develop an expression for the divergence of the radiative heat flux, one must consider the whole enclosure. The control volume will absorb a fraction of the incoming radiant energy and will emit radiative energy proportional to the fourth power of its temperature. The incoming radiative energy to the control volume is the sum of the directional radiation intensities in all possible directions which can be expressed as [1,3]

$$g = \int_{4\pi} i' d\omega \tag{3}$$

where g and i' represent the incoming radiant energy and the directional radiation intensity, respectively, and $d\omega$ is the differential solid angle. Assuming that the control

volume is chosen small enough so that the emitted energy in the control volume is not attenuated in the control volume, the net radiative heat flux out of the control volume, in other words the divergence of the radiative heat flux for a gray medium in local thermodynamic equilibrium with an absorption coefficient 'a', can be expressed as [1-3]

$$\nabla q^r = 4a\sigma T^4 - ag \tag{4}$$

where σ is the Stefan-Boltzman constant.

Substituting Eq. (4) and Eq. (2) into Eq. (1) gives

$$-k\nabla^2 T + 4a\sigma T^4 - ag = q''' \tag{5}$$

which is the energy equation for an absorbing, emitting, and isotropically scattering gray medium with constant and uniform properties. The terms in Eq. (5) represent the net conductive heat transfer out of the control volume, the emitted energy from the control volume, absorbed energy in the control volume, and the heat generated in the control volume due to internal heat sources, respectively. In order to solve Eq. (5) for temperature field expressions for the incident radiation energy and boundary conditions for temperature are needed. The incident radiation equation will be developed in the next section and the boundary conditions will be stated at the end of this chapter.

C. Incident Radiation Equation

In order to obtain an expression for the incident radiation which is the sum of the directional intensities in all directions, the directional intensity of radiation needs to be approximated. Several processes affect the directional intensity at a point. In order to formulate these, the change in the directional intensity as it passes through an infinitesimal length 'ds' in the interior of the enclosure which contains an absorbing, emitting, and isotropically scattering gray medium will be considered [2].

The directional intensity will increase due to the emission from the medium. Since the emitted energy is proportional to the fourth power of its temperature with the proportionality constant being $4a\sigma$ and since the emitted energy is independent of the direction, the increase in the directional intensity due to emission from the medium in a particular direction will be

$$i'_e = a\frac{\sigma T^4}{\pi} \tag{6}$$

The directional intensity will be attenuated due to absorption and scattering. The absorption will result in attenuation of the directional intensity and scattering will result in the attenuation of the intensity in a particular direction. Thus, both of these effects can be expressed as

$$i'_a = -(a + \sigma_s)i' \tag{7}$$

Another process that affects the directional intensity is the incoming scattering. The scattering is assumed to be isotropic, thus, the probability that a scattering will occur in a specific direction is the ratio of the scattering coefficient, σ_s to the solid angle, 4π. Since the incident radiation at a point is the the sum of the directional intensities in all directions then the probability of having a scattering which will result in an increase in the directional intensity can be expressed as

$$i'_s = \frac{\sigma_s}{4\pi} g \tag{8}$$

The sum of the above effects should be equal to the change in the directional intensity as it passes through a length 'ds' which can be written as

$$\frac{di'}{ds} = i'_a + i'_s + i'_e \tag{9}$$

If an extinction coefficient is defined such that

$$\beta = a + \sigma_s \tag{10}$$

and a nondimensional length κ such that

$$\kappa = \beta s \tag{11}$$

and scaling the physical length scale by the extinction coefficient in Eq. (9) gives

$$\frac{di'}{d\kappa} = -\kappa i' + (1 - \Omega)\frac{\sigma T^4}{\pi} + \frac{\Omega}{4\pi} g \qquad (12)$$

where another nondimensional parameter, the isotropic scattering albedo $\Omega = \sigma_s/\beta$ has been introduced. In order to find the directional intensity at a point κ in the medium, this first order differential equation can be integrated to give

$$i'(\kappa) = i'(0)\exp(-\kappa) + \int_0^{\kappa} (i_s' + i_e')\exp(-(\kappa - \kappa^*))d\kappa^* \qquad (13)$$

where $i'(0)$ is the value of the directional radiation at the boundary and κ^* is the dummy variable of integration. For a diffusely emitting and reflecting gray wall the directional intensity can be expressed as

$$i'(0) = \frac{q_w^+}{\pi} \qquad (14)$$

where q_w^+ is the outgoing component of the radiative heat flux at the boundary. The positive direction for the heat flux vector is chosen parallel to the inward normal of the surface. Substituting Eq. (14) into Eq. (13) results in

$$i'(\kappa) = \frac{q_w^+}{\pi}\exp(-\kappa) + \int_0^{\kappa} (i_s' + i_e')\exp(-(\kappa - \kappa^*))d\kappa^* \qquad (15)$$

Now that the directional intensity is approximated in terms of temperature, incident radiation and the optical properties of the enclosure, we can integrate Eq. (15) over the entire solid angle to obtain an equation for the incident radiation. Performing the integration gives

$$g(\kappa) = \int_{4\pi} \frac{q_w^+}{\pi} \exp(-\kappa) d\omega \; + \; \int_{4\pi} \int_0^{\kappa} (i_s' + i_e') \exp(-(\kappa - \kappa^*)) d\kappa^* d\omega \qquad (16)$$

The single integral in Eq. (16) represents the fraction of energy that originates from the boundary of the system that reaches a point κ in the medium. The double integral represents the contribution of the medium to the incident radiation at point κ. The radiation energy originating in the medium in the form of emission and scattering reaches point κ after being attenuated by a factor which depends on the optical distance between the points. The locus of points κ^* depends on the solid angle. Note that the incident radiation equation is an integral equation and is linear in T^4.

The geometry of the enclosure does not explicitly appear in Eq. (16). The differential solid angle and the optical distance of the medium needs to be expressed in terms of the geometrical parameters of the enclosure. Only

the final form of the equations will be presented in this study in the next section. The details of the derivation of these equations can be found in [4].

D. Nondimensional Form of Equations

In order to generalize the governing equations and to obtain a better understanding of the physical phenomenon associated with this problem, the energy equation and the incident radiation equation can be transformed into a nondimensional form. Although there may be several different methods of selecting these nondimensional quantities, it seems reasonable to choose the optical distance as the length scale and normalize the energy flux values with respect to a reference black body emissive power. The temperature can be normalized with respect to a reference temperature. If the reference temperature is denoted by 'T_r' and the reference emissive power is selected as '$E_b = \sigma T_r^4$' then the following dimensionless quantities are obtained;

Dimensionless Temperature : $u = T/T_r$

Dimensionless Incident Radiation : $G = g/E_b$

Dimensionless Heat Flux : $\psi = q/E_b$

Dimensionless Heat Generation Rate : $Q = q'''/4\beta E_b$

Isotropic Scattering Albedo : $\Omega = \sigma_s/\beta$

Stark Number : $N = k\beta T_r/4E_b$

Dimensionless Length : $y = \beta y'$

The incident radiation equation in nondimensional form can be expressed as

$$
\begin{aligned}
G(y,z) = \frac{2}{\pi} \Bigg\{ & \int_{-\alpha_1}^{\alpha_2} \psi_1^+ Ki_2\left(\frac{z}{\cos\alpha}\right) d\alpha \\
& + \int_0^z \int_{-\alpha_1}^{\alpha_2} \left((1-\Omega)u^4 + \frac{\Omega}{4}G\right) Ki_1\left(\frac{z-z^*}{\cos\alpha}\right) \frac{d\alpha dz^*}{\cos\alpha} \\
& + \int_{-\phi_1}^{\phi_2} \psi_2^+ Ki_2\left(\frac{Z-z}{\cos\alpha}\right) d\phi \\
& + \int_z^Z \int_{-\phi_1}^{\phi_2} \left((1-\Omega)u^4 + \frac{\Omega}{4}G\right) Ki_1\left(\frac{z^*-z}{\cos\phi}\right) \frac{d\phi dz^*}{\cos\phi} \\
& + \int_{-\theta_1}^{\theta_2} \psi_3^+ Ki_2\left(\frac{y}{\cos\theta}\right) d\theta \\
& + \int_0^y \int_{-\theta_1}^{\theta_2} \left((1-\Omega)u^4 + \frac{\Omega}{4}G\right) Ki_1\left(\frac{y-y^*}{\cos\theta}\right) \frac{d\theta dy^*}{\cos\theta} \\
& + \int_{-\gamma_1}^{\gamma_2} \psi_4^+ Ki_2\left(\frac{Y-y}{\cos\gamma}\right) d\gamma \\
& + \int_y^Y \int_{-\gamma_1}^{\gamma_2} \left((1-\Omega)u^4 + \frac{\Omega}{4}G\right) Ki_1\left(\frac{y^*-y}{\cos\gamma}\right) \frac{d\gamma dy^*}{\cos\gamma} \Bigg\}
\end{aligned}
\tag{17}
$$

where ψ_1^+, ψ_2^+, ψ_3^+, ψ_4^+ are the outgoing components of the radiative heat flux at the bottom, top, left, and right

walls, respectively, and the energy equation becomes

$$-N\nabla^2 u + (1 - \Omega)u^4 = (1 - \Omega)\frac{G}{4} + Q \qquad (18)$$

where the integrations in Eq. (17) are explicitly stated in terms of geometrical parameters. The configuration used is shown in Figure 1. The Ki_n functions appearing in the incident energy equation are explained in Appendix A. They are the Bickley functions, and are analogous to the exponential integral function appearing in one-dimensional radiative transfer problems with participating media.

The nondimensional form of the governing equations indicates that the governing parameters for this problem are the optical length, the scattering albedo, and the Stark number for a given set of boundary conditions. The effect of the optical thickness of the enclosure, that is the extinction coefficient multiplied by the physical length of the enclosure, can be seen from Eq. (15). The extinction coefficient which has units of inverse length can be considered as the inverse of the average distance a photon travels before making an interaction. Therefore, a high value of optical length implies that a photon will interact with the medium in its vicinity. The radiative transfer will lose its integral character and will approach a diffusion type process. On the other hand if the optical thickness of the medium is small, the interaction of photons

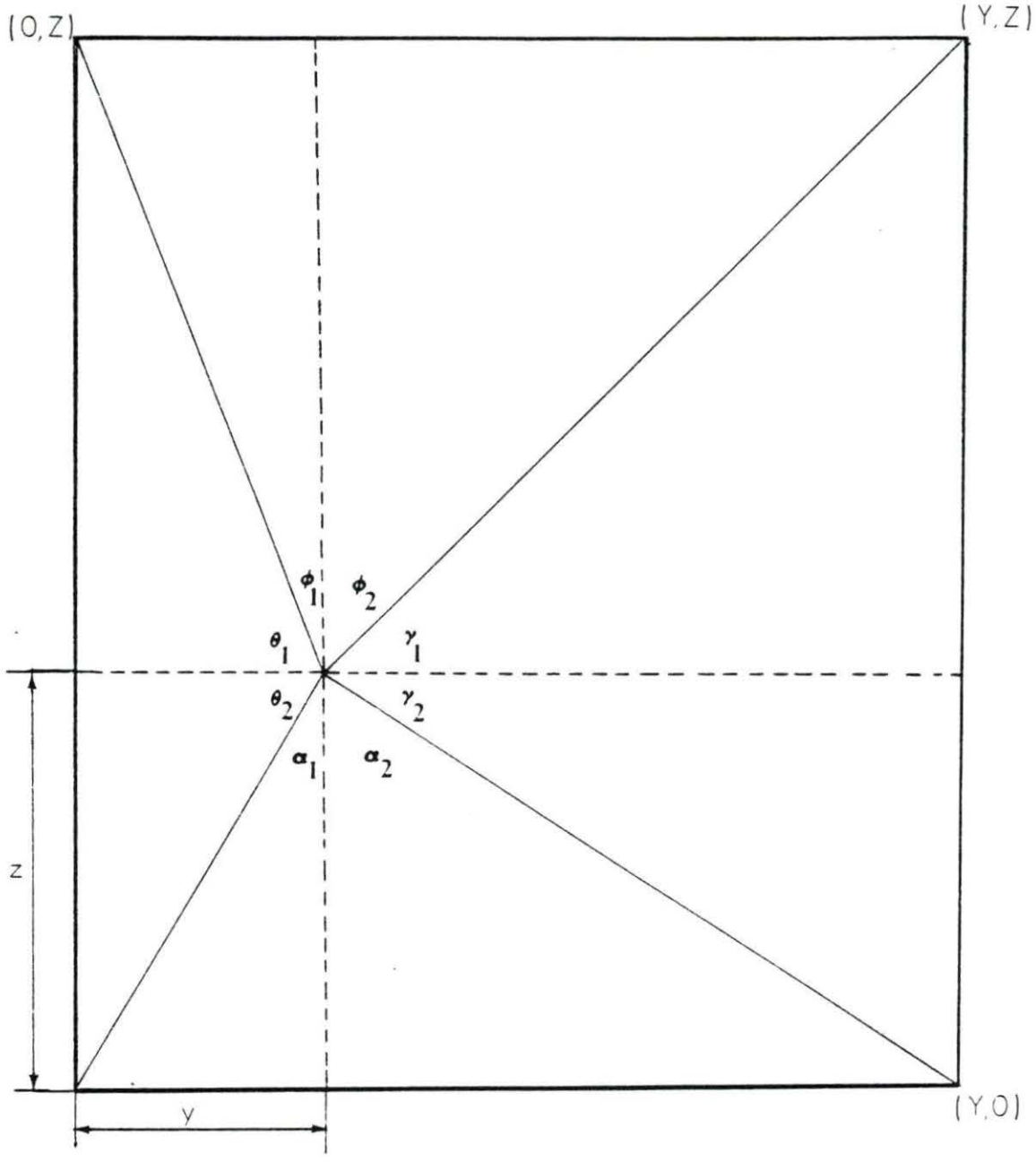

FIGURE 1. The rectangular enclosure configuration

within the medium will be negligible. The radiative transfer will approach that in a nonparticipating medium. These limiting cases are referred as the the optically thick and optically thin limits. Approximate solutions are easily obtained when one of these limiting cases is applicable. However, for most engineering systems neither of the above limiting cases are applicable. In this study intermediate values of the optical thickness are considered.

The Stark number describes the relative importance of the conductive heat transfer to that of radiative heat transfer. A high value of the Stark number implies that conduction is the dominant mode of heat transfer. Radiation heat transfer becomes more important than conduction heat transfer for values of Stark number less than unity. If the Stark Number is zero then the system under consideration is a purely radiating system and the energy equation is no longer a second order partial differential equation but reduces to

$$G = 4u^4 \tag{19}$$

which implies that solving the incident radiation will provide the temperature solution, hence, the number of unknowns is reduced to one.

Another important parameter appearing in the energy equation is the scattering albedo. Two limiting cases of

scattering albedo can be identified. If the albedo is zero then the medium is purely absorbing and emitting. The incident radiation equation is no longer an integral equation but depends only on the fourth power of temperature. Thus, the incident radiation does not have to be considered as a variable [3]. In order to obtain the energy equation corresponding to this case Eq. (17) with $\Omega=0$ can be substituted into Eq. (18) to give

$$
\begin{aligned}
-N\nabla^2 u + u^4 = \frac{1}{2\pi} \Bigg\{ & \int_{-a_1}^{a_2} \psi_1^{+} \mathrm{Ki}_1\left(\frac{z}{\cos a}\right) da \\
& + \int_{0}^{Z} \int_{-a_1}^{a_2} u^4 \, \mathrm{Ki}_1\left(\frac{z - z^*}{\cos a}\right) \frac{da\,dz^*}{\cos a} \\
& + \int_{-a_1}^{\phi_2} \psi_2^{+} \mathrm{Ki}_1\left(\frac{Z - z}{\cos \phi}\right) d\phi \\
& + \int_{z}^{Z} \int_{-\phi_1}^{\phi_2} u^4 \mathrm{Ki}_1\left(\frac{z^* - z}{\cos \phi}\right) \frac{d\phi\,dz^*}{\cos \phi} \\
& + \int_{-\theta_1}^{\theta_2} \psi_1^{+} \mathrm{Ki}_1\left(\frac{y}{\cos \theta}\right) d\theta \\
& + \int_{0}^{y} \int_{-\theta_1}^{\theta_2} u^4 \mathrm{Ki}_1\left(\frac{y - y^*}{\cos \theta}\right) \frac{d\theta\,dy^*}{\cos \theta} \\
& + \int_{-\gamma_1}^{\gamma_2} \psi_2^{+} \mathrm{Ki}_1\left(\frac{Y - y}{\cos \gamma}\right) d\gamma
\end{aligned}
$$

$$+ \int_{Y}^{Y} \int_{-\gamma_1}^{\gamma_2} u^4 Ki_1\left(\frac{y^* - y}{\cos\gamma}\right) \frac{d\gamma dy^*}{\cos\gamma} \Bigg\} \qquad (20)$$

This is the form of the energy equation used in [4]. The temperature distribution can be obtained from Eq. (20). The other extreme case is the case when the scattering albedo is unity. In this case, the medium neither absorbs nor emits radiation. As can be seen from the energy equation, the energy equation reduces to a conduction equation and is uncoupled from the incident energy equation. In this case, the radiative and conductive transfer mechanisms are independent of each other, thus, simple addition of the heat flux values obtained from a pure radiation problem and a pure conduction problem having the same boundary conditions gives the total heat flux values. To see this, if we take Ω=1 in Eq. (17) and Eq. (18) then the incident radiation equation becomes

$$G(y,z) = \frac{2}{\pi} \Bigg\{ \int_{-a_1}^{a_2} \psi_1^+ Ki_2\left(\frac{z}{\cos a}\right) da$$

$$+ \int_{0}^{z} \int_{-a_1}^{a_2} \frac{G}{4} Ki_1\left(\frac{z - z^*}{\cos a}\right) \frac{da dz^*}{\cos a}$$

$$+ \int_{-\phi_1}^{\phi_2} \psi_2^+ Ki_2\left(\frac{Z - z}{\cos a}\right) d\phi$$

$$+ \int_0^Z \int_{-\phi_1}^{\phi_2} \frac{G}{4} \, Ki_1\left(\frac{z^* - z}{\cos\phi}\right) \frac{d\phi dz^*}{\cos\phi}$$

$$+ \int_{-\theta_1}^{\theta_2} \psi_3^+ Ki_2\left(\frac{y}{\cos\theta}\right) d\theta$$

$$+ \int_0^Y \int_{-\theta_1}^{\theta_2} \frac{G}{4} \, Ki_1\left(\frac{y - y^*}{\cos\theta}\right) \frac{d\theta dy^*}{\cos\theta}$$

$$+ \int_{-\gamma_1}^{\gamma_2} \psi_4^+ Ki_2\left(\frac{Y - y}{\cos\gamma}\right) d\gamma$$

$$+ \int_y^Y \int_{-\gamma_1}^{\gamma_2} \frac{G}{4} \, Ki_1\left(\frac{y^* - y}{\cos\gamma}\right) \frac{d\gamma dy^*}{\cos\gamma} \Bigg\} \qquad (21)$$

and the energy equation is simply

$$-N\nabla^2 u = Q \qquad (22)$$

If Eq. (19) is substituted into Eq. (21) the energy equation for a gray medium in radiative equilibrium is obtained. It should be noted that this observation is not valid when heat flux boundary conditions are used.

The values of the nondimensional parameters covered in this study are for intermediate optical thickness, i.e., of the order of unity, and the range of Stark numbers considered was from unity to 0.01. The scattering albedo was varied between zero and unity.

E. Heat Flux Equations

The total heat flux at a wall is the sum of the conductive and radiative heat fluxes. The radiative heat flux is the difference between the radiative energy leaving the surface and incident on the surface per unit area in a direction normal to the surface [1]. The surface will receive radiant energy from the medium and the other walls of the enclosure. If we consider that the directional intensity represents the radiative energy per unit area normal to its direction, then the total incident radiative energy per unit surface area can be computed by [2]

$$q_w^- = \int i' \cos\alpha d\omega \tag{23}$$

where $\cos\alpha$ is the cosine of the angle between the direction of the directional intensity and the normal of the surface. The radiative energy leaving a surface is the sum of the reflected portion of the incoming radiative energy and the emitted radiative energy. For a diffuse gray wall with an emissivity of 'ϵ', the outgoing component of the radiative heat flux is given by [1-3]

$$q_w^+ = \epsilon\sigma T^4 + (1 - \epsilon)q_w^- \tag{24}$$

Therefore, the net radiative heat flux at a wall can be calculated by

$$q^r = q_w^+ - q_w^- = \epsilon(\sigma T^4 - q_w^-) \tag{25}$$

The conductive heat flux is proportional to the temperature gradient at the wall and is given by

$$q^c = -k\frac{\partial T}{\partial n}\Big)_w \tag{26}$$

The nondimensional form of the heat flux equations are found to be

$$\psi^r = \epsilon(u^4 - \psi_w^-) \tag{27}$$

and for the outgoing component of radiative heat flux

$$\psi_w^+ = \epsilon u^4 + (1 - \epsilon)\psi_w^- \tag{28}$$

and for the conductive heat flux

$$\psi^c = -4N\frac{\partial u}{\partial n}\Big)_w \tag{29}$$

The specific forms of the radiative heat flux equations for a rectangular enclosure have been derived in [4]. Upon modifying these equations to take scattering into account, the incoming radiative heat flux at the bottom wall can be expressed as

$$\psi_1^-(y) = \frac{2}{\pi}\left\{ \int_{-a_1}^{\phi_2} \psi_2^+ Ki_3\left(\frac{Z}{\cos\phi}\right)\cos\phi d\phi \right. \tag{30}$$

$$\left. + \int_0^Z \int_{-\phi_1}^{\phi_2} \left((1 - \Omega)u^4 + \frac{\Omega}{4}G\right) Ki_2\left(\frac{z^*}{\cos\phi}\right) d\phi dz^* \right.$$

$$+ \int_0^{\theta_1} \psi_3^+ Ki_3\left(\frac{Y}{\cos\theta}\right)\sin\theta d\theta$$

$$+ \int_0^{Y}\int_0^{\theta_1} \left((1-\Omega)u^4 + \frac{\Omega}{4}G\right)Ki_2\left(\frac{Y-Y^*}{\cos\theta}\right)\, tg\theta d\theta dY^*$$

$$+ \int_0^{\gamma_1} \psi_4^+ Ki_3\left(\frac{Y-y}{\cos\gamma}\right)\sin\gamma d\gamma$$

$$+ \int_y^{Y}\int_0^{\gamma_1} \left((1-\Omega)u^4 + \frac{\Omega}{4}G\right)Ki_2\left(\frac{Y^*-y}{\cos\gamma}\right)\, tg\gamma d\gamma dY^* \Bigg\}$$

and the net heat flux is given by

$$\psi_1(y) = -4N\frac{\partial u}{\partial z}\Big)_{z=0} + \epsilon(u(y,0)^4 + \psi_1^-(y)) \qquad (31)$$

Similarly, for the top wall one can obtain

$$\psi_2^-(y) = \frac{2}{\pi}\left\{ \int_{-a_1}^{a_2} \psi_1^+ Ki_3\left(\frac{Z}{\cos a}\right)\cos a da \right. \qquad (32)$$

$$+ \int_0^{Z}\int_{-a_1}^{a_2} \left((1-\Omega)u^4 + \frac{\Omega}{4}G\right)Ki_2\left(\frac{Z-z^*}{\cos a}\right)\, da dz^*$$

$$+ \int_0^{\theta_2} \psi_3^+ Ki_3\left(\frac{Y}{\cos\theta}\right)\sin\theta d\theta$$

$$+ \int_0^{Y}\int_0^{\theta_2} \left((1-\Omega)u^4 + \frac{\Omega}{4}G\right)Ki_2\left(\frac{Y-Y^*}{\cos\theta}\right)\, tg\theta d\theta dY^*$$

$$+ \int_0^{\gamma_2} \psi_4^+ Ki_3\left(\frac{Y - y}{\cos\gamma}\right)\sin\gamma d\gamma$$

$$+ \int_y^Y \int_0^{\gamma_2} \left((1 - \Omega)u^4 + \frac{\Omega}{4}G\right)Ki_2\left(\frac{y^* - y}{\cos\gamma}\right) \, tg\gamma d\gamma dy^* \Bigg\}$$

and the net heat flux is given by

$$\psi_2(y) = 4N\frac{\partial u}{\partial z}\Big)_{z=z} + \epsilon(u(y,Z)^4 + \psi_2^-(y)) \tag{33}$$

The left side wall incoming radiative heat flux is given by

$$\psi_3^-(z) = \frac{2}{\pi}\Bigg\{ \int_{-\gamma_1}^{\gamma_2} \psi_4^+ Ki_3\left(\frac{Y}{\cos\gamma}\right)\cos\gamma d\gamma \tag{34}$$

$$+ \int_0^Y \int_{-\gamma_1}^{\gamma_2} \left((1 - \Omega)u^4 + \frac{\Omega}{4}G\right)Ki_2\left(\frac{y^*}{\cos\gamma}\right) \, d\gamma dy^*$$

$$+ \int_0^{a_1} \psi_1^+ Ki_3\left(\frac{z}{\cos a}\right)\sin a da$$

$$+ \int_0^z \int_0^{a_1} \left((1 - \Omega)u^4 + \frac{\Omega}{4}G\right)Ki_2\left(\frac{z - z^*}{\cos a}\right) \, tgadadz^*$$

$$+ \int_{-\phi_1}^{\phi_2} \psi_2^+ Ki_3\left(\frac{Z - z}{\cos\phi}\right)\sin\phi d\phi$$

$$+ \int_z^Z \int_0^{\phi_2} \left((1 - \Omega)u^4 + \frac{\Omega}{4}G\right)Ki_2\left(\frac{z^* - z}{\cos\phi}\right) \, tg\phi d\phi dz^* \Bigg\}$$

and the net heat flux is given by

$$\psi_3(z) = -4N\frac{\partial u}{\partial y}\Big)_{y=0} + \epsilon(u(0,z)^4 + \psi_3^-(z)) \qquad (35)$$

The configuration used for these equations is shown in Figure 2. The double integral terms appearing in the incoming heat flux equations represent the contribution of the medium to the radiative heat flux. The single integrals represent the effect of the other walls. The emissivity of the walls affects the medium temperature through its effect on the outgoing component of the radiative heat flux even though it does not appear explicitly in the energy and incident radiation equations.

F. Boundary Conditions

The incident radiation equation is an integral equation and does not require any boundary conditions. However, the temperature of the surrounding walls and the wall emissivities are included in the incident radiation equation through the single integral terms. Although it has been noted that the incident radiation equation is linear, strictly speaking this holds true for only black wall cases where the outgoing components of the radiative heat flux depend on the temperature of the wall only. For a gray wall the outgoing component depends on the temperature and the incident radiation distribution in the enclosure.

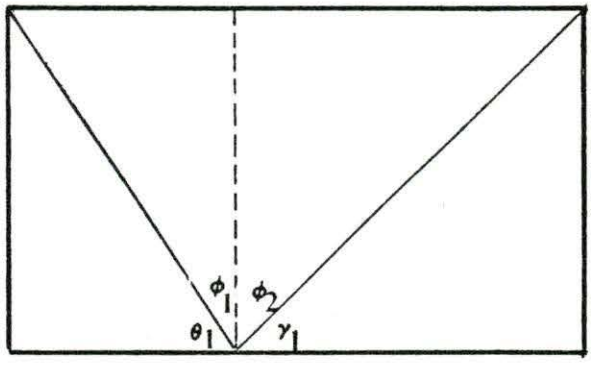

a) Bottom Wall

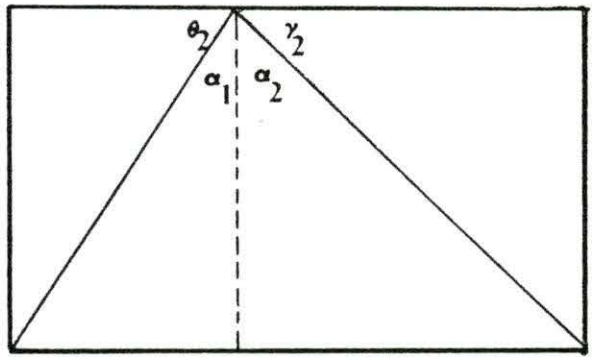

b) Top Wall

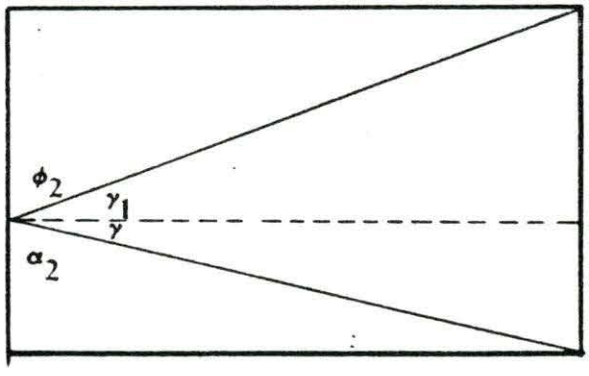

c) Left Side Wall

FIGURE 2. The configuration used for developing heat flux equations

The energy equation is a nonlinear elliptic differential equation except for the case of a unity isotropic scattering albedo. In order to solve the energy equation the boundary conditions must be specified on all the surrounding walls. These boundary conditions can either be a specification of the temperature or the temperature gradient at the walls.

In this study, two types of boundary conditions are considered. The first type is to specify the temperature on all the walls. The second type of boundary condition considered is the convective heat flux boundary condition. If a coolant with a nondimensional temperature of u is used to extract heat from one of the walls of the enclosure an energy balance on the wall gives

$$-4N\frac{\partial u}{\partial n} + \psi^r = 4NBi(u - u_\infty) \tag{36}$$

where the Biot number is defined as

$$Bi = \frac{h}{k\beta} \tag{37}$$

and β is the extinction coefficient of the medium. Eq. (36) relates the temperature and the temperature gradient at the wall to the temperature and incident radiation distribution in the medium through the radiative heat flux. As noted earlier the radiative and conductive heat transfer mechanisms are independent of each other if the isotropic

scattering albedo is unity. However, if a convective type boundary condition is used the two heat transfer mechanisms are coupled to each other by specifying the total heat transfer at the wall.

III. METHOD OF SOLUTION

The incident radiation and energy equations are complex enough to preclude an analytical solution in their general form, thus, a numerical approximation is necessary. The incident radiation equation, a double integral equation, can be solved by a direct method if the temperature field and the outgoing components of the radiative heat fluxes are known. However, the accuracy of the numerical approximation to the incident radiation can not exceed the accuracy achieved in the evaluation of the integrals. In order to evaluate the integrals accurately, a large number of integration points should be used, which renders the direct solution techniques inefficient. Furthermore, the numerical integration requires the values of the incident radiation and temperature to be known at the integration points. Therefore, an efficient numerical interpolation scheme is desirable. On the other hand, the energy equation is a nonlinear elliptic partial differential equation with nonlinear mixed type boundary conditions which necessitates an iterative type of solution technique. One can conclude that the numerical method to be used should be able to supply the values of the dependent variables over the whole domain and be suitable for an iterative type computation.

As can be seen from the above discussion, the incident radiation and the energy equation are two different types of

equations which have to be solved simultaneously, and a numerical method suitable for one of the equations may not be the best choice for the other one. Among the several methods that are applicable to this problem, the finite element method formulated by using a Galerkin weighted residuals approach is selected for this problem.

The Galerkin finite element method has been applied to combined mode heat transfer problems successfully [4,7,14-19]. Razzaque used a Galerkin finite element technique to obtain solutions for the radiative equilibrium and combined conduction and radiation of an absorbing and emitting gray medium in a two-dimensional rectangular enclosure [4]. Wu and Ferguson [14] and Fernandes et al. [15] applied the Galerkin finite element method to the interaction of conduction and radiation in one-dimension for a gray participating medium. Another similar study of one-dimensional radiation-conduction problem is reported by Nice [16]. Although all studies mentioned above utilize a Galerkin finite element technique, there are differences between the treatments of nonlinearities. Yet two important conclusions common to all of the above studies are

- The Galerkin finite element method is a viable method for solving combined conduction and radiation problems involving a gray participating medium.

- It is difficult to achieve convergence for small Stark numbers.

The solution of integral equations by the Galerkin finite element method is reported to be an efficient accurate scheme [17-19]. The basic advantage of the finite element method as applied to this problem comes from the interpolation scheme built into the finite element equations; the integrals appearing in the incident radiation equation can be evaluated accurately. Another feature of the finite element technique is the discretization of the heat flux boundary conditions so that the characteristics of the original differential equation are preserved better than they would be with the finite difference methods [20,21]. Although variable material properties are not considered in this problem finite element technique can easily handle such problems.

Having described the motivation for choosing the finite element technique for the numerical approximation to this problem, the method will be described briefly in Section A. The iterative procedures used will be described in Section B. Although an elaborate error analysis has not been performed, a simple check on the accuracy of the results will be presented in Section C.

A. Finite Element Formulation

The finite element method consists of finding the expansion coefficients of the interpolating functions which are used to approximate the dependent variable so that the error introduced by the approximation is minimized according to certain criteria. In the Galerkin formulation of the finite element method, this criterion is specified as being the vanishing of the weighted error if the weighting functions are chosen the same as the interpolating functions [21-23].

In order to apply the procedure, the domain is first divided into smaller subdomains called finite elements. The dependent variable is approximated over each element by a linear sum of the interpolating functions. The interpolating functions are generally chosen to be polynomials in spatial coordinates. Depending on the order of polynomial selected the nodes are assigned to the elements such that the interpolating polynomials are uniquely determined. Another criterion used in specifying the interpolating functions is to require that they vanish outside an element and be equal to unity at the nodes of the element. The approximation to the dependent variable expressed in terms of the interpolating functions is substituted into the differential equation and the resulting error is weighted by the interpolating functions. Since the

only unknowns in the weighted error are the expansion coefficients of the interpolating functions associated with the nodes, equating the weighted error to zero permits the resulting equation to be solved for the expansion coefficients. Once the expansion coefficients are known the dependent variable can be calculated everywhere in the domain.

In order to demonstrate the application of the above procedure, an elliptic partial differential equation defined on a finite domain can be considered. Consider a partial differential equation of the form

$$-A\nabla^2 u + Bu = F \tag{38}$$

with proper boundary conditions, where A, B and F can be functions of the dependent variable as well as the independent variables. The incident radiation and the energy equation can be cast into the form of the above equation by a proper selection of A, B and F. Approximate the dependent variable as

$$u \simeq u^a = \sum_{j=1}^{N} u_j \phi_j \tag{39}$$

where u_j are the unknown values and ϕ_j are the interpolating polynomials for each node. Substituting this approximation into the partial differential equation and weighting by the interpolating functions ϕ's one obtains

$$\int\int (-A\nabla^2 u^a + Bu^a)\phi_i d\tau = \int\int F\phi_i d\tau \tag{40}$$

where $d\tau$ is the differential area element of the domain, and the double integrations are over the whole domain. If we apply integration by parts (or Gauss divergence theorem) to the first term the resulting equation is

$$\int\int (A\nabla u^a \nabla\phi_i + Bu^a\phi_i)d\tau - \int A\frac{\partial u^a}{\partial n}\phi_i d\sigma = \int\int F\phi_i d\tau \tag{41}$$

where $d\sigma$ is the differential surface element belonging to the boundary. Since the interpolating functions are defined so that they vanish outside an element the above equation can be computed over each element individually and then summed. The surface integral appearing in Eq. (41) vanishes for elements inside the domain. Only for those elements which have an element boundary coincident with the boundary of the original domain will the surface integral term not vanish if the derivative of the dependent variable is specified. Suppose that the boundary condition along a boundary is given as

$$-A\frac{\partial u}{\partial n} + \psi = H(u - u_\infty) \tag{42}$$

where ψ is a known function of the dependent and independent variables. Then one can use this equation to obtain

$$\int -A\frac{\partial u^a}{\partial n}\phi_i d\sigma = \int Hu^a\phi_i d\sigma - \int (Hu_\infty + \psi)\phi_i d\sigma \tag{43}$$

Substituting Eq. (43) into Eq. (41) gives

$$\sum_{j=1}^{N} u_j \left\{ \int\int (A\nabla\phi_i\nabla\phi_j + B\phi_i\phi_j)d\tau + \int H\phi_i\phi_j d\sigma \right\} =$$

$$\int\int F\phi_i d\tau + \int (Hu_\infty + \psi)\phi_i d\sigma \tag{44}$$

which can be expressed in the matrix notation as

$$[K_{ij}][U_j] - [F_i] = 0 \tag{45}$$

where

$$[K_{ij}] = \int\int (A\nabla\phi_i\nabla\phi_j + B\phi_i\phi_j)d\tau + \int H\phi_i\phi_j d\sigma \tag{46}$$

is named the 'stiffness matrix' and

$$[F_i] = \int\int F\phi_i d\tau + \int (Hu_\infty + \psi)\phi_i d\sigma \tag{47}$$

is the 'load vector' [21-23]. Therefore, the original partial differential equation has been reduced to a system of equations which can be solved by an appropriate technique.

In order to find the specific form of Eq. (45) for the incident radiation the following substitutions can be made

$$A = H = \psi = 0$$

$B = 1$

$F =$ right hand side of Eq. (17)

to give

$$[K_{ij}]_G[G_j] - [F_i]_G = 0 \tag{48a}$$

where

$$[K_{ij}]_G = \int\int \phi_i \phi_j d\tau \tag{48b}$$

$$[F_i]_G = \int\int F\phi_i d\tau \tag{48c}$$

and G_j denotes the nodal values of the incident radiation. For the energy equation in a similar manner, the following substitutions

$A = N$

$B = (1 - \Omega)u^3$

$F = (1 - \Omega)\frac{G}{4} + Q$

$H = NBi$

$\psi = -\frac{\psi^r}{4}$

yields

$$[K_{ij}]_U [U_j] - [F_i]_U = 0 \tag{49a}$$

where

$$[K_{ij}]_U = \int\int (N\nabla\phi_i\nabla\phi_j + (1 - \Omega)u^3\phi_i\phi_j)d\tau + \int NBi\phi_i\phi_j d\sigma \qquad (49b)$$

and

$$[F_i]_U = \int\int ((1 - \Omega)\frac{G}{4} + Q)\phi_i d\tau + \int (NBiu_\infty + \frac{\psi^r}{4})\phi_i d\sigma \qquad (49c)$$

Therefore, the numerical approximation to the governing equations has been obtained. The system of equations defined by Eq. (48) and Eq. (49) constitute a nonlinear system of equations that needs to be solved for the unknown nodal values of the incident radiation and the temperature. The next section will describe some of the possible numerical procedures that can be used to solve Eq. (48) and Eq. (49).

B. Solution Technique

1. Incident radiation equation

The algebraic form of the incident radiation equation, that is Eq. (48), can be solved by a suitable linear equation solver provided that the integrals are approximated by a numerical quadrature method and the values of the

incident radiation, temperature and the outgoing components of the heat fluxes are known at the integration points. Among the various numerical integration schemes, Gaussian quadrature was selected to approximate the integrals. The range of the integrals was divided into two, and a 6 point Gaussian rule was used. The reason for this selection lies in the fact that most of the computational time required is spent to compute the integrals. Therefore, an integration rule which has a high accuracy with the minimum number of integrand evaluations was sought. The integrands in the incident radiation equation are smooth functions with rapidly decreasing derivatives, hence the Gaussian quadrature is expected to perform well. The order selected was based on a comparison of the results obtained by the Gaussian quadratures of several orders with the adaptive Romberg integration for selected representative integrands. A Gaussian quadrature of order 6 was found to be a good compromise between numerical accuracy and computational time requirement.

Once an initial guess for the temperature, incident radiation and the outgoing components of the heat fluxes is available then, using this information, the right hand side of the incident radiation equation can be computed. Therefore, Eq. (48) can be solved for the nodal values of the incident radiation.

2. Energy equation

The energy equation can be treated in several ways. The simplest approach would be to keep the nonlinear terms at the right hand side of the equation. In this case,

$$[K_{ij}]_U = \int\int (N\nabla\phi_i\nabla\phi_j)d\tau + \int NBi\phi_i\phi_j d\sigma \qquad (50a)$$

and

$$[F_i]_U = \int\int \left((1 - \Omega)(\frac{G}{4} - u^4) + Q \right)\phi_i d\tau + \int (NBiu_\infty + \frac{\psi^r}{4})\phi_i d\sigma \qquad (50b)$$

in Eq. (49a). The advantage of this approach is that the stiffness matrix is linear through out the iterations and needs to be factored only once. The new values of temperature can be obtained by simple back substitution after the force vector is computed. Unfortunately, this method tends to diverge for Stark numbers less than 0.1. This can be observed by noting that a small change in the temperature will be amplified by its fourth power first in the incident radiation equation and then in the energy equation. The problem is more severe for a small scattering albedo since $(1-\Omega)$ appears as the coefficient of temperature in both equations. The same behavior was observed in one-dimensional solutions of the radiation-conduction problem by

finite elements in other studies [14-16]. One way of circumventing the numerical difficulties associated with rapidly changing temperature values is simply to reduce the change in the temperature by using an under-relaxation parameter [14,16]. In this case the iteration converges, however, the number of iterations is very high. For a one-dimensional problem, this may not be a major drawback, but in a two-dimensional problem the slow convergence of the method is formidable. Also the selection of a suitable under-relaxation parameter is by no means trivial.

Another approach to the numerical solution of Eq. (18) can be sought by introducing the emission term into the stiffness matrix. In this case the stiffness matrix has to be computed at every iteration. This form of the equations is given by Eq. (49). This scheme is slightly better than the first one and has been used successfully for Stark numbers up to 0.05 in [4]. The same problem, namely slow convergence for small Stark numbers, is reported [4].

Since treating the energy equation as a linear equation and using successive substitutions at every iteration does not yield satisfactory results, one has to resort to other methods for small Stark numbers. A Newton-Raphson type of procedure can be used. In this technique, a correction to an approximation to the solution is obtained by solving

$$\Lambda(U) + \frac{d\Lambda}{dU} \Delta U = 0 \qquad (51)$$

where

$$\Lambda(U) = [K_{ij}]_U \, [U_j] - [F_i]_U$$

for the correction terms ΔU [22]. This method is better than the above methods. Several versions of this method can be applied depending on the application [22,24]. The basic difference of this method is the need to compute the Jacobian of the system of equations, sometimes referred as the tangential matrix [22,23] at every iteration. However, as a simplification the Jacobian can be kept constant for a number of iterations which results in a higher number of iterations to satisfy the same convergence requirement [22].

If the energy equation is treated as a nonlinear equation then an iteration step to obtain the updated values of the temperature field consists of 'inner' iterations to solve the nonlinear system of equations. The inner iterations compute the Jacobian and obtain corrections to the previous iterates. If the energy equation is treated as a linear equation then an iteration to update the new values of temperature consists of solving the linear system of equations.

3. Heat flux computations

For problems with black walls and specified temperature boundary conditions, the outgoing components of the radiative heat fluxes that are required to evaluate the

single integrals in the incident radiation equation are only a function of the wall temperature. Therefore, the heat flux computations need to be done only once after the convergence has been obtained. However, for problems with gray walls the outgoing component of the radiative heat flux is the sum of the emitted and reflected heat fluxes, and the incoming heat flux is dependent on the incident radiation. Thus, the incoming components of the radiative heat flux should be updated after every iteration. When convective heat flux boundary conditions are imposed on one or more of the walls, the emission term in the outgoing component of the radiative heat flux varies at every iteration, therefore, it has to be updated at every iteration.

The evaluation of single integrals in the incident radiation equation requires that the outgoing components of the radiative heat fluxes be known at irregularly spaced integration points. For problems with gray walls, the incoming components of the radiative heat flux can not be computed by using the exact expressions because of the computational time requirement. In order to circumvent this problem, the outgoing and incoming components of the radiative heat fluxes were computed at regularly placed points on the walls and a quadratic interpolation was used to obtain the values at other points.

One computational problem that has been pointed out by

previous studies of this problem is the treatment of the corner nodes [4,5]. If the temperature of two adjacent walls are specified and differ from each other then there is a discontinuity at the corner wall. This effect is very pronounced in heat flux computations near the corner nodes where a discontinuity in temperature exists. A reasonable approximation is to take the corner value to be the average of the temperatures of the two adjacent walls. Depending on the corner temperature value a peak in the heat flux values near the corner has been observed. In this study, for problems without convective type boundary conditions, the bottom wall temperature was taken as uniform and quadratic interpolation was used for the side wall temperatures.

4. Iteration procedure

The overall iteration procedure can be described as:

1. Assign initial values to the incident radiation, temperature and outgoing components of heat fluxes.
2. Compute the right hand side of the incident radiation equation and solve for new values of incident radiation.
3. Solve for temperature by using the newly computed values of the incident radiation and other information to obtain a new temperature field.
4. For problems with gray walls or convective heat

flux boundary conditions using the newly computed incident radiation and temperature values compute the outgoing and incoming components of the heat flux on the surrounding walls.

5. Test for convergence.

The convergence criterion used in this study is based on the absolute difference between two successive iterations, and is required to be less than 0.001 for the incident radiation and temperature values.

C. Numerical Verification

In order to establish the accuracy of the code developed and to obtain a rough estimate of the errors introduced into the results through various approximations involved in the solution procedure outlined in the previous section, some numerical checks were performed. Since there are no analytical results available, the numerical solution of the exact equations of radiative equilibrium as reported by Larsen [9], and Crosbie and Schrenker [13] were used for comparison. Both methods are exact in the sense that the exact governing equations are solved and the only errors in the results are numerical errors introduced in the discretization of the equations. The comparison will be made for a black square enclosure containing a gray medium. The bottom wall has a nondimensional temperature of unity

and all other wall temperatures are zero. Table 1 compares the bottom, top and side wall heat fluxes and Table 2 compares the incident radiation values along the centerline.

TABLE 1. Comparison of heat flux values for a square black enclosure containing a gray medium in radiative equilibrium

	Bottom Wall			Side Wall			Top Wall		
z or y	[9]	[13]	FEM	[9]	[13]	FEM	[9]	[13]	FEM
.1	.832	.827	.830	.524	.518	.520	.189	.190	.190
.2	.798	.796	.796	.437	.431	.434	.212	.213	.213
.3	.778	.777	.776	.368	.366	.365	.229	.230	.230
.4	.768	.767	.766	.310	.308	.309	.240	.240	.240
.5	.764	.764	.763	.260	.259	.259	.243	.244	.244
.6	.768	.767	.766	.218	.217	.218	.240	.244	.240
.7	.778	.777	.776	.182	.181	.181	.229	.230	.230
.8	.798	.796	.796	.149	.149	.149	.212	.213	.213
.9	.832	.827	.830	.119	.119	.119	.189	.190	.190

The results of this study show excellent agreement for the case compared. For this problem the enclosure was divided into 16 uniform elements and linear shape functions were used for the incident radiation which results in 25 nodal unknowns. The element force and stiffness matrix integrations were performed by using four Gauss points over each element. The evaluation of integrals appearing in Eq. (17) was done by a 6 point Gauss quadrature formula in each variable.

TABLE 2. Comparison of centerline incident radiation values for a square black enclosure containing a gray medium in radiative equilibrium

	Centerline Incident Radiation		
z	[9]	[13]	FEM
0.0	-	2.517	2.4804
0.1	2.084	2.076	2.0763
0.2	1.736	1.732	1.7329
0.3	1.444	1.444	1.4435
0.4	1.200	1.196	1.2014
0.5	1.000	1.000	1.0000
0.6	0.832	0.832	0.8326
0.7	0.692	0.692	0.6918
0.8	0.568	0.568	0.5701
0.9	0.456	0.460	0.4602
1.0	-	0.345	0.3545

As Table 2 suggests the agreement for the incident radiation is very good except for the bottom and top wall incident radiation values. The relative percent error in the top wall incident radiation is 1.48 % and for the bottom wall the relative error in bottom wall incident radiation is 2.2 %. At all other locations along the centerline the differences between the solutions are less than 0.1 %.

IV. RESULTS

The results of the computations performed for the analysis of the combined mode radiative and conductive heat transfer are summarized below. The results will be presented in two major sections. First the results of several cases with specified temperature boundary conditions will be summarized. The second section will contain the results of problems with heat flux boundary conditions on one or more of the surrounding walls. In each section, the black wall cases will be presented first. The effect of Stark number and isotropic scattering albedo will be discussed. An attempt to compare the results from this study to previously published results will be made. Additional results are included in Appendix B.

A. Results for First Type Boundary Conditions

The results will be presented for a square enclosure with a hot wall and three cold walls. The hot wall is the bottom wall and its temperature is used as the reference temperature for most of the cases. The bottom wall temperature is specified as unity and the other wall temperatures as 0.5. The square enclosure was divided into 16 uniform elements. For temperature, 9-noded quadratic elements with Lagrangian shape functions were used. For incident radiation, 4-noded linear elements were used. The

numerical integrations required to compute the coefficient matrix and the force vector were calculated by using Gaussian quadrature.

1. Results for a square black enclosure

Figure 3 shows the centerline temperature profiles for various Stark numbers for an absorbing and emitting gray medium in a black enclosure. The limiting cases of an infinite Stark number corresponding to a pure conducting medium and a zero Stark number corresponding to a pure radiating medium are also included. The radiative transfer becomes more important with decreasing Stark number. Existence of radiative transfer results in an increase in the medium temperature compared to a pure conduction case. For Stark numbers larger than unity, the temperature profiles are very close to a pure conducting case and the effect of radiation is negligible. On the other hand, for small Stark numbers, such as 0.01, the medium temperature profiles differ considerably from that of a pure radiation case. The conductive heat transfer mechanism does not allow a temperature slip between the wall and the medium temperature next to it as the radiative transfer mechanism does. Therefore, the medium temperature is forced to match the wall temperature near the walls due to the existence of the conduction.

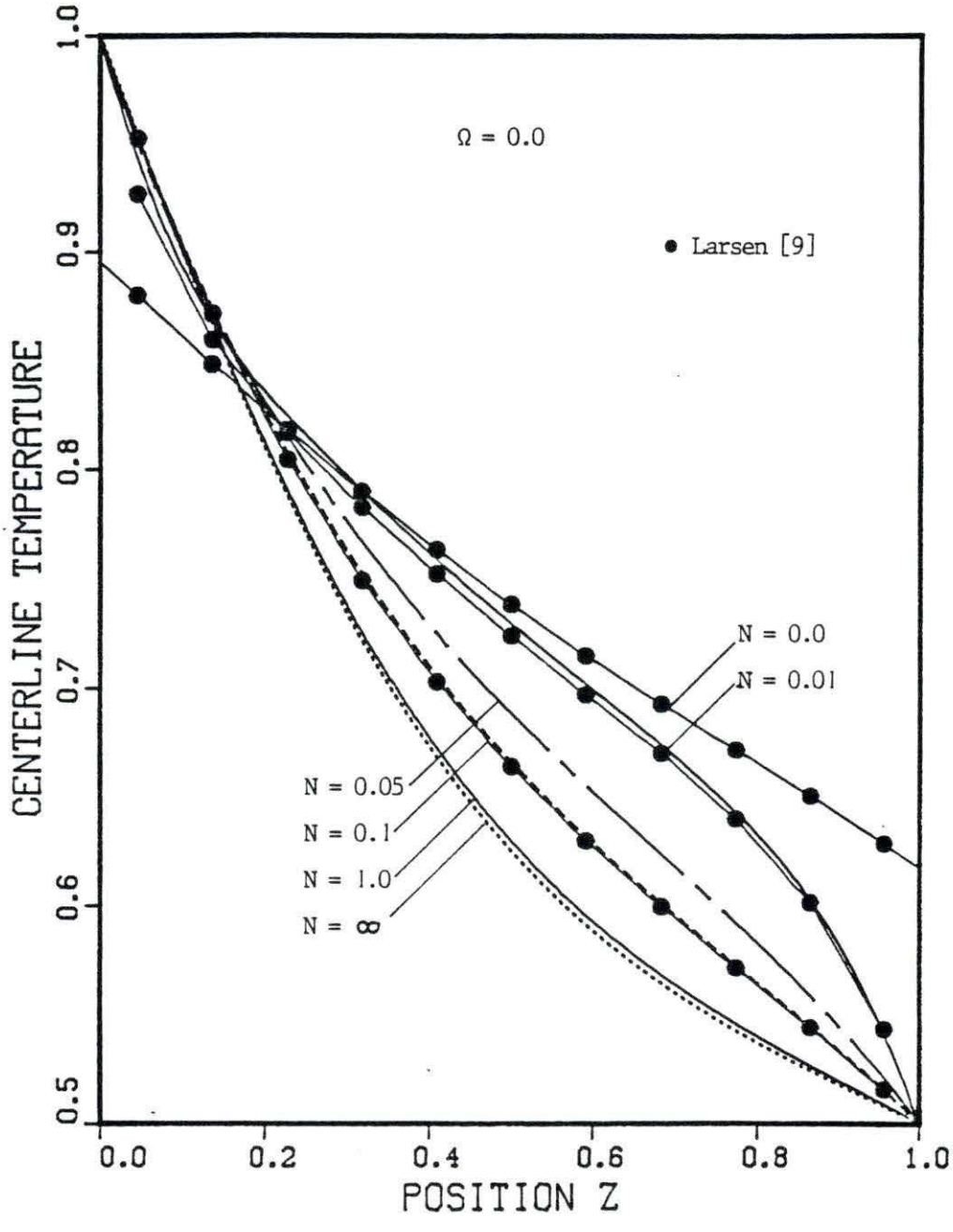

FIGURE 3. Centerline temperature profiles in a square enclosure with black walls for various values of Stark number

The results obtained for the centerline temperature values agree well with the previously published values of Larsen [9] who used the Exchange Factor Method (EFM). A comparison of the numerical values of the centerline temperature values for a square enclosure with an absorbing and emitting gray medium is given in Table 3.

TABLE 3. Comparison of centerline temperature values for an absorbing and emitting gray medium contained in a black square enclosure with $u(y,0)=1.0$ and $u(0,z)=u(y,1)=u(1,z)=0.5$

Stark Number	N = 0.01			N = 0.1		
	Nondimensional Centerline Temperature					
Z	Ref [9]	% E	FEM	Ref [9]	% E	FEM
0.0	1.000	0.0	1.000	1.000	0.0	1.000
0.1	0.879	1.6	0.893	0.902	0.2	0.903
0.2	0.829	0.3	0.831	0.823	0.3	0.826
0.3	0.789	0.5	0.793	0.759	0.5	0.763
0.4	0.755	0.5	0.758	0.707	0.4	0.709
0.5	0.724	0.2	0.725	0.663	0.5	0.666
0.6	0.694	0.3	0.696	0.626	0.3	0.628
0.7	0.664	0.2	0.665	0.594	0.2	0.595
0.8	0.629	0.1	0.630	0.563	0.1	0.564
0.9	0.582	0.1	0.581	0.533	0.0	0.533
1.0	0.500	0.0	0.500	0.500	0.0	0.500

The net heat flux values at the bottom wall are shown in Figure 4. As can be observed from this figure, a decrease in Stark number results in a decrease in the net heat flux from the hot (bottom) wall. For Stark number

equal to zero the net heat flux is simply the net radiative heat flux and for Stark number equal to infinity the net heat flux is the conductive heat flux only. For other values of Stark numbers, the heat flux is the sum of the conductive and radiative heat fluxes. The ratio of conductive heat flux to total heat flux decreases as the Stark number decreases since the medium has a thermal conductivity equivalent to 4N. The decrease in the total heat flux is due to a decrease in the Stark number, since the temperature gradients at the hot wall increase with decreasing Stark number.

The comparison of bottom wall net heat flux values with the results of other studies indicates a reasonable agreement except near the corner of the enclosure. The discrepancy near the corner is due to the treatment of the discontinuity in the temperature. As discussed in Section II-B, the temperature of the side wall near the corner nodes is interpolated quadratically, resulting in higher temperatures on the side wall, therefore, causing a decrease in the net heat flux at the bottom wall near the corner. The numerical values of the bottom wall heat flux are compared with those of Larsen [9], and Ratzel [5] in Table 4. The results from this study are in close agreement with the results from Larsen.

The effect of the isotropic scattering albedo on the

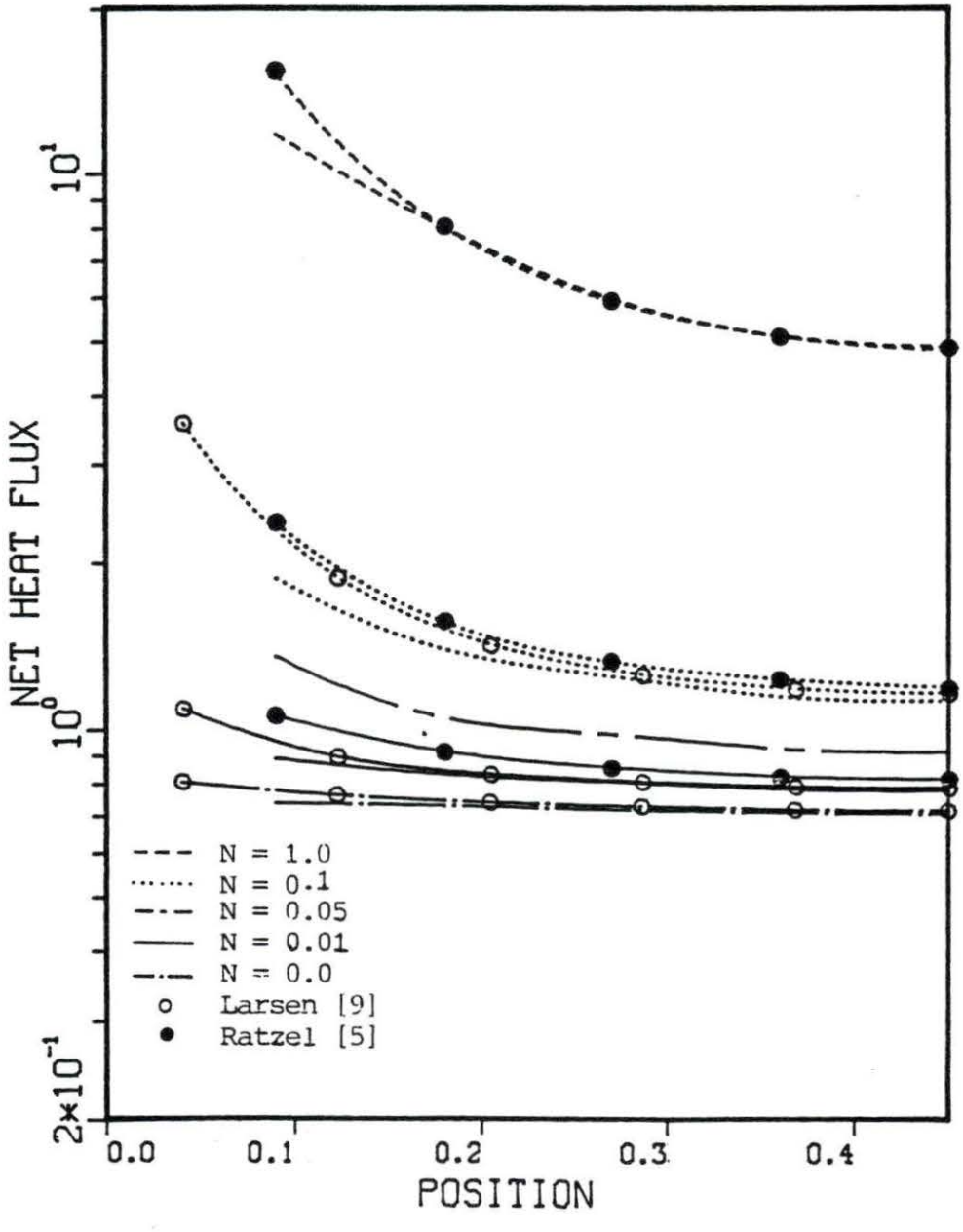

FIGURE 4. Net heat flux distribution at the bottom wall in a square enclosure with black walls for various values of Stark number

TABLE 4. Comparison of bottom wall heat flux values for an absorbing and emitting gray medium contained in a black square enclosure with u(y,0)=1.0 and u(0,z)=u(y,1)=u(1,z)=0.5 for N=0.01

	Bottom Wall Net Heat Flux				
Z	Ref [9]	% E	Ref [5]	% E	FEM
0.1	0.975	9.1	1.062	18.8	0.894
0.2	0.852	4.8	0.915	12.5	0.835
0.3	0.811	1.2	0.855	6.7	0.801
0.4	0.793	1.0	0.826	5.2	0.785
0.5	0.787	0.7	0.817	4.6	0.781
0.6	0.793	1.0	0.826	5.2	0.785
0.7	0.811	1.2	0.855	6.7	0.801
0.8	0.852	4.8	0.915	12.5	0.835
0.9	0.975	9.1	1.062	18.8	0.894

centerline temperature profiles is shown in Figures 5-7 for an absorbing, emitting and isotropically scattering gray medium contained in a black square enclosure for various Stark numbers. The effect of scattering albedo is to decrease the medium temperature compared to the temperature of an absorbing-emitting medium. This is basically due to the decrease in the amount of absorption in the medium. This effect is important for cases where radiation heat transfer is the dominant mode of heat transfer, that is for small Stark numbers. For Stark numbers greater than 0.1 the scattering effects are negligible. As discussed earlier, a unity scattering albedo implies that the radiative and conductive heat transfer mechanisms are independent of each other and the energy equation reduces to a pure conduction

equation. When the scattering albedo is zero the medium is an absorbing-emitting gray medium, and the interaction between the radiation and conduction is greatest.

The effect of scattering on hot wall heat flux can be observed from Figure 8. An increase in scattering albedo causes a decrease in the hot wall net heat flux due to a reduction in the temperature gradients near the wall. The magnitude of this decrease is small.

2. Results for a square gray enclosure

When the surrounding walls of the enclosure are not black the outgoing component of the radiative heat flux on a particular wall is the sum of the emitted and reflected components and is given by Eq. (27). The centerline temperature profiles for various Stark numbers are shown in Figures 9-10. The medium is enclosed with gray walls each having the same emissivity. As Figure 9 suggests the overall effect of a decrease in wall emissivity is a decrease in the medium temperature. This is basically due to a reduction in the energy emitted by the hot wall. Since there is less energy available in the interior of the enclosure for absorption, the temperature of the medium decreases. However, the existence of conductive heat transfer forces the medium temperature to be equal to the wall temperature and the temperature gradients near the wall remain almost constant. Another effect of a reduction in

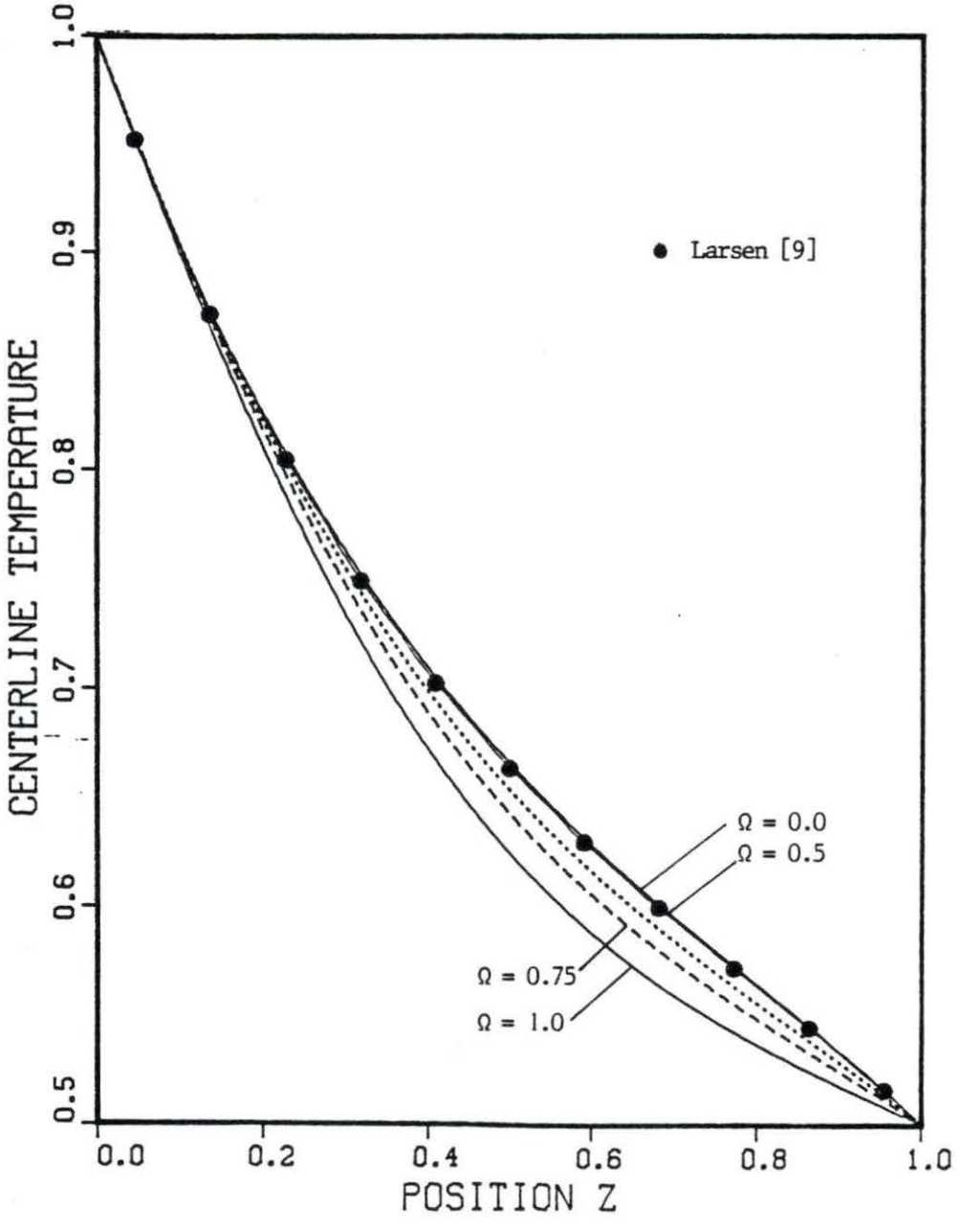

FIGURE 5. Centerline temperature profiles in a square enclosure with black walls for various values of isotropic scattering albedo with N=0.1

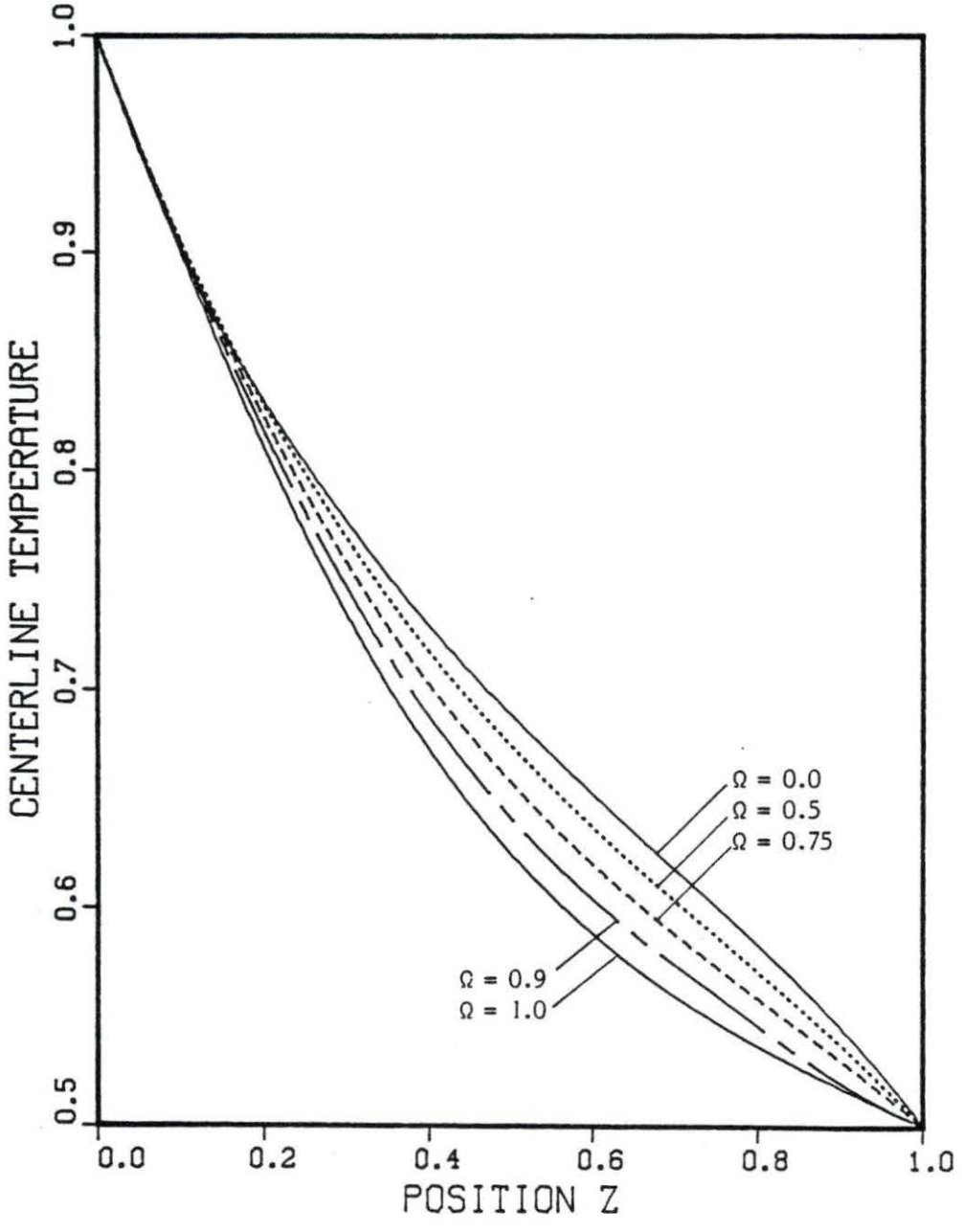

FIGURE 6. Centerline temperature profiles in a square enclosure with black walls for various values of isotropic scattering albedo with N=0.05

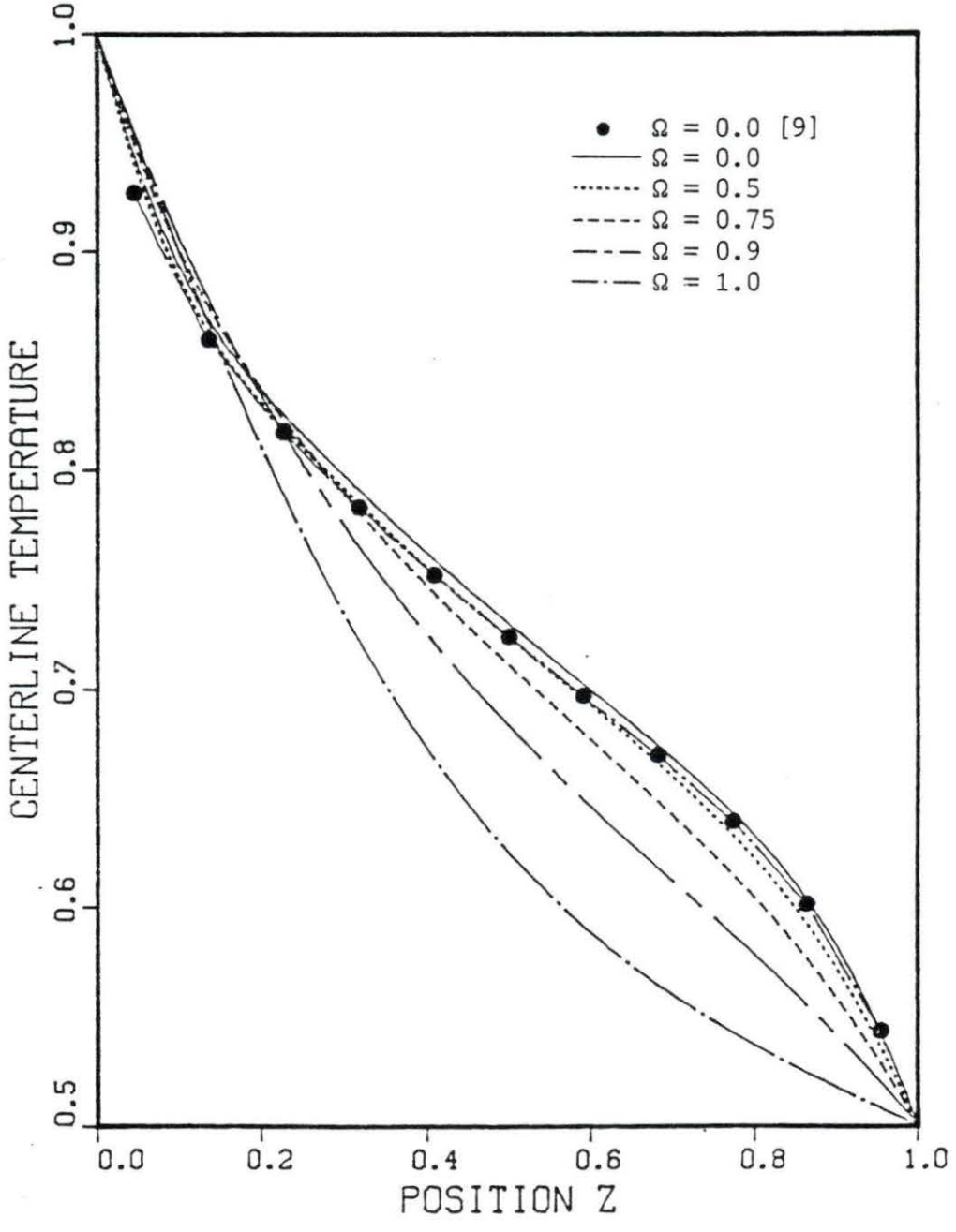

FIGURE 7. Centerline temperature profiles in a square enclosure with black walls for various values of isotropic scattering albedo with N=0.01

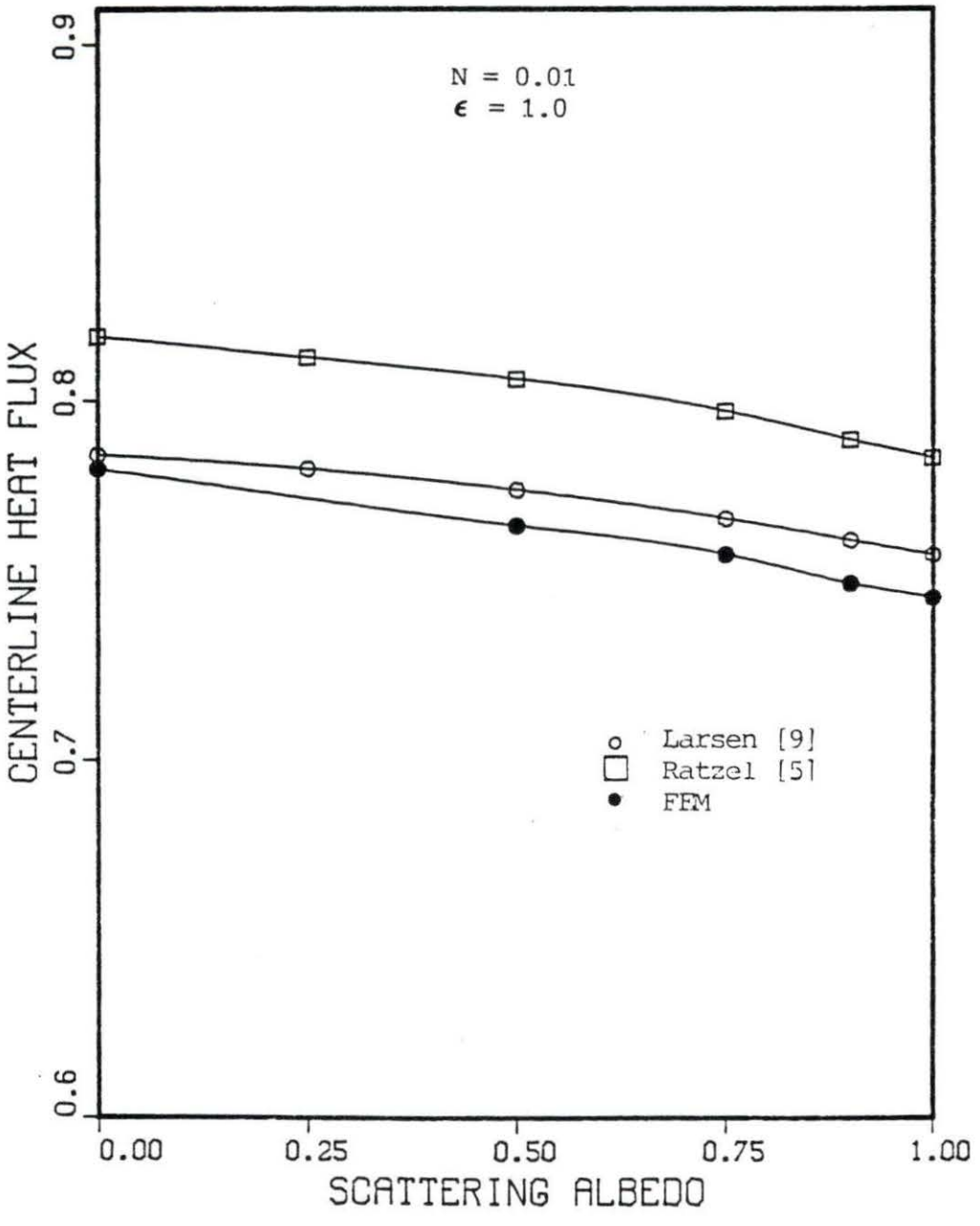

FIGURE 8. Effect of isotropic scattering albedo on centerline bottom wall net heat flux in a square enclosure with black walls with N=0.01

wall emissivity is to flatten the temperature distribution inside the medium due to additional redistribution of energy provided by reflection from the walls. As expected the wall emissivity has more influence on the temperature and heat flux distribution when the radiation is dominant mode of heat transfer.

The heat flux distributions for the bottom wall for a gray enclosure are shown in Figure 11. The decrease in the net heat flux at the hot wall is due a decrease in the net radiative heat flux. The conductive heat flux remains almost the same and is not affected by the decrease in the wall emissivity.

Figure 12 and Figure 13 show the effect of hot wall emissivity on the centerline temperature distribution and bottom wall heat flux for Stark number equal to 0.05. In this case all the walls except the bottom wall are black. By decreasing the hot wall emissivity, the hot wall in a way becomes cooler since the radiative heat flux incident on the medium from the hot wall decreases. A zero hot wall emissivity implies that there is no emitted radiant energy incident on the medium from the hot wall. However, the existence of conduction raises the temperature of the medium near the hot wall.

The effect of the isotropic scattering albedo on centerline temperature profiles when the enclosure walls are

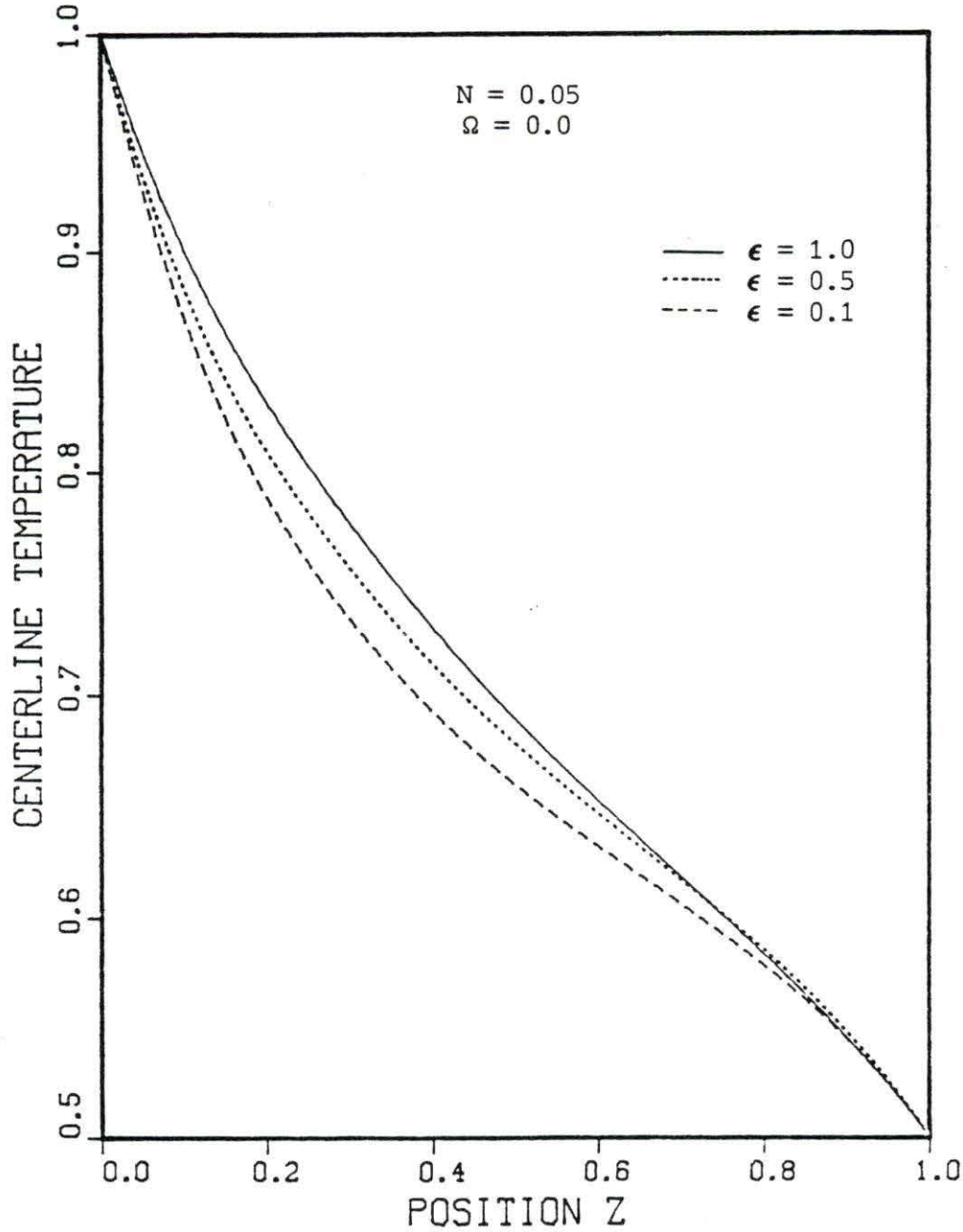

FIGURE 9. Centerline temperature profiles in a square enclosure with gray walls for various values of wall emissivity with N=0.05

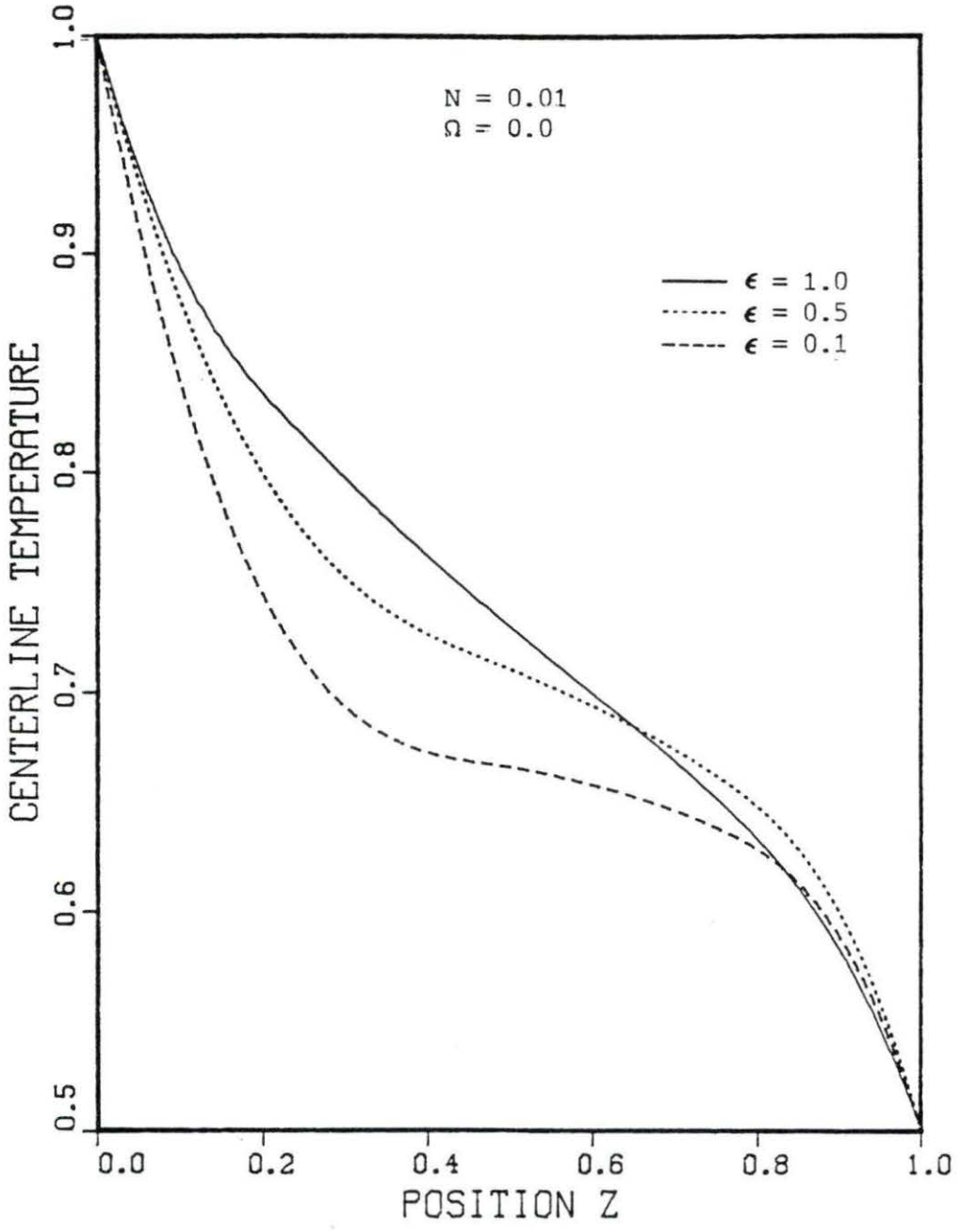

FIGURE 10. Centerline temperature profiles in a square enclosure with gray walls for various values of wall emissivity with N=0.01

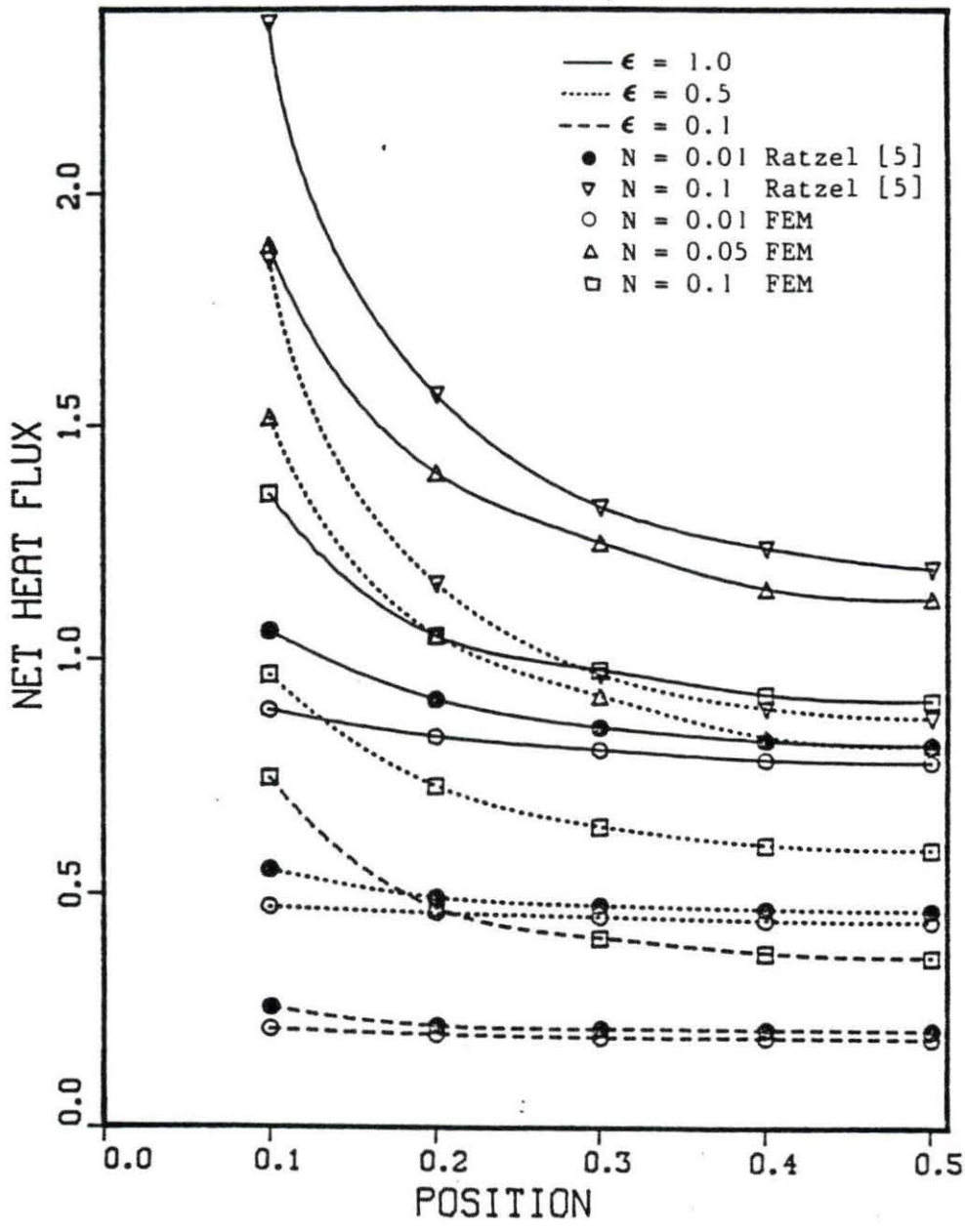

FIGURE 11. Net heat flux distribution at the bottom wall in a square enclosure with gray walls for various values of wall emissivity and Stark number

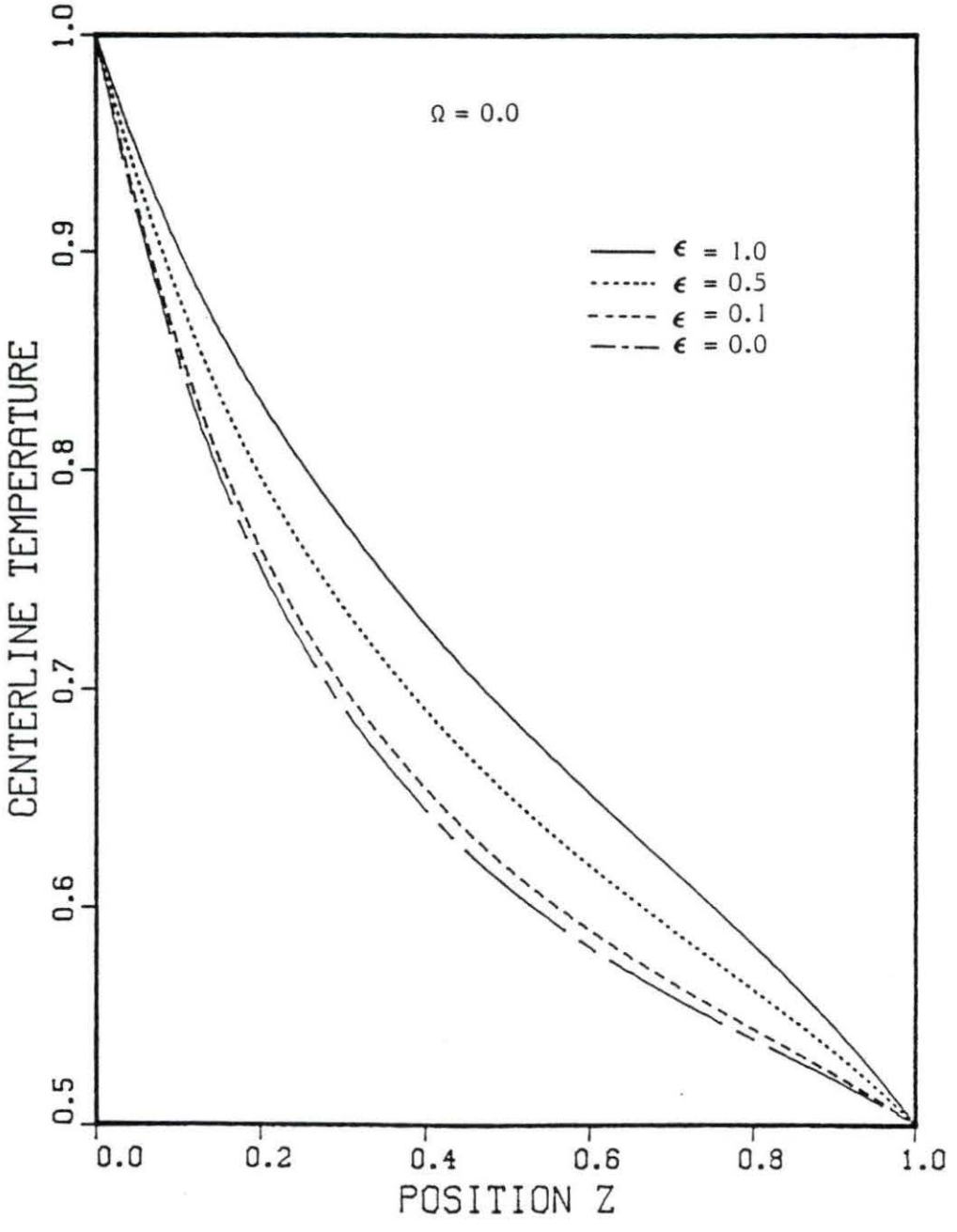

FIGURE 12. Centerline temperature profiles in a square enclosure with gray walls for various values of bottom wall emissivity with N=0.05

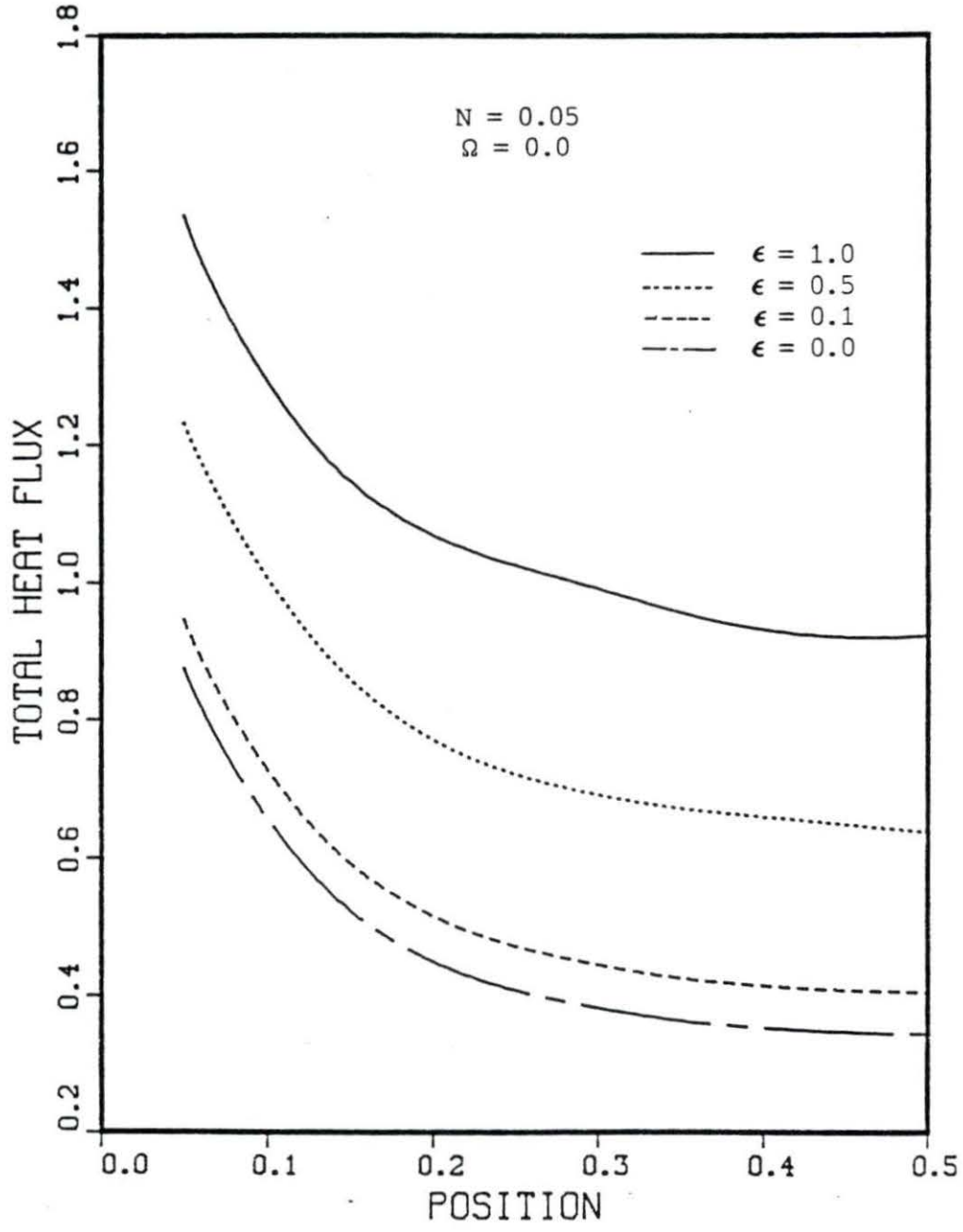

FIGURE 13. Net heat flux distribution at the bottom wall in a square enclosure with gray walls for various values of bottom wall emissivity with N=0.05

gray are shown in Figures 14-15 for various Stark numbers. The change in the interior medium temperature is more significant when compared to a black enclosure. For small Stark numbers, the scattering and gray wall effects cause the medium temperature to decrease near the bottom wall and to increase near the top wall. The interior medium temperature is flattened due to existence of gray walls.

The variation of bottom wall heat flux in a gray enclosure with isotropic scattering is shown in Figure 16. Also shown are the bottom wall heat flux values obtained by Ratzel by using a P-3 approximation [5]. The combined effect of increasing isotropic scattering albedo and decreasing wall emissivity results in a decrease in the bottom wall heat flux. The effect of the discontinuity of the temperature at the bottom wall corner node is felt less when the walls are gray. For practical purposes, the bottom wall heat flux can be considered as a constant value.

B. Results for Heat Flux Boundary Conditions

In this section, the results for a square enclosure containing an absorbing, emitting and isotropically scattering gray medium will be presented. The bottom wall is cooled with a coolant having a zero nondimensional temperature. The other wall and bottom wall corner nodes are kept at 0.5 nondimensional temperature.

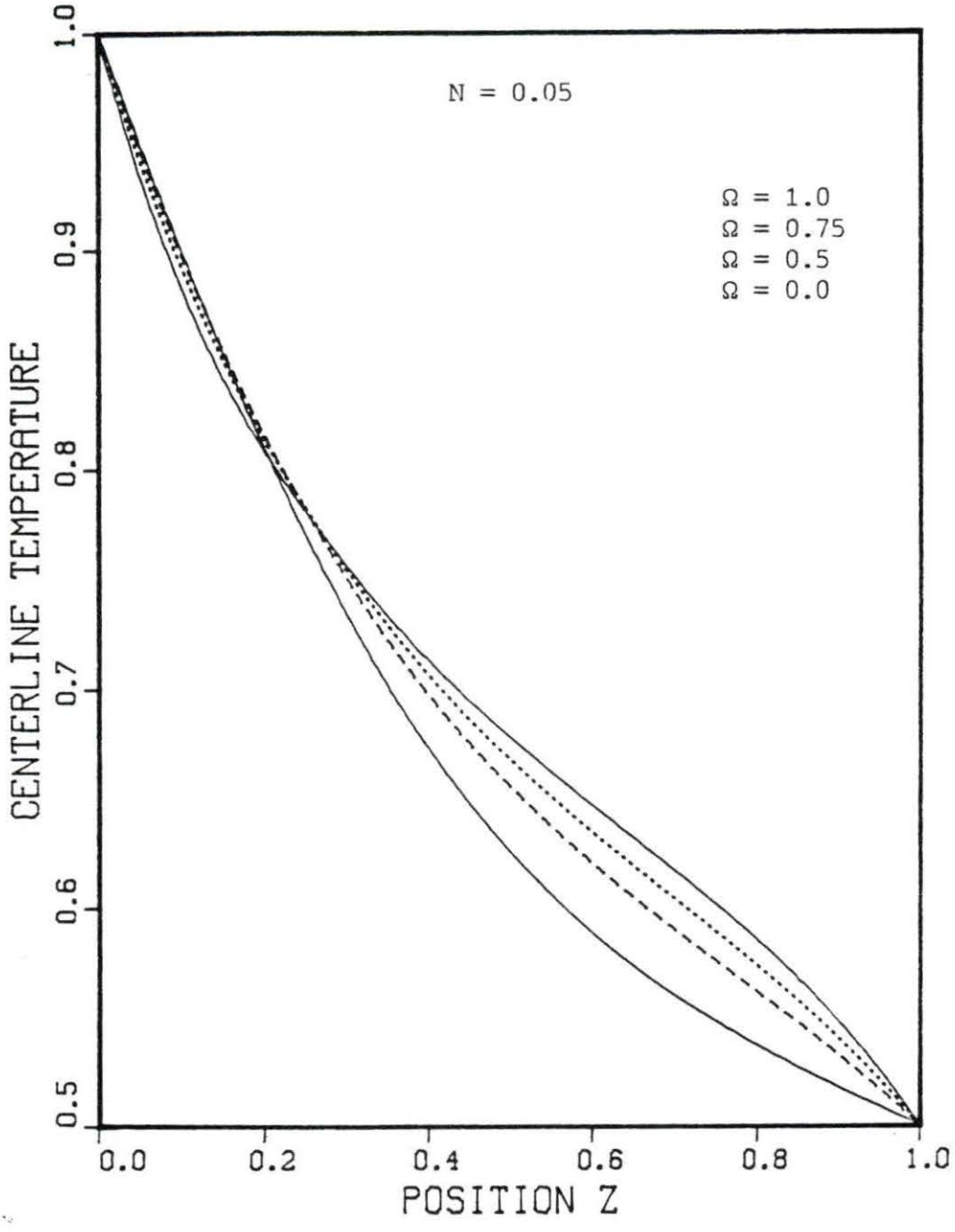

FIGURE 14. Centerline temperature profiles in a square enclosure with gray walls for various values of isotropic scattering albedo with N=0.05

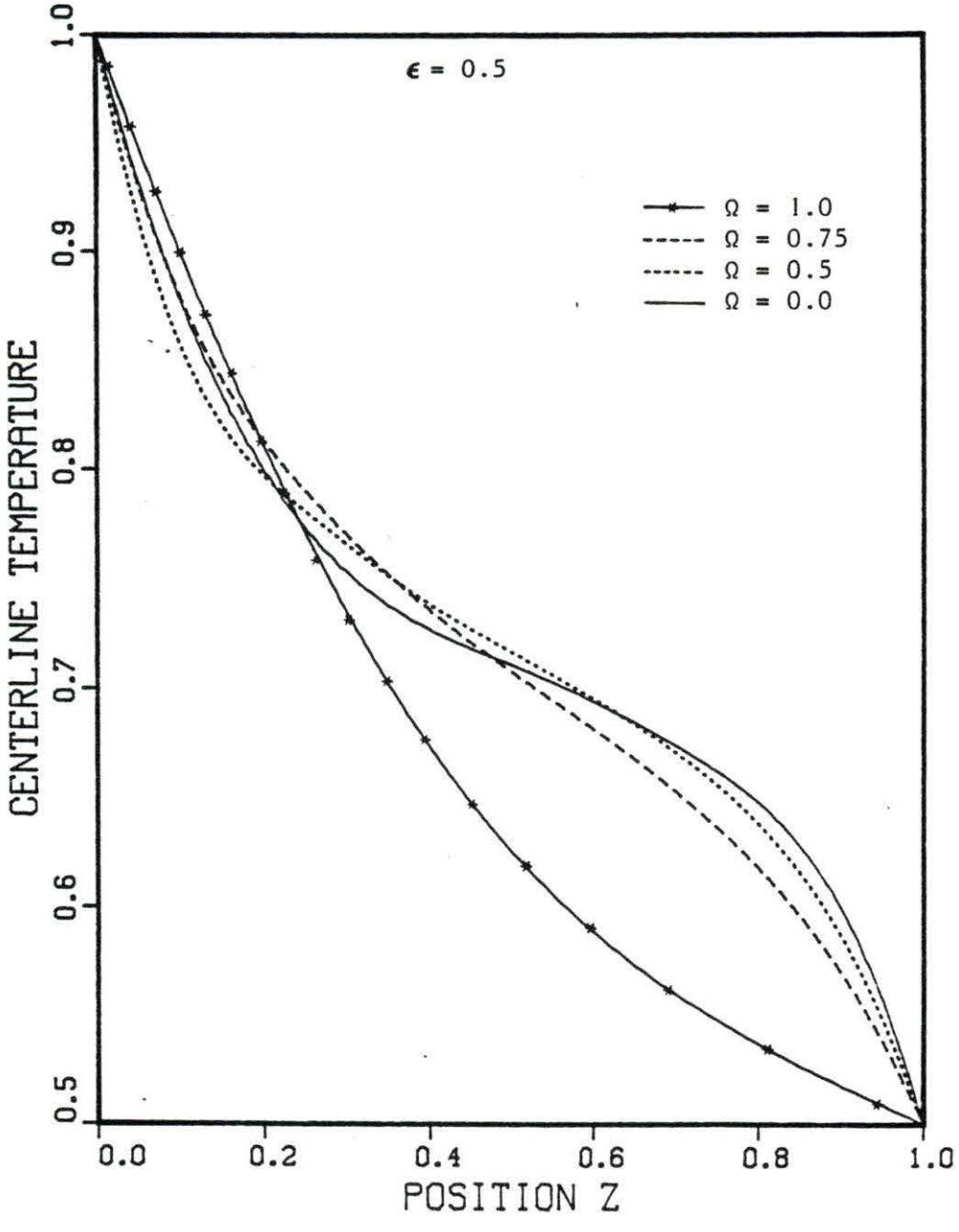

FIGURE 15. Centerline temperature profiles in a square enclosure with gray walls for various values of isotropic scattering albedo with N=0.01

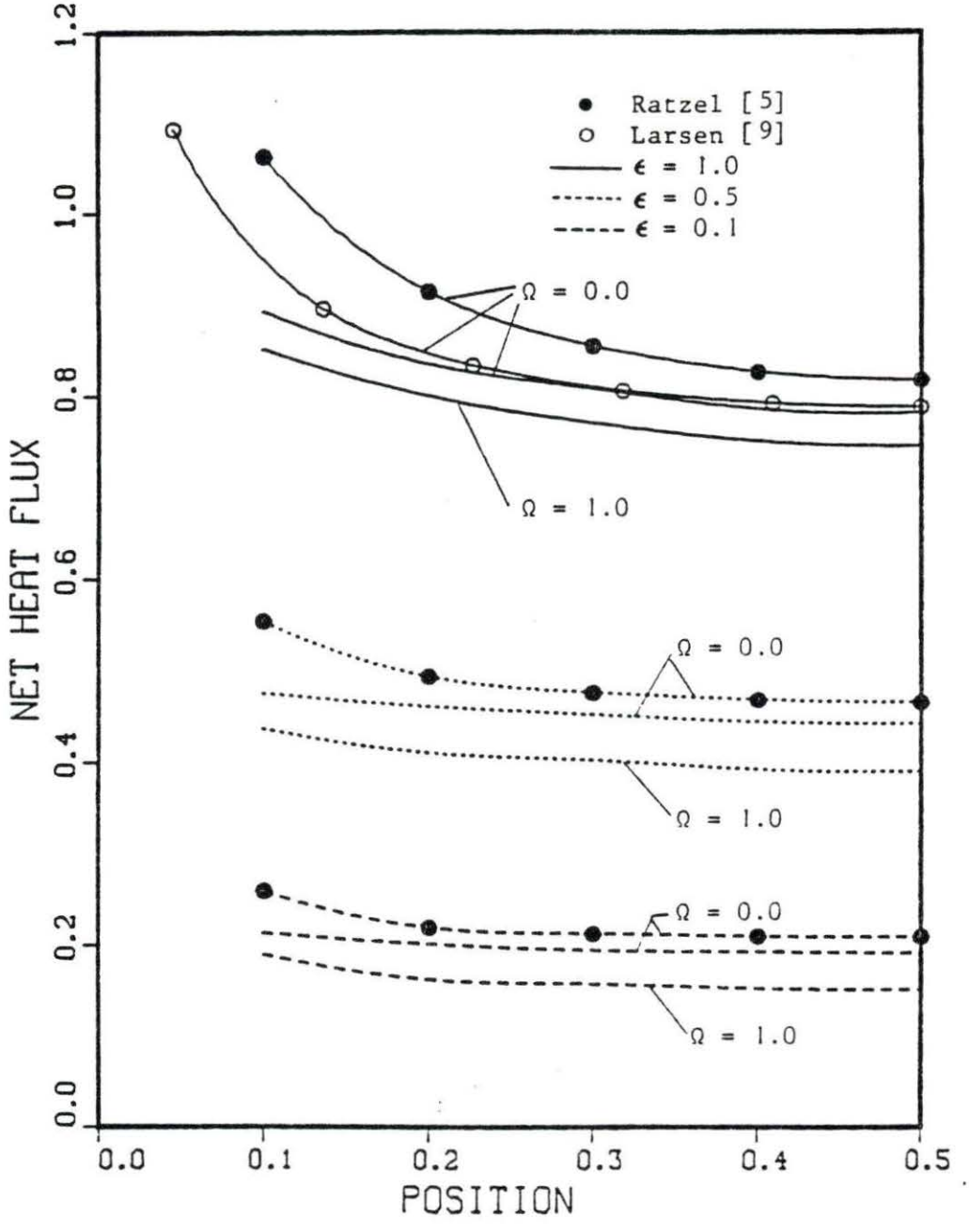

FIGURE 16. Net heat flux distribution at the bottom wall in a square enclosure with gray walls for various values of isotropic scattering albedo and wall emissivity with N=0.01

The enclosure was divided into 16 uniform elements. Quadratic serendipity elements which have 8 nodes were used for incident radiation. The temperature was approximated by using quadratic Lagrangian elements having 9 nodes. The element force and stiffness matrix integrations were computed by using a 4-point Gaussian quadrature formula. The convergence criterion was set at 0.001 based on the absolute value of the maximum difference in incident radiation and temperature values between two consecutive iterations.

The effect of Biot number on the centerline temperature profile in a black square enclosure with an absorbing and emitting gray medium with a Stark number equal to 0.1 is shown in Figure 17. When the Biot number is zero, which implies a zero heat flux from the bottom wall, the temperature and incident radiation distribution in the medium is uniform since all of the other walls are at the same temperature. On the other hand for a Biot number approaching infinity, the bottom wall temperature approaches the coolant temperature. For other cases, the medium temperature decreases with increasing Biot number since more energy is carried away from the bottom wall. The decrease in temperature is localized to regions near the bottom wall.

The bottom wall net heat flux values for the above problem are shown in Figure 18. At the bottom wall corner

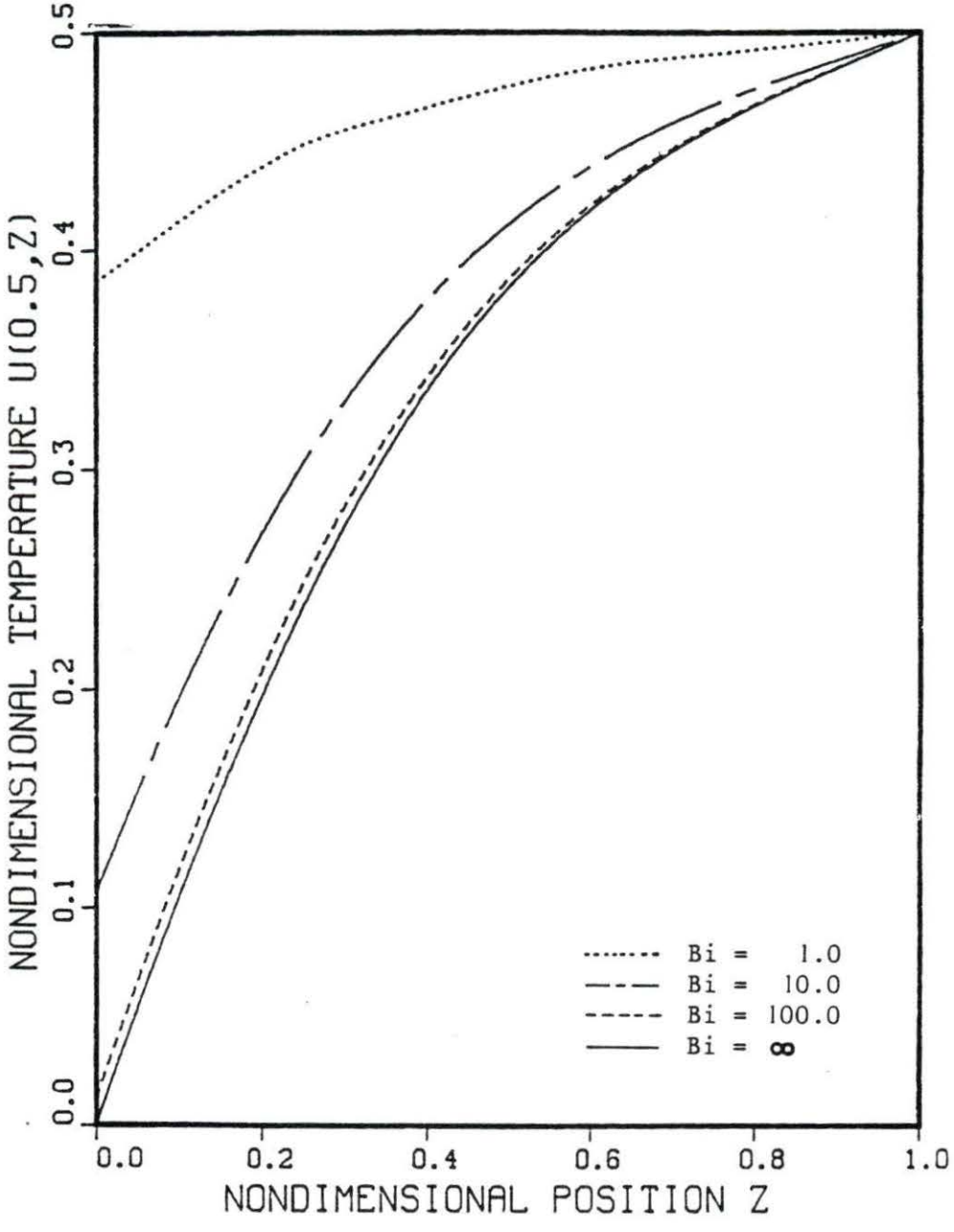

FIGURE 17. Centerline temperature profiles in a square enclosure with black walls for various values of Biot number for N=0.1

node the heat flux is discontinuous. The conductive heat flux at the corner node is zero, because there are no temperature gradients since the corner node temperature is specified as the same as the side wall temperature. The radiative heat flux is also discontinuous at the corner node [13]. However, the convective heat flux is proportional to the temperature of the bottom wall. Therefore, conductive and radiative heat fluxes are unable to match the convective heat flux near the corners.

The boundary conditions although satisfied at the nodes are not satisfied near the corner. This is an indication of the coarseness of the finite element mesh used. A finer mesh with smaller element sizes, hence with nodes closer to the bottom wall corner, would have provided solutions that can adequately resolve the heat flux variations near the corner node. However, in this study, such an attempt was not made.

Figure 19 shows the distribution of bottom wall heat flux values for various Stark numbers with Biot number equal to 10 and 100. Although the nondimensional parameter 4NBi which can be considered as the ratio of the convective heat flux and the radiative heat flux at the boundary is expected to be the significant parameter, the values obtained indicate that the Stark number and Biot number independently affect the temperature and heat flux distribution. As can

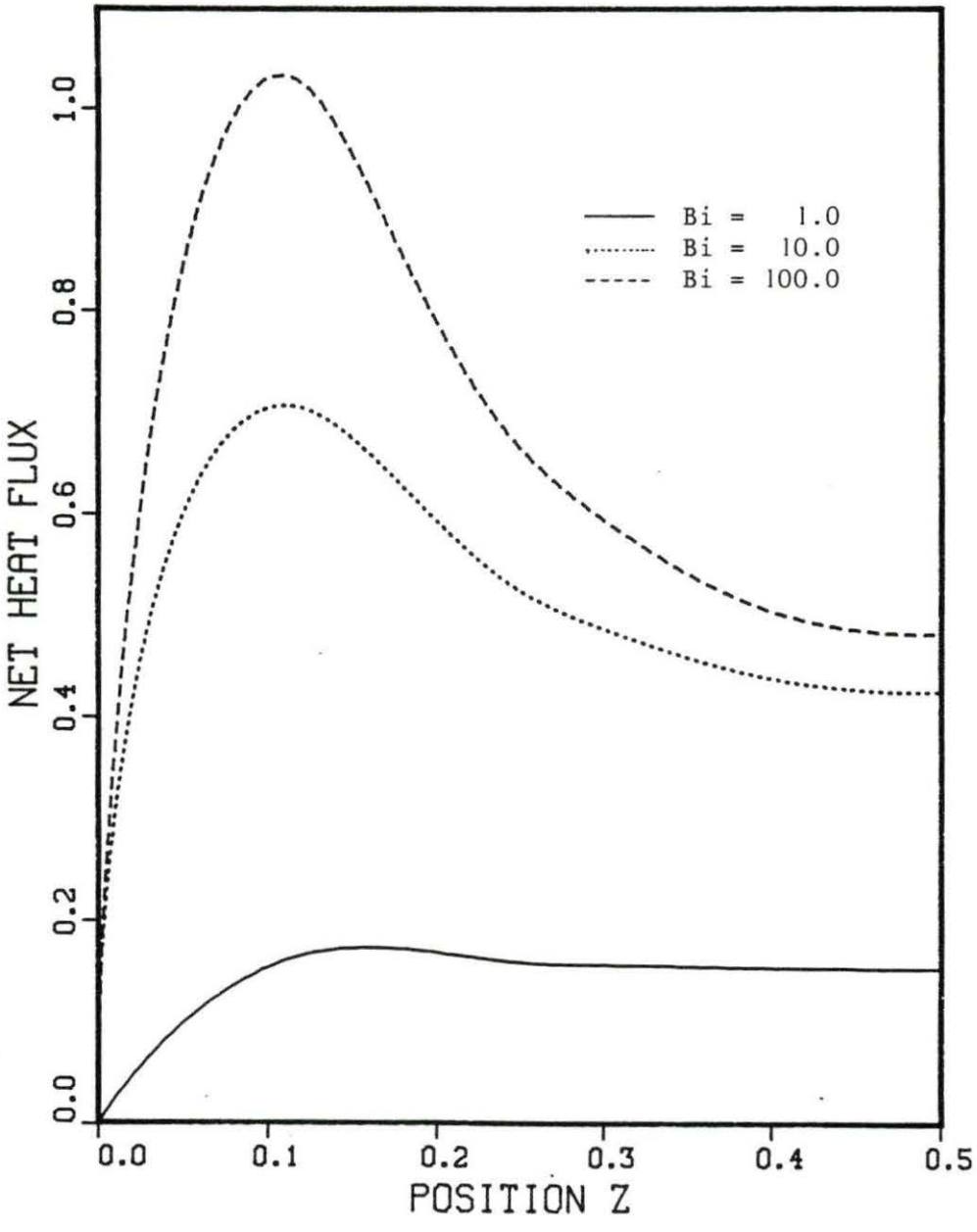

FIGURE 18. Net heat flux distribution at the bottom wall in a square enclosure with black walls for various values of Biot number for N=0.1

be seen from Figure 19 for the same value of 4NBi the temperature and heat flux values differ considerably. The Stark number, which can be considered to be proportional to the medium thermal conductivity, has similar effects to those discussed in the previous section. An increase in Stark number results in higher bottom wall heat flux values due to an increase in the conductive heat transfer and therefore, lower medium temperatures.

The effect of the isotropic scattering albedo on centerline temperatures and on bottom wall heat flux values are shown in Figure 20 and Figure 21, respectively. The medium Stark number is 0.01 and the enclosure walls are black. The decrease in centerline temperature due to increasing scattering albedo is because of the reduction in the energy available for absorption and emission, since for the same extinction coefficient the absorption coefficient decreases with increasing scattering albedo. For Stark numbers larger than 0.1 the effect of scattering is not significant. The existence of convective heat flux at the bottom wall reduces the effect of the scattering albedo to a certain extent. The radiative heat flux decreases due to an increase in the scattering albedo, however, since the total heat flux at the bottom wall is specified as proportional to the bottom wall temperature, the conductive heat flux compensates for the decrease in the radiative heat flux.

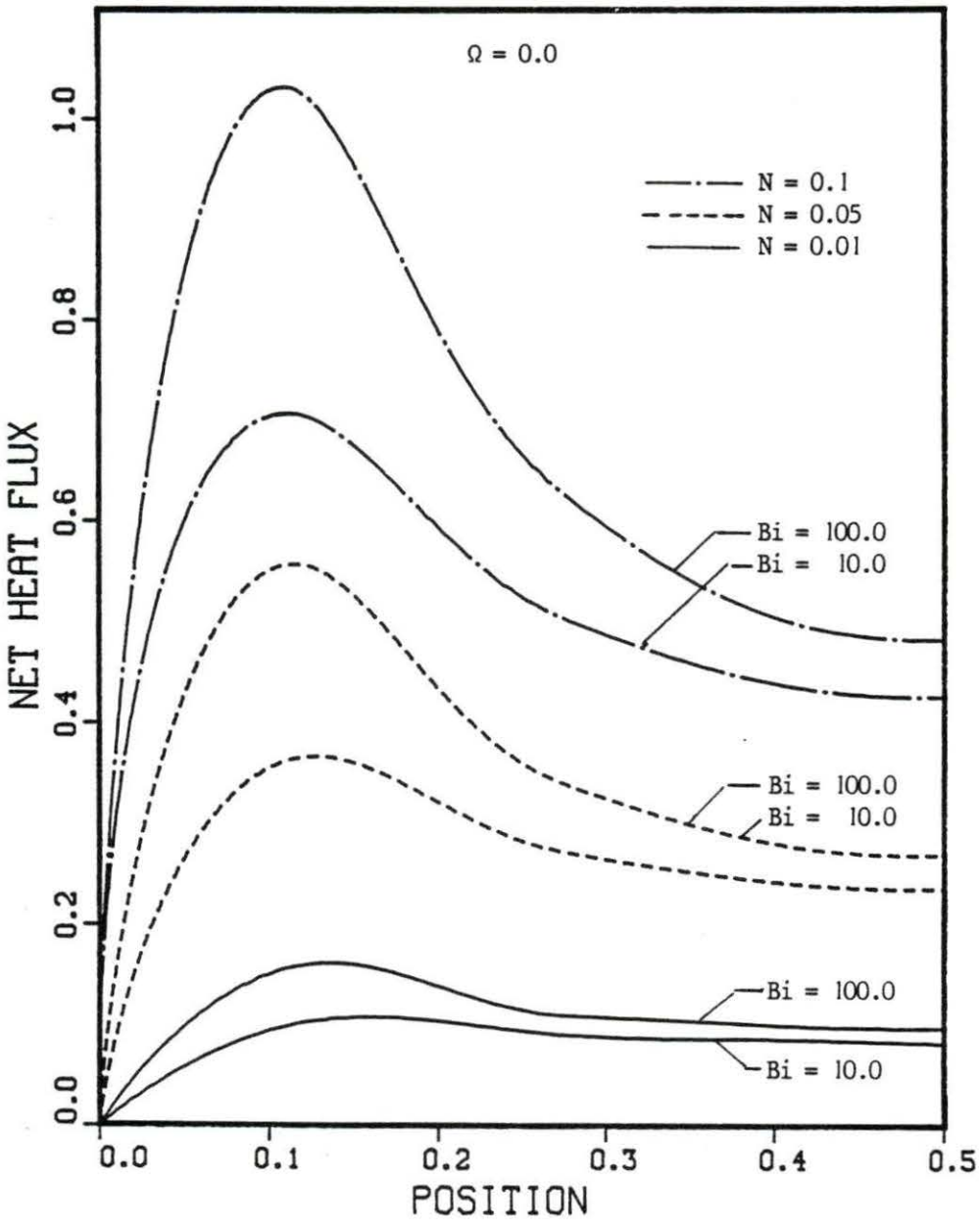

FIGURE 19. Net heat flux distribution at the bottom wall in a square enclosure with black walls for various values of Stark number with Bi=10 and Bi=100

Hence, the net effect of scattering is reduced.

Figure 22 shows the effect of emissivity of the walls on the centerline temperature for a radiation dominated case with convective heat flux boundary conditions. All the walls have the same emissivity and the medium Stark number is equal to 0.01. Since a decrease in wall emissivity reduces the net radiative heat flux, the medium temperature also decreases. The hot walls, top and side walls, have less energy available for the medium compared to a black enclosure. The bottom wall temperature also decreases due to a decrease in the wall emissivity.

The bottom wall heat flux values are shown in Figure 23. As expected the net heat flux values also decrease with decreasing wall emissivity. Although conductive heat transfer mechanism compensates for the reduction in the radiative heat flux, the convective heat flux is less when compared to the black wall case due to the decrease in the bottom wall temperature.

C. Summary

The results of the previous two sections can be summarized as below.

- The radiative mode of heat transfer is dominant for values of Stark number less than 0.1. For higher values of Stark number conduction is the basic mode

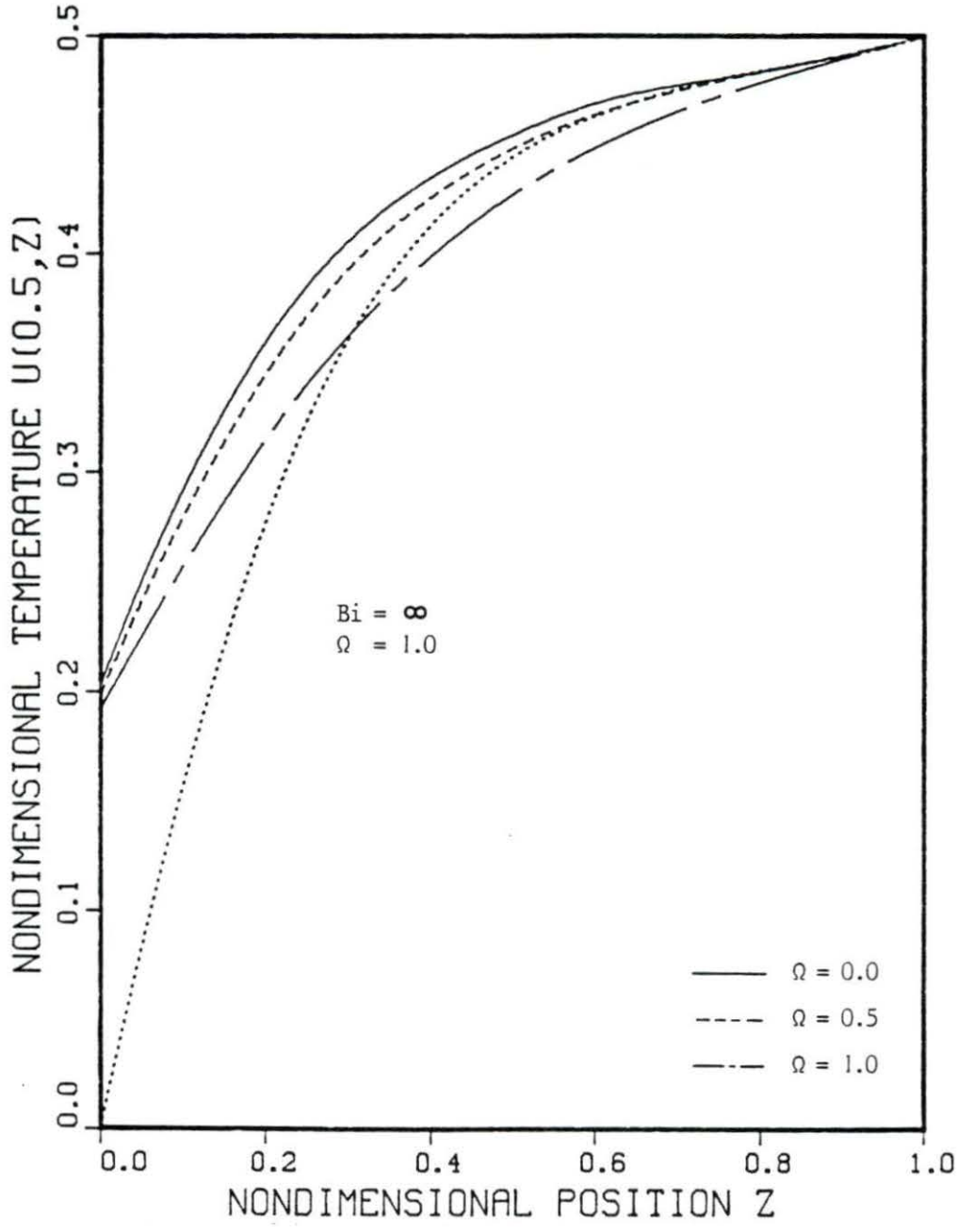

FIGURE 20. Centerline temperature profiles in a square enclosure with black walls for various values of isotropic scattering albedo for N=0.01 and Bi=10

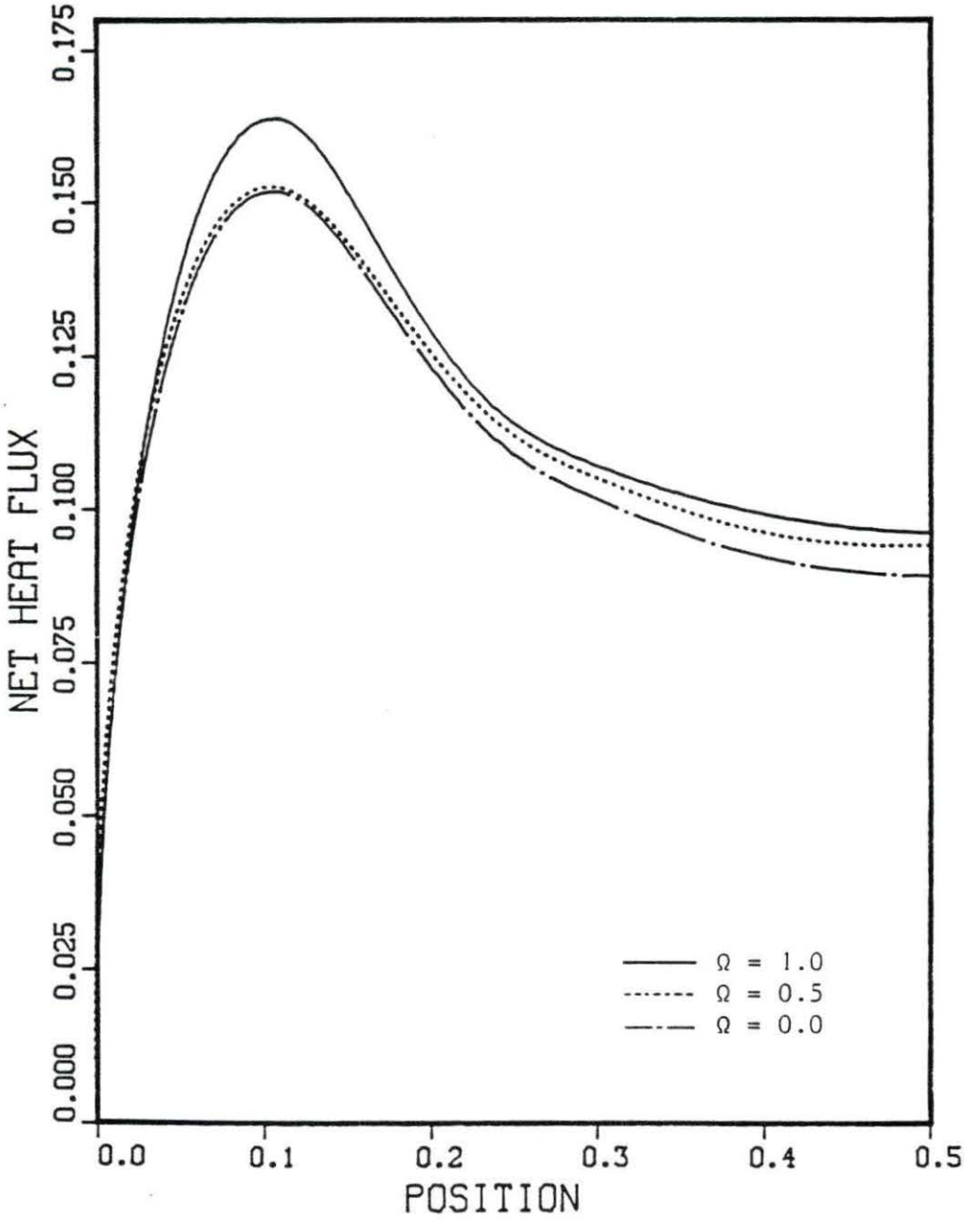

FIGURE 21. Net heat flux distribution at the bottom wall in a square enclosure with black walls for various values of isotropic scattering albedo for N=0.01 and Bi=10

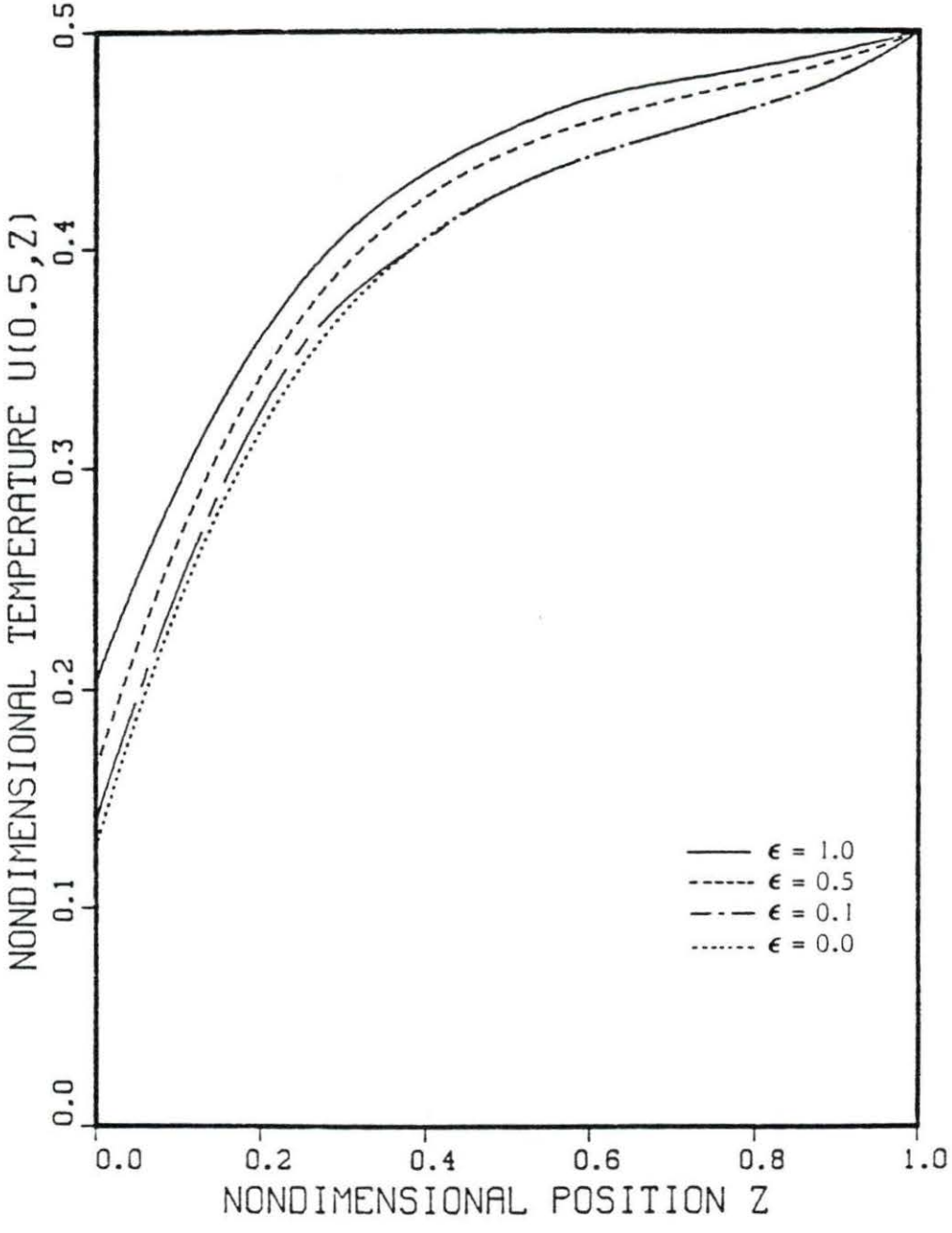

FIGURE 22. Centerline temperature profiles in a square enclosure with gray walls for various values of wall emissivity for N=0.01 and Bi=10

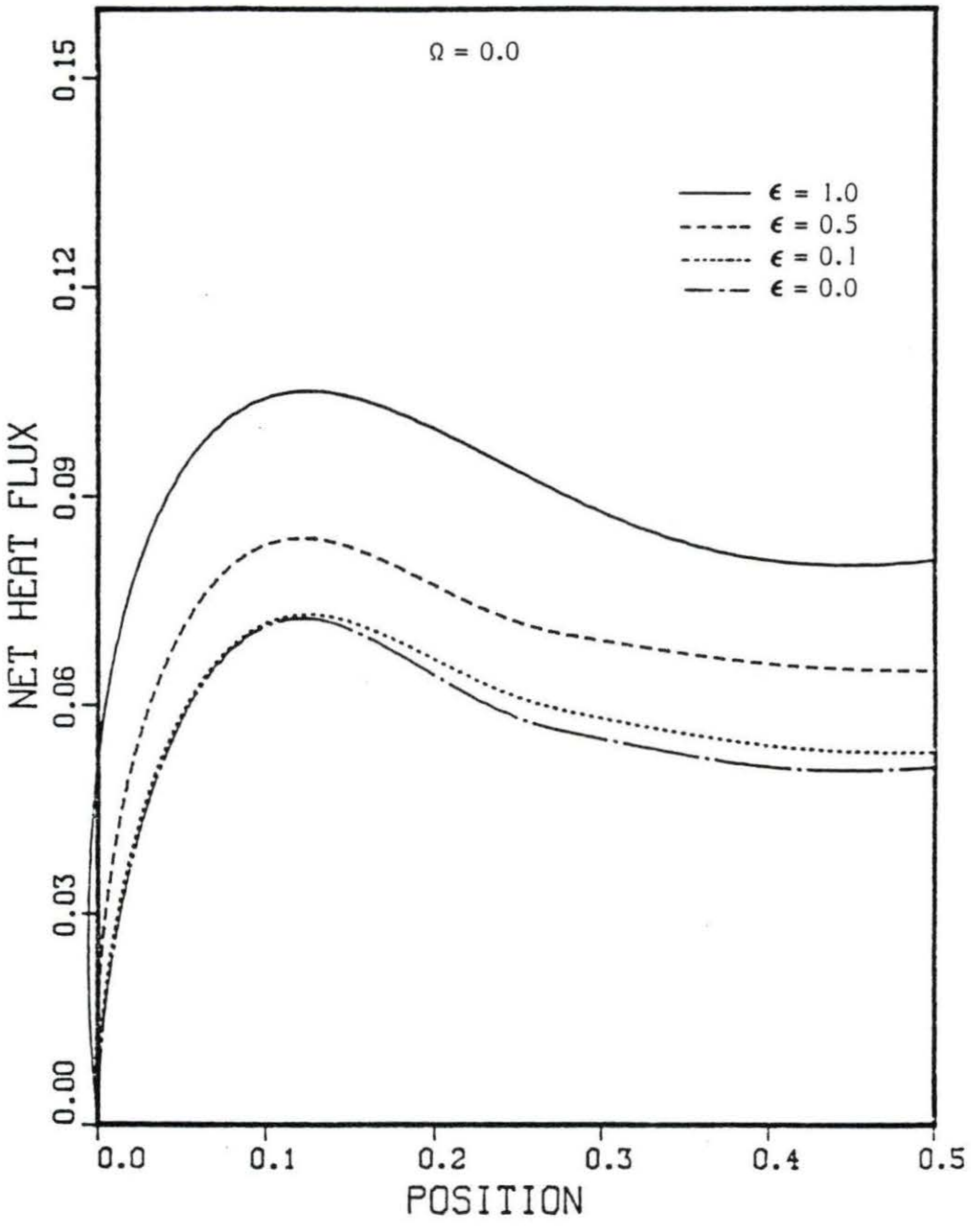

FIGURE 23. Net heat flux distribution at the bottom wall in a square enclosure with gray walls for various values of wall emissivity for N=0.01 and Bi=10

of heat transfer and radiation effects are negligible.

- The radiative properties of the medium and the enclosure affect the medium temperature distribution and the heat flux values for radiation dominant cases. Their effect on the conductive heat flux is relatively small.
- The existence of radiation increases the medium temperature and decreases the heat flux values when compared to a pure conducting medium.
- The effects of a decrease in wall emissivity are lower medium temperatures and lower heat flux rates due to a decrease in the net radiative heat flux.
- The scattering is important for radiation dominant cases with the scattering albedo greater than 0.5. The medium temperature and heat flux decreases with increasing isotropic scattering albedo. The magnitude of reduction in the heat flux rate is small. The effect of scattering in a gray enclosure is more significant than the effect of scattering in a black enclosure.
- When the enclosure is cooled with a coolant the medium temperature distribution and the net heat flux values on the surrounding walls depend on the Biot number and the Stark number rather than their

product. The effect of a high Biot number is to reduce the medium temperature especially near the bottom wall. The Stark number basically controls the penetration of the effects of the Biot number. For a high value of Stark number and for the same Biot number, the temperature near the top wall is less than it would be for a lower Stark number.

- The effects of the radiative properties of the medium and the surrounding surfaces are reduced when heat flux conditions are applied.
- The equivalence of radiative equilibrium and pure scattering for an enclosure having the same surface properties is not valid when heat flux boundary conditions are present.

D. Discussion

In this study, the exact equations governing the heat transfer in a conducting, absorbing, emitting and isotropically scattering gray medium with constant properties were solved by the finite element method. Two types of boundary conditions were considered; prescribed temperature on the surfaces and convective heat flux boundary conditions. The effects of the Stark number, isotropic scattering albedo, wall emissivities and Biot number on the temperature and heat flux distribution were

investigated. Comparisons with different formulations of the same problem were made.

Two contributions of this study are the investigation of scattering in gray enclosures and the inclusion of convective type heat flux boundary conditions. The method employed can easily incorporate nonisotropic scattering independent of the incidence angle and temperature dependent properties as long as the medium is gray.

Although the aspect ratio of the medium is a very important physical parameter, its effects have not been investigated in this study. A more realistic study of two-dimensional combined mode radiation and conduction problem should be able to analyze nongray mediums. The formulation and the numerical method used in this study is not capable of solving nongray medium problems in a reasonable amount of computer time.

The accuracy of the numerical results could have been improved, especially for small Stark numbers and for problems with convective heat flux boundary conditions, if a finer mesh was used. However, this was not attempted.

The formulation of the governing equations needs to be considered in more detail. The variables used were the incident radiation and the temperature, and they were treated separately. The incident radiation equation was numerically easy to solve with the finite element method,

however, it consumed most of the computation time. The energy equation, despite its simple appearance, was hard to solve with the finite element method. Therefore, the problem was divided into two simpler subproblems, one easy to solve yet time consuming, the other numerically hard to solve.

The treatment of the incident radiation equation is not suitable for an efficient numerical algorithm. Further work on this equation seems to be essential before attempting to solve more practical problems.

V. REFERENCES

1. M. N. Ozisik. Radiative Transfer and Interactions with Conduction and Convection. John Wiley & Sons, New York, 1973.

2. R. Siegel and J. R. Howell. Thermal Radiation Heat Tranfer. McGraw Hill, New York, 1981.

3. E. M. Sparrow and R. D. Cess. Radiation Heat Transfer. McGraw Hill, New York, 1978.

4. M. M. Razzaque. "Finite Element Analysis of Combined Mode Heat Transfer Including Radiation in Gray Participating Media". Ph.D. Dissertation. University of Texas at Austin, Austin, Texas, 1982.

5. A. C. Ratzel. "P-N Differential Approximation for Solution of One and Two Dimensional Radiation and Conduction Energy Transfer in Gray Participating Media". Ph.D. Dissertation. University of Texas at Austin, Austin, Texas, 1980.

6. T. M. Shih and Y. N. Chen. "A Discretized Intensity Method Proposed for Two-Dimensional Systems Enclosing Radiative and Conductive Media". J. Num. Heat Transfer 6:117-134, 1983.

7. R. Fernandes and J. Francis. "Combined Conductive and Radiative Heat Transfer in an Absorbing, Emitting and Scattering Cylindrical Medium". J. Heat Transfer 104:594-601, 1982.

8. H. C. Hottel and E. S. Cohen. "Radiant Heat Exchange in a Gas-filled Enclosure: Allowance for Non-uniformity of Gas Temperature". AICHE J. 4:3-14, 1958.

9. M. E. Larsen. "The Exchange Factor Method: An Alternative Zonal Formulation for Analysis of Radiating Enclosures Containing Participating Media". Ph.D. Dissertation. University of Texas at Austin, Austin, Texas, 1983.

10. W. A. Fiveland. "Discrete-Ordinates Solution of the Radiation Transport Equation for Rectangular Enclosures". J. Heat Transfer 106:699-706, 1984.

11. W. W. Yuen and L. W. Wong. "Analysis of Radiative Equilibrium in a Rectangular Enclosure with Gray Medium". J. Heat Transfer 106:433-439, 1984.

12. W. W. Yuen and C. F. Ho. "Analysis of Two-Dimensional Radiative Heat Transfer in a Gray Medium with Internal Heat Generation". Int. J. Heat Mass Transfer 28:17-23, 1985.

13. A. L. Crosbie and R. G. Schrenker. "Radiative Transfer in a Two-Dimensional Rectangular Medium Exposed to Diffuse Radiation". J. Quant. Spectrosc. Radiat. Transfer 103:339-372, 1984.

14. S. T. Wu and R. E. Ferguson. "Application of Finite Element Techniques to the Interaction of Conduction and Radiation in Participating Media". In Heat Transfer and Thermal Control, pp. 61-92. Edited by A. L. Crosbie. AIAA, New York, 1981.

15. R. Fernandes, J. Francis and J. N. Reddy. "A Finite Element Approach to Combined Conductive and Radiative Heat Transfer in a Planar Medium". In Heat Transfer and Thermal Control, pp. 93-109. Edited by A. L. Crosbie. AIAA, New York, 1981.

16. M. L. Nice. "Application of Finite Element Method to Heat Transfer in a Participating Medium". In Numerical Properties and Methodologies in Heat Transfer, pp. 497-514. Edited by T. M. Shih. Hemisphere Publishing Co., Washington D. C., 1983.

17. J. P. Wong and G. Aquirre-Ramirez. "Numerical Solution of Integral Equations by Finite Element Method". Proceedings of the 12th Annual Meeting, pp. 560-567, Society of Engineering Science, Washington D. C., 1975.

18. J. N. Reddy and V. D. Murty. "Finite Element Solution of Integral Equations Arising in Radiative Heat Transfer and Laminar Boundary Layer Theory". J. Num. Heat Transfer 1:389-401, 1978.

19. O. C. Zienkiewicz. The Finite Element Method. 3rd edition. McGraw Hill, New York, 1977.

20. M. Kaviany. "One Dimensional Conduction-Radiation Heat Transfer Between Parallel Surfaces Subject to Convective Boundary Conditions". Int. J. Heat Mass Transfer 28:497-499, 1985.

21. K. H. Huebner and E. A. Thornton. The Finite Element Method for Engineering. 2nd edition. John Wiley and Sons, New York, 1982.

22. W. F. Ames. Nonlinear Partial Differential Equations in Engineering. Academic Press, New York, 1965.

23. T. M. Shih. Numerical Heat Transfer. Hemisphere Publishing Co., Washington D. C., 1983.

24. W. W. Yuen and L. W. Wong. "Numerical Computation of an Important Integral Function in Two Dimensional Radiative Transfer". J. Quant. Spectrosc. Radiat. Transfer 29:145-149, 1983.

25. R. J. J. Stamm'ler and M. J. Abbate. Methods of Steady-State Reactor Physics in Nuclear Design. Academic Press, New York, 1983.

VI. APPENDIX A

The Ki_n functions are known as the Bickley-Naylor functions and are defined as [4,24,25]

$$Ki_n(x) = \int_0^{\pi/2} \exp\left(\frac{-x}{\cos\theta}\right) \cos^{n-1}\theta d\theta$$

$$= \int_0^{\infty} \frac{\exp(-x\cosh u)}{\cosh^n u} du$$

$$= \int_1^{\infty} \exp(-xt) \frac{dt}{t^n \sqrt{t^2-1}}$$

The zeroth order Ki_n function is equal to the modified Bessel function of the second kind and order zero. The following relationships are valid among the Ki_n functions

$$\frac{d}{dx}\left(Ki_n(x)\right) = -Ki_{n-1}(x)$$

$$Ki_n(x) = Ki_n(0) - \int_0^x Ki_{n-1}(t)dt$$

$$Ki_n(x) = \int_x^{\infty} Ki_{n-1}(t)dt$$

These functions are related to the exponential integral functions by the following equation [24]

$$E_n(x) = \frac{2}{\pi} \int_0^{\pi/2} Ki_n\left(\frac{x}{\cos\theta}\right) \cos^{n-2}\theta dt.$$

Several numerical approximations to these functions are published [4,9,24,25]. The numerical approximations used in this study are based on the expressions given in [4].

VII. APPENDIX B

Numerical values of the temperature distribution in the medium and the net heat flux values on the surrounding walls are tabulated for some selected cases. The contour plots of temperature are also included. For the cases with first type boundary conditions, the bottom wall is at a nondimensional temperature of 1.0 and the other walls are at a nondimensional temperature of 0.5. For the cases with heat flux boundary conditions, only the bottom wall is cooled with a coolant having a nondimensional temperature of 0.0 and the other walls are kept at 0.5 nondimensional temperature. In the contour plots, the vertical axis is the z-axis and the horizontal axis is the y-axis.

TABLE 5. Temperature distribution and wall net heat flux values in a black square enclosure with N=0.01 for scattering albedo equal to 0.0

Stark Number = 0.01 Scattering Albedo = 0.0
Wall Emissivity : Bottom = 1.0 Top = 1.0 Side = 1.0
Wall Temperature : Bottom = 1.0 Top = 0.5 Side = 0.5

Temperature Distribution

Z \ Y	0.000	0.100	0.200	0.300	0.400	0.500
0.0	1.000	1.000	1.000	1.000	1.000	1.000
0.1	0.540	0.783	0.866	0.883	0.890	0.893
0.2	0.481	0.696	0.787	0.815	0.826	0.832
0.3	0.507	0.664	0.742	0.774	0.786	0.793
0.4	0.499	0.640	0.710	0.740	0.753	0.759
0.5	0.500	0.618	0.679	0.707	0.720	0.725
0.6	0.500	0.602	0.655	0.680	0.691	0.696
0.7	0.500	0.585	0.630	0.651	0.661	0.665
0.8	0.500	0.566	0.602	0.618	0.627	0.630
0.9	0.500	0.542	0.564	0.574	0.579	0.581
1.0	0.500	0.500	0.500	0.500	0.500	0.500

Wall Heat Fluxes

Z OR Y	Bottom Wall	Side Wall	Top Wall
0.1	0.894	-0.671	-0.175
0.2	0.835	-0.467	-0.205
0.3	0.801	-0.403	-0.226
0.4	0.785	-0.328	-0.238
0.5	0.781	-0.271	-0.242
0.6	0.785	-0.224	-0.238
0.7	0.801	-0.182	-0.226
0.8	0.835	-0.145	-0.205
0.9	0.894	-0.108	-0.175
Average	0.832	-0.311	-0.214
% Error	-0.565		

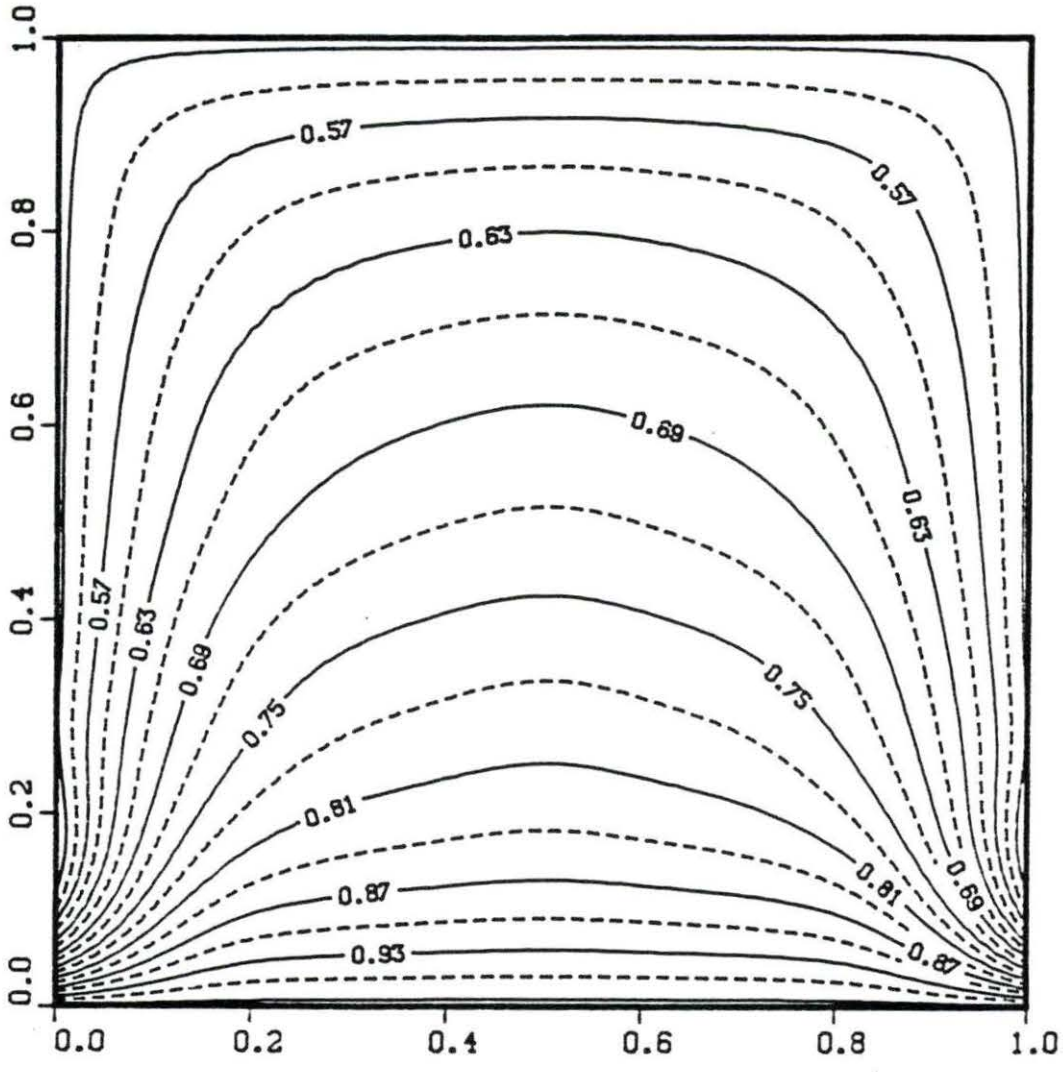

FIGURE 24. Temperature distribution in a black square enclosure with N=0.01 for scattering albedo equal to 0.0

TABLE 6. Temperature distribution and wall net heat flux values in a black square enclosure with N=0.05 for scattering albedo equal to 0.0

Stark Number = 0.05 Scattering Albedo = 0.0
Wall Emissivity : Bottom = 1.0 Top = 1.0 Side = 1.0
Wall Temperature : Bottom = 1.0 Top = 0.5 Side = 0.5

Temperature Distribution

Z \ Y	0.000	0.100	0.200	0.300	0.400	0.500
0.0	1.000	1.000	1.000	1.000	1.000	1.000
0.1	0.540	0.763	0.855	0.887	0.901	0.905
0.2	0.481	0.664	0.760	0.805	0.826	0.832
0.3	0.507	0.622	0.701	0.747	0.769	0.776
0.4	0.499	0.594	0.660	0.701	0.722	0.730
0.5	0.500	0.575	0.628	0.663	0.682	0.688
0.6	0.500	0.560	0.602	0.631	0.646	0.652
0.7	0.500	0.546	0.579	0.601	0.613	0.617
0.8	0.500	0.532	0.555	0.571	0.579	0.582
0.9	0.500	0.518	0.531	0.539	0.543	0.545
1.0	0.500	0.500	0.500	0.500	0.500	0.500

Wall Heat Fluxes

Z OR Y	Bottom Wall	Side Wall	Top Wall
0.1	1.429	-1.347	-0.182
0.2	1.094	-0.725	-0.226
0.3	0.985	-0.611	-0.256
0.4	0.934	-0.449	-0.275
0.5	0.921	-0.363	-0.282
0.6	0.934	-0.290	-0.275
0.7	0.985	-0.225	-0.256
0.8	1.094	-0.170	-0.226
0.9	1.429	-0.116	-0.182
Average	1.183	-0.477	-0.240
% Error	-1.028		

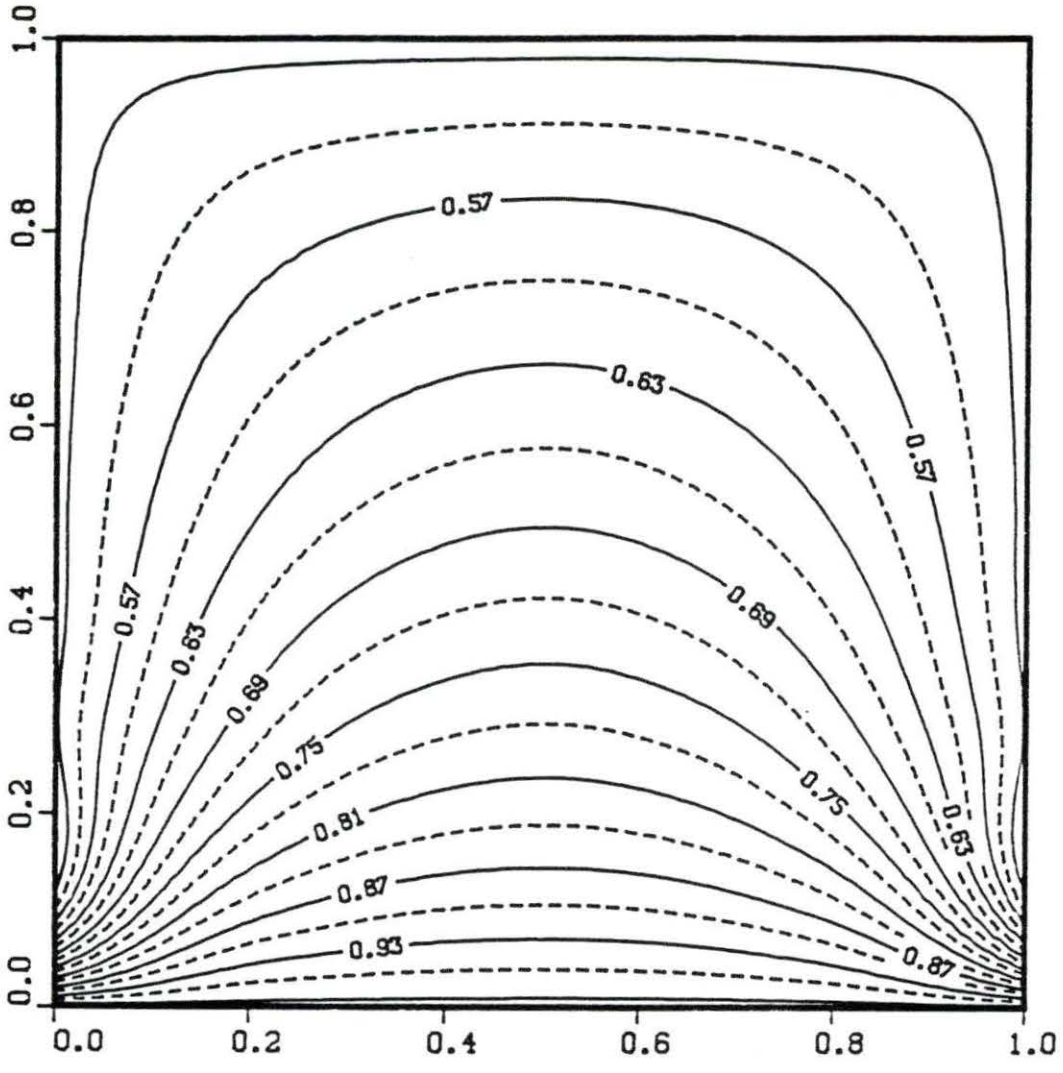

FIGURE 25. Temperature distribution in a black square enclosure with N=0.05 and for scattering albedo equal to 0.0

TABLE 7. Temperature distribution and wall net heat flux values in a black square enclosure with N=0.1 for scattering albedo equal to 0.0

Stark Number = 0.10 Scattering Albedo = 0.0
Wall Emissivity : Bottom = 1.0 Top = 1.0 Side = 1.0
Wall Temperature : Bottom = 1.0 Top = 0.5 Side = 0.5

Temperature Distribution

Z \ Y	0.000	0.100	0.200	0.300	0.400	0.500
0.0	1.000	1.000	1.000	1.000	1.000	1.000
0.1	0.540	0.773	0.853	0.882	0.900	0.903
0.2	0.481	0.651	0.749	0.798	0.820	0.826
0.3	0.507	0.600	0.682	0.733	0.755	0.763
0.4	0.499	0.579	0.639	0.680	0.703	0.710
0.5	0.500	0.560	0.607	0.640	0.659	0.666
0.6	0.500	0.546	0.582	0.608	0.623	0.628
0.7	0.500	0.534	0.561	0.580	0.592	0.595
0.8	0.500	0.523	0.542	0.554	0.562	0.565
0.9	0.500	0.513	0.522	0.528	0.532	0.534
1.0	0.500	0.500	0.500	0.500	0.500	0.500

Wall Heat Fluxes

Z OR Y	Bottom Wall	Side Wall	Top Wall
0.1	1.932	-2.385	-0.193
0.2	1.432	-0.957	-0.246
0.3	1.295	-0.749	-0.284
0.4	1.153	-0.570	-0.309
0.5	1.144	-0.446	-0.317
0.6	1.153	-0.348	-0.309
0.7	1.295	-0.265	-0.284
0.8	1.432	-0.193	-0.246
0.9	1.932	-0.127	-0.193
Average	1.617	-0.671	-0.264
% Error	0.635		

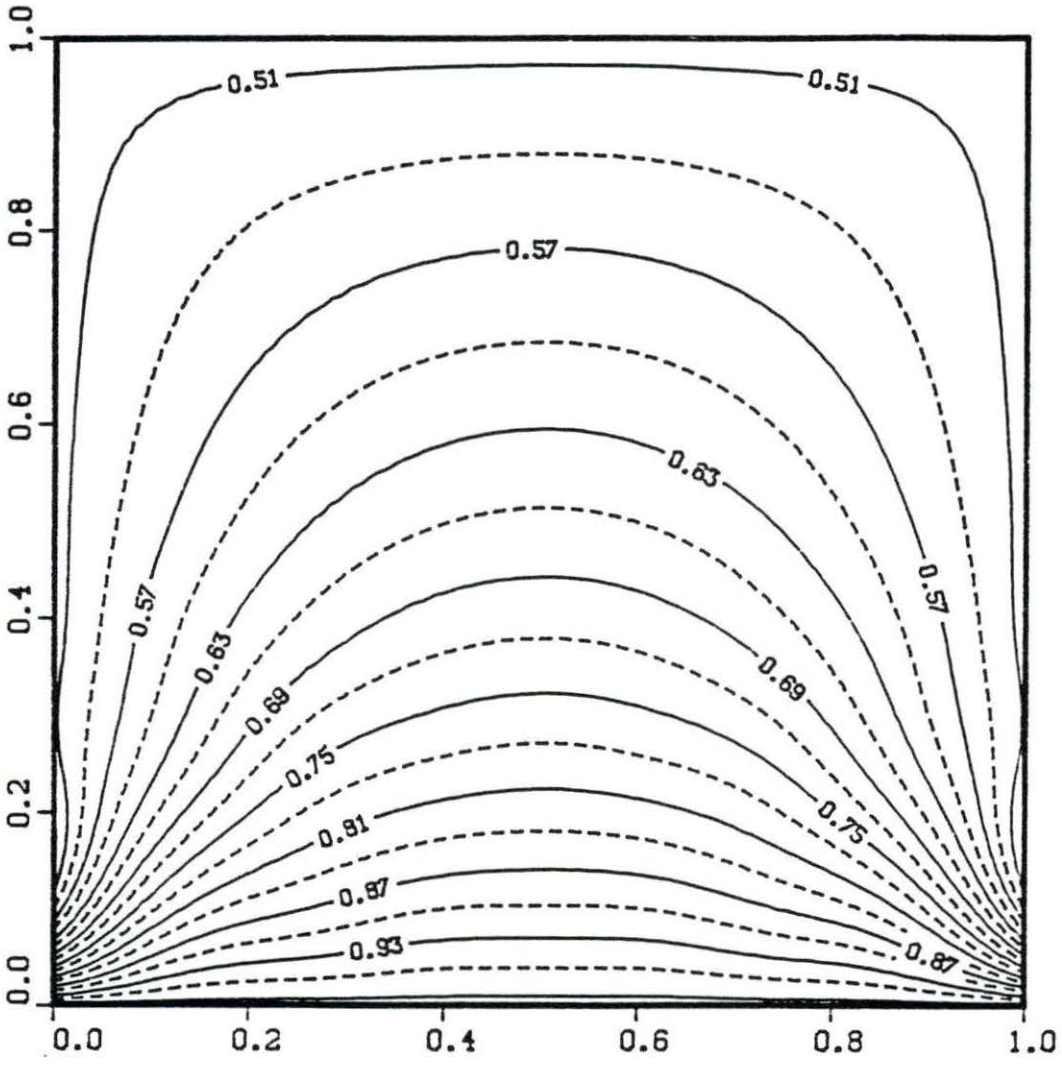

FIGURE 26. Temperature distribution in a black square enclosure with N=0.1 and for scattering albedo equal to 0.0

TABLE 8. Temperature distribution and wall net heat flux values in a gray square enclosure with N=0.01 for wall emissivity equal to 0.5 and for scattering albedo equal to 0.0

Stark Number = 0.01 Scattering Albedo = 0.0
Wall Emissivity : Bottom = 0.5 Top = 0.5 Side = 0.5
Wall Temperature : Bottom = 1.0 Top = 0.5 Side = 0.5

Temperature Distribution

Z \ Y	0.000	0.100	0.200	0.300	0.400	0.500
0.0	1.000	1.000	1.000	1.000	1.000	1.000
0.1	0.540	0.774	0.846	0.859	0.864	0.866
0.2	0.481	0.690	0.770	0.792	0.801	0.804
0.3	0.507	0.662	0.733	0.758	0.768	0.772
0.4	0.499	0.642	0.707	0.731	0.742	0.746
0.5	0.500	0.625	0.684	0.707	0.718	0.722
0.6	0.500	0.612	0.665	0.687	0.697	0.701
0.7	0.500	0.598	0.645	0.665	0.674	0.677
0.8	0.500	0.582	0.621	0.638	0.646	0.649
0.9	0.500	0.555	0.581	0.592	0.597	0.599
1.0	0.500	0.500	0.500	0.500	0.500	0.500

Wall Heat Fluxes

Z OR Y	Bottom Wall	Side Wall	Top Wall
0.1	0.481	-0.363	-0.103
0.2	0.427	-0.254	-0.124
0.3	0.418	-0.224	-0.136
0.4	0.411	-0.188	-0.143
0.5	0.410	-0.164	-0.145
0.6	0.411	-0.144	-0.143
0.7	0.418	-0.125	-0.136
0.8	0.427	-0.107	-0.124
0.9	0.481	-0.084	-0.103
Average	0.447	-0.184	-0.129
% Error	3.628		

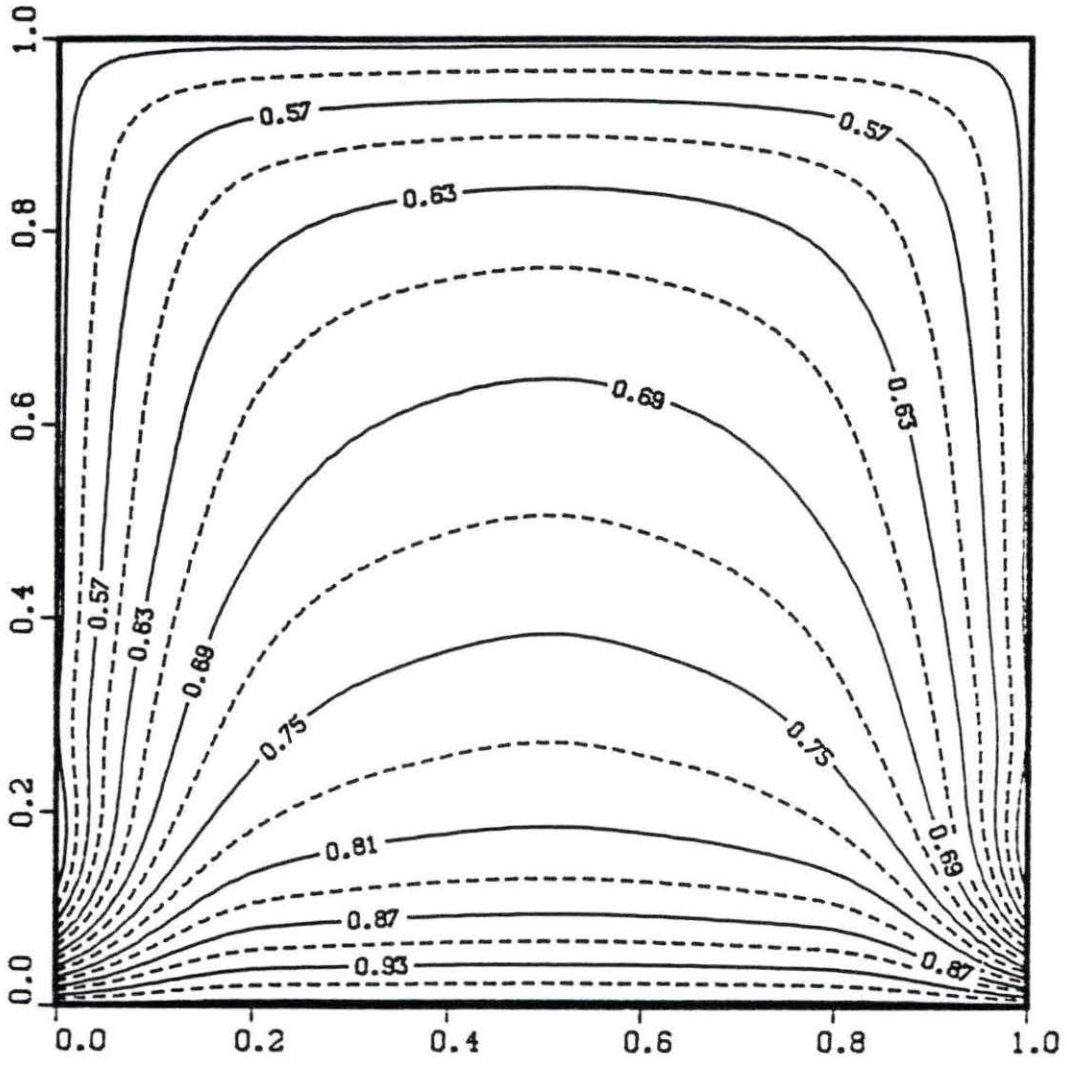

FIGURE 27. Temperature distribution in a gray square enclosure with N=0.01 for wall emissivity equal to 0.5 and for scattering albedo equal to 0.0

TABLE 9. Temperature distribution and wall net heat flux values in a black square enclosure with N=0.01 for wall emissivity equal to 0.5 and for scattering albedo equal to 0.5

Stark Number = 0.01 Scattering Albedo = 0.5
Wall Emissivity : Bottom = 0.5 Top = 0.5 Side = 0.5
Wall Temperature : Bottom = 1.0 Top = 0.5 Side = 0.5

Temperature Distribution

Z \ Y	0.000	0.100	0.200	0.300	0.400	0.500
0.0	1.000	1.000	1.000	1.000	1.000	1.000
0.1	0.540	0.776	0.835	0.846	0.858	0.858
0.2	0.481	0.674	0.756	0.784	0.794	0.797
0.3	0.507	0.637	0.715	0.750	0.761	0.765
0.4	0.499	0.623	0.688	0.720	0.734	0.738
0.5	0.500	0.610	0.669	0.698	0.712	0.716
0.6	0.500	0.598	0.651	0.678	0.691	0.695
0.7	0.500	0.585	0.631	0.656	0.668	0.670
0.8	0.500	0.569	0.608	0.625	0.633	0.638
0.9	0.500	0.545	0.570	0.575	0.578	0.587
1.0	0.500	0.500	0.500	0.500	0.500	0.500

Wall Heat Fluxes

Z OR Y	Bottom Wall	Side Wall	Top Wall
0.1	0.475	-0.371	-0.103
0.2	0.443	-0.245	-0.123
0.3	0.440	-0.207	-0.128
0.4	0.428	-0.179	-0.131
0.5	0.428	-0.158	-0.141
0.6	0.428	-0.140	-0.131
0.7	0.440	-0.123	-0.128
0.8	0.443	-0.105	-0.123
0.9	0.475	-0.084	-0.103
Average	0.457	-0.179	-0.123
% Error	-5.326		

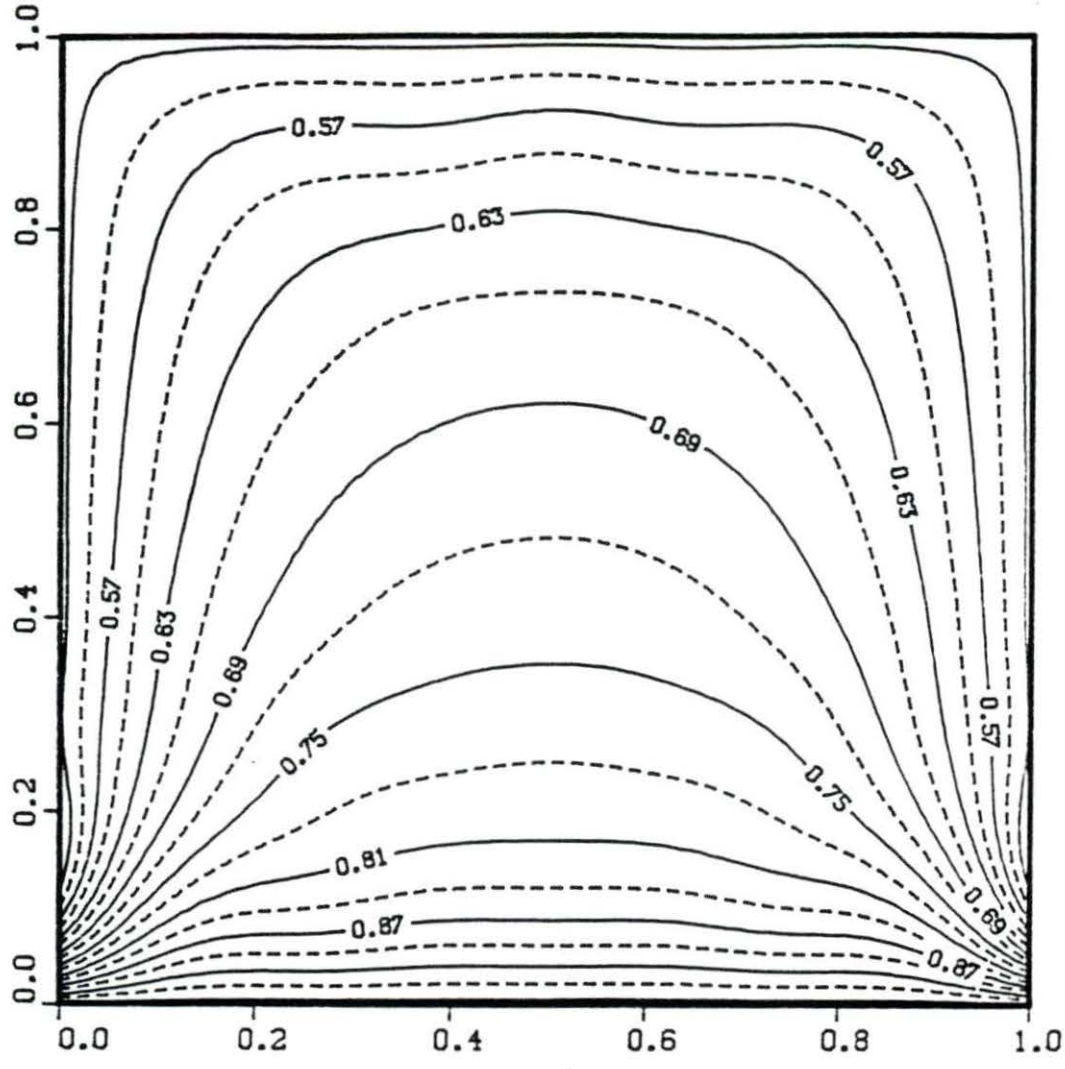

FIGURE 28. Temperature distribution in a black square enclosure with N=0.01 for wall emissivity equal to 0.5 and for scattering albedo equal to 0.5

TABLE 10. Temperature distribution and wall net heat flux values in a black square enclosure with N=0.01 for wall emissivity equal to 0.1 and for scattering albedo equal to 1.0

Stark Number = 0.01 Scattering Albedo = 1.0
Wall Emissivity : Bottom = 0.1 Top = 0.1 Side = 0.1
Wall Temperature : Bottom = 1.0 Top = 0.5 Side = 0.5

Temperature Distribution

Z \ Y	0.000	0.100	0.200	0.300	0.400	0.500
0.0	1.000	1.000	1.000	1.000	1.000	1.000
0.1	0.540	0.765	0.846	0.876	0.897	0.900
0.2	0.481	0.637	0.731	0.780	0.803	0.811
0.3	0.507	0.581	0.655	0.704	0.726	0.734
0.4	0.499	0.559	0.608	0.644	0.666	0.673
0.5	0.500	0.540	0.576	0.603	0.619	0.625
0.6	0.500	0.528	0.553	0.572	0.584	0.588
0.7	0.500	0.519	0.535	0.549	0.557	0.560
0.8	0.500	0.511	0.522	0.530	0.535	0.537
0.9	0.500	0.505	0.510	0.514	0.517	0.517
1.0	0.500	0.500	0.500	0.500	0.500	0.500

Wall Heat Fluxes

Z OR Y	Bottom Wall	Side Wall	Top Wall
0.1	0.188	-0.215	-0.026
0.2	0.138	-0.078	-0.028
0.3	0.125	-0.062	-0.030
0.4	0.112	-0.049	-0.031
0.5	0.111	-0.041	-0.031
0.6	0.112	-0.036	-0.031
0.7	0.125	-0.031	-0.030
0.8	0.138	-0.028	-0.028
0.9	0.188	-0.025	-0.026
Average	0.159	-0.063	-0.029
% Error	2.351		

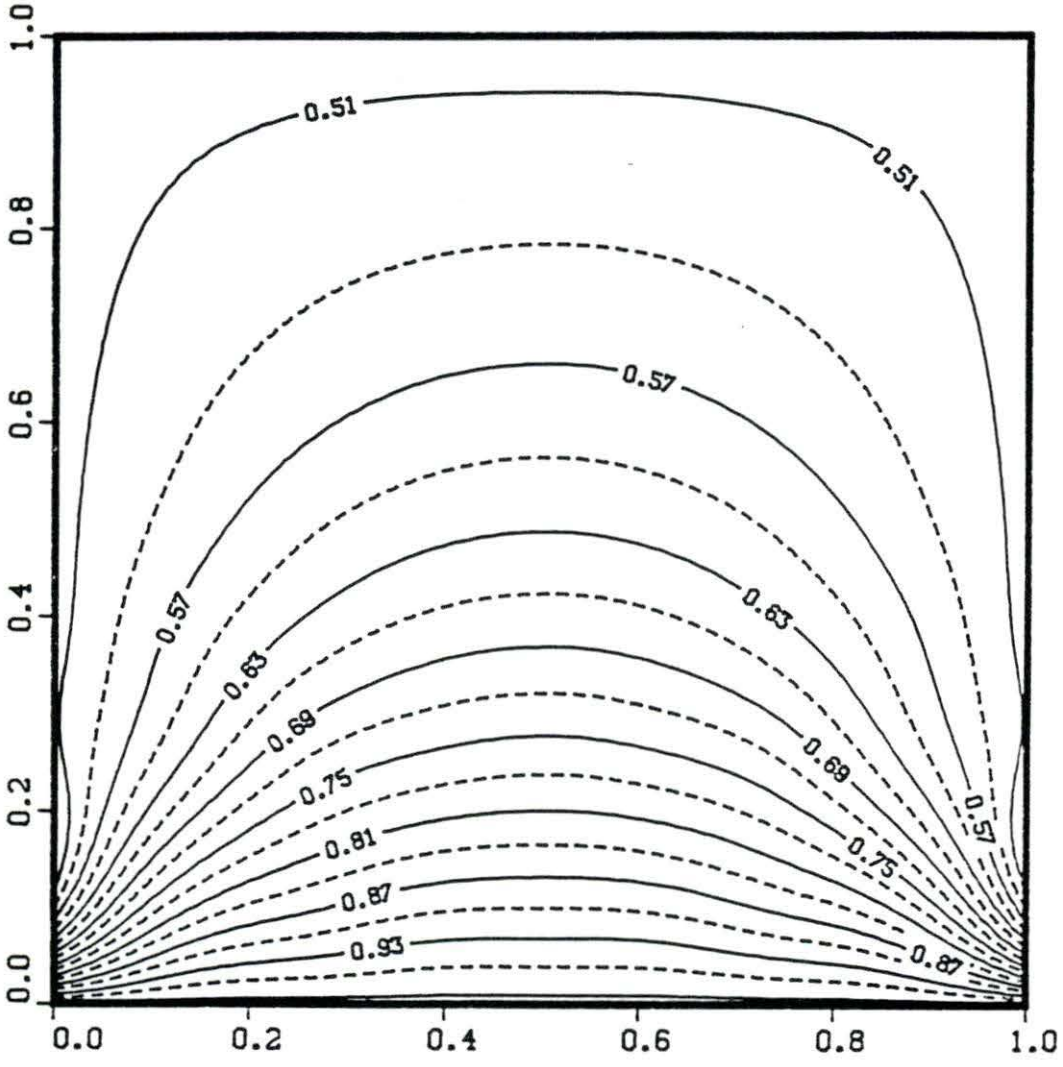

FIGURE 29. Temperature distribution in a black square enclosure with N=0.01 for wall emissivity equal to 0.1 and for scattering albedo equal to 1.0

TABLE 11. Temperature distribution and wall net heat flux values in a black square enclosure with N=0.1 for scattering albedo equal to 0.0 and Bi=1.0

Stark Number = 0.10 Scattering Albedo = 0.0
Wall Emissivity : Bottom = 1.0 Top = 1.0 Side = 1.0
Wall Temperature : Top = 0.5 Side = 0.5

Temperature Distribution

0.0	0.500	0.431	0.405	0.393	0.385	0.383
0.1	0.500	0.460	0.436	0.422	0.414	0.412
0.2	0.500	0.475	0.456	0.444	0.437	0.434
0.3	0.500	0.483	0.469	0.459	0.454	0.452
0.4	0.500	0.488	0.478	0.471	0.466	0.465
0.5	0.500	0.492	0.484	0.479	0.476	0.475
0.6	0.500	0.494	0.489	0.485	0.483	0.482
0.7	0.500	0.496	0.492	0.490	0.488	0.488
0.8	0.500	0.497	0.495	0.494	0.492	0.492
0.9	0.500	0.499	0.498	0.497	0.496	0.496
1.0	0.500	0.500	0.500	0.500	0.500	0.500

Wall Heat Fluxes

Z OR Y	Bottom Wall	Side Wall	Top Wall
0.1	-0.172	-0.220	-0.008
0.2	-0.179	-0.132	-0.016
0.3	-0.157	-0.090	-0.021
0.4	-0.157	-0.062	-0.023
0.5	-0.154	-0.046	-0.025
0.6	-0.157	-0.033	-0.023
0.7	-0.157	-0.024	-0.021
0.8	-0.179	-0.015	-0.016
0.9	-0.172	-0.006	-0.008
Average	-0.152	0.070	0.018
% Error	-3.793		

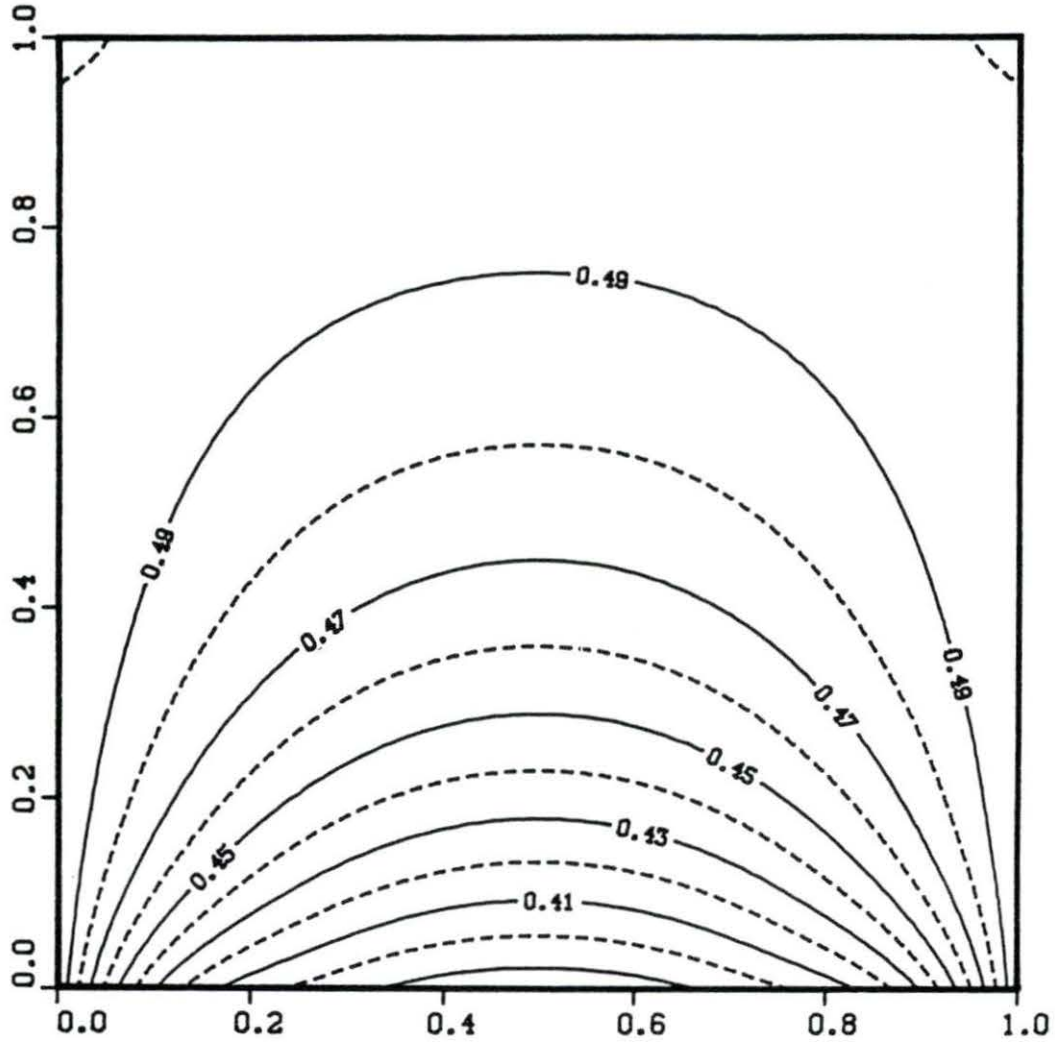

FIGURE 30. Temperature distribution in a black square enclosure with N=0.1 for scattering albedo equal to 0.0 and Bi=1.0

TABLE 12. Temperature distribution and wall net heat flux values in a black square enclosure with N=0.1 for scattering albedo equal to 0.0 and Bi=10.0

Stark Number = 0.10 Scattering Albedo = 0.0
Wall Emissivity : Bottom = 1.0 Top = 1.0 Side = 1.0
Wall Temperature : Top = 0.5 Side = 0.5

Temperature Distribution

Z \ Y	0.000	0.100	0.200	0.300	0.400	0.500
0.0	0.500	0.208	0.136	0.124	0.109	0.106
0.1	0.500	0.339	0.261	0.222	0.202	0.196
0.2	0.500	0.404	0.339	0.299	0.278	0.271
0.3	0.500	0.437	0.389	0.356	0.338	0.332
0.4	0.500	0.458	0.422	0.397	0.382	0.377
0.5	0.500	0.471	0.446	0.427	0.416	0.412
0.6	0.500	0.480	0.463	0.448	0.444	0.453
0.7	0.500	0.486	0.475	0.465	0.462	0.466
0.8	0.500	0.492	0.484	0.479	0.475	0.472
0.9	0.500	0.496	0.492	0.490	0.488	0.489
1.0	0.500	0.500	0.500	0.500	0.500	0.500

Wall Heat Fluxes

Z OR Y	Bottom Wall	Side Wall	Top Wall
0.1	-0.749	-0.901	-0.031
0.2	-0.655	-0.486	-0.044
0.3	-0.473	-0.309	-0.063
0.4	-0.442	-0.202	-0.057
0.5	-0.426	-0.145	-0.026
0.6	-0.442	-0.112	-0.057
0.7	-0.473	-0.075	-0.063
0.8	-0.655	-0.044	-0.044
0.9	-0.749	-0.101	-0.031
Average	-0.523	0.264	0.046
% Error	-9.881		

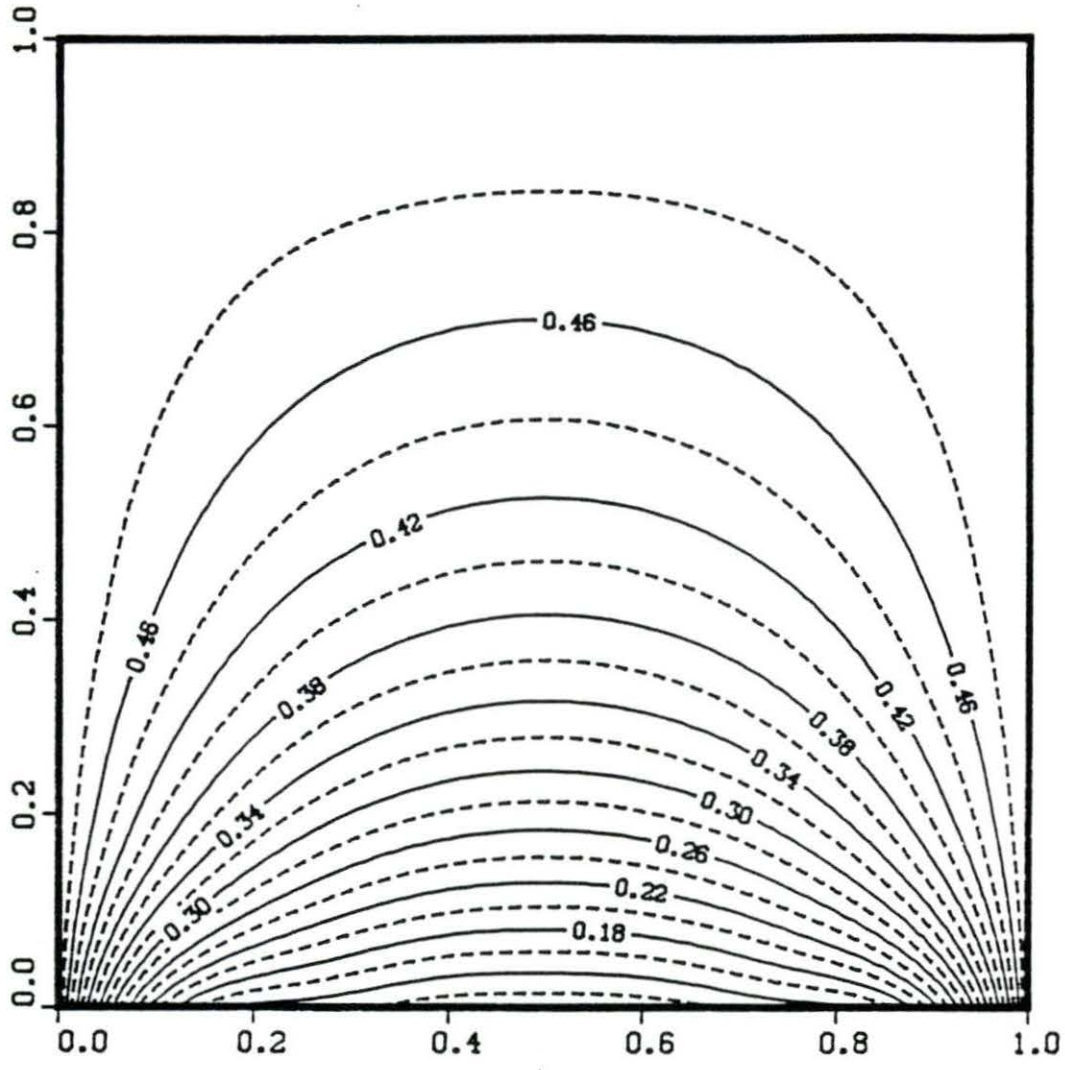

FIGURE 31. Temperature distribution in a black square enclosure with N=0.1 for scattering albedo equal to 0.0 and Bi=10.0

TABLE 13. Temperature distribution and wall net heat flux values in a black square enclosure with N=0.05 for scattering albedo equal to 0.0 and Bi=10.0

Stark Number = 0.05 Scattering Albedo = 0.0
Wall Emissivity : Bottom = 1.0 Top = 1.0 Side = 1.0
Wall Temperature : Top = 0.5 Side = 0.5

Temperature Distribution

Z \ Y	0.000	0.100	0.200	0.300	0.400	0.500
0.0	0.500	0.216	0.146	0.134	0.120	0.117
0.1	0.500	0.345	0.270	0.233	0.214	0.208
0.2	0.500	0.409	0.348	0.310	0.290	0.284
0.3	0.500	0.441	0.396	0.366	0.349	0.343
0.4	0.500	0.461	0.429	0.405	0.392	0.387
0.5	0.500	0.473	0.450	0.434	0.423	0.420
0.6	0.500	0.481	0.466	0.454	0.447	0.444
0.7	0.500	0.487	0.477	0.469	0.464	0.462
0.8	0.500	0.492	0.485	0.481	0.477	0.476
0.9	0.500	0.496	0.493	0.490	0.489	0.488
1.0	0.500	0.500	0.500	0.500	0.500	0.500

Wall Heat Fluxes

Z OR Y	Bottom Wall	Side Wall	Top Wall
0.1	-0.390	-0.454	-0.021
0.2	-0.347	-0.248	-0.030
0.3	-0.259	-0.161	-0.036
0.4	-0.243	-0.109	-0.040
0.5	-0.234	-0.078	-0.041
0.6	-0.243	-0.056	-0.040
0.7	-0.259	-0.161	-0.036
0.8	-0.347	-0.028	-0.030
0.9	-0.390	-0.017	-0.021
Average	-0.280	0.146	0.033
% Error	3.295		

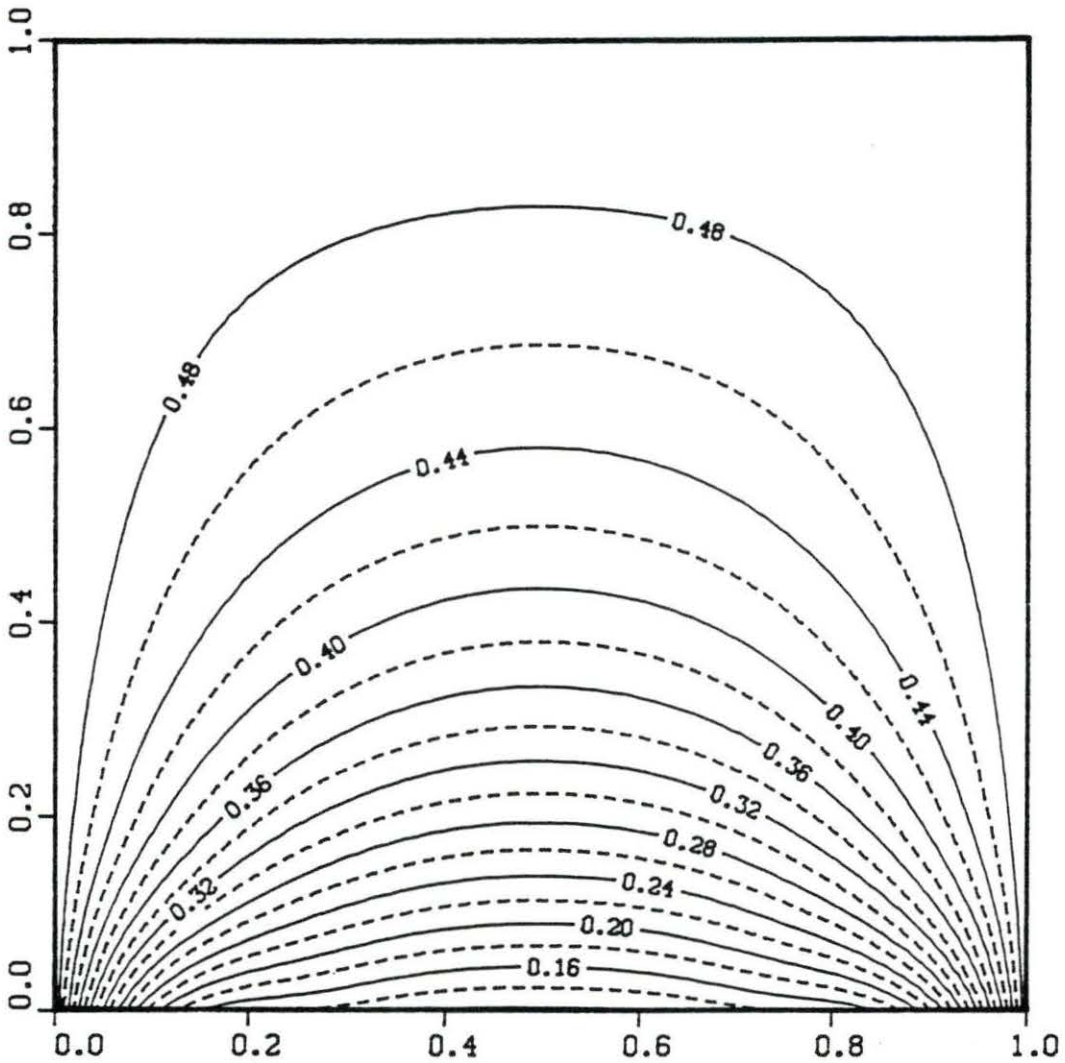

FIGURE 32. Temperature distribution in a black square enclosure with N=0.05 for scattering albedo equal to 0.0 and Bi=10.0

TABLE 14. Temperature distribution and wall net heat flux values in a black square enclosure with N=0.01 for scattering albedo equal to 0.0 and Bi=100.0

Stark Number = 0.01 Scattering Albedo = 0.0
Wall Emissivity : Bottom = 1.0 Top = 1.0 Side = 1.0
Wall Temperature : Top = 0.5 Side = 0.5

Temperature Distribution

Z \ Y	0.000	0.100	0.200	0.300	0.400	0.500
0.0	0.500	0.076	0.014	0.032	0.024	0.024
0.1	0.500	0.295	0.212	0.182	0.166	0.162
0.2	0.500	0.395	0.329	0.292	0.275	0.269
0.3	0.500	0.438	0.394	0.367	0.352	0.347
0.4	0.500	0.461	0.432	0.413	0.402	0.398
0.5	0.500	0.474	0.455	0.441	0.434	0.431
0.6	0.500	0.482	0.468	0.459	0.454	0.452
0.7	0.500	0.487	0.478	0.472	0.468	0.467
0.8	0.500	0.491	0.485	0.481	0.479	0.478
0.9	0.500	0.495	0.492	0.490	0.489	0.488
1.0	0.500	0.500	0.500	0.500	0.500	0.500

Wall Heat Fluxes

Z OR Y	Bottom Wall	Side Wall	Top Wall
0.1	-0.163	-0.157	-0.016
0.2	-0.139	-0.086	-0.019
0.3	-0.105	-0.058	-0.021
0.4	-0.100	-0.042	-0.022
0.5	-0.096	-0.032	-0.023
0.6	-0.100	-0.025	-0.022
0.7	-0.105	-0.019	-0.021
0.8	-0.139	-0.015	-0.019
0.9	-0.163	-0.011	-0.016
Average	-0.115	0.049	0.020
% Error	-2.978		

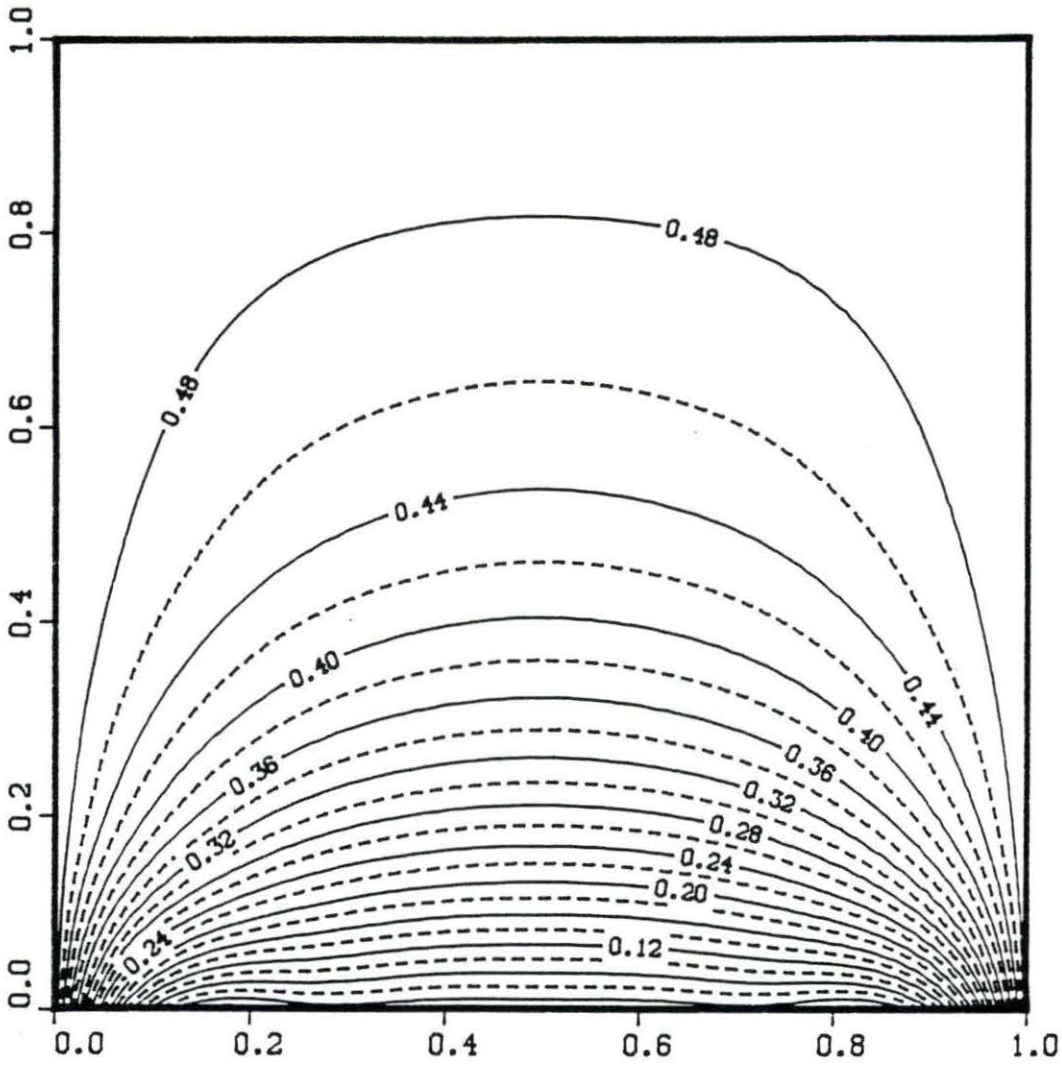

FIGURE 33. Temperature distribution in a black square enclosure with N=0.01 for scattering albedo equal to 0.0 and Bi=100.0

TABLE 15. Temperature distribution and wall net heat flux values in a black square enclosure with N=0.01 for scattering albedo equal to 0.5 and Bi=100.0

Stark Number = 0.01 Scattering Albedo = 0.5
Wall Emissivity : Bottom = 1.0 Top = 1.0 Side = 1.0
Wall Temperature : Top = 0.5 Side = 0.5

Temperature Distribution

Z \ Y	0.000	0.100	0.200	0.300	0.400	0.500
0.0	0.500	0.076	0.014	0.032	0.023	0.023
0.1	0.500	0.287	0.201	0.168	0.152	0.147
0.2	0.500	0.386	0.314	0.274	0.255	0.249
0.3	0.500	0.431	0.382	0.350	0.332	0.327
0.4	0.500	0.457	0.423	0.400	0.386	0.382
0.5	0.500	0.472	0.449	0.433	0.423	0.420
0.6	0.500	0.481	0.465	0.454	0.448	0.445
0.7	0.500	0.487	0.477	0.469	0.465	0.463
0.8	0.500	0.491	0.485	0.480	0.478	0.477
0.9	0.500	0.495	0.492	0.490	0.489	0.488
1.0	0.500	0.500	0.500	0.500	0.500	0.500

Wall Heat Fluxes

Z OR Y	Bottom Wall	Side Wall	Top Wall
0.1	-0.161	-0.158	-0.015
0.2	-0.136	-0.088	-0.018
0.3	-0.102	-0.060	-0.020
0.4	-0.096	-0.042	-0.022
0.5	-0.093	-0.032	-0.022
0.6	-0.096	-0.025	-0.022
0.7	-0.102	-0.019	-0.020
0.8	-0.136	-0.014	-0.018
0.9	-0.161	-0.010	-0.015
Average	-0.113	0.050	0.019
% Error	-5.242		

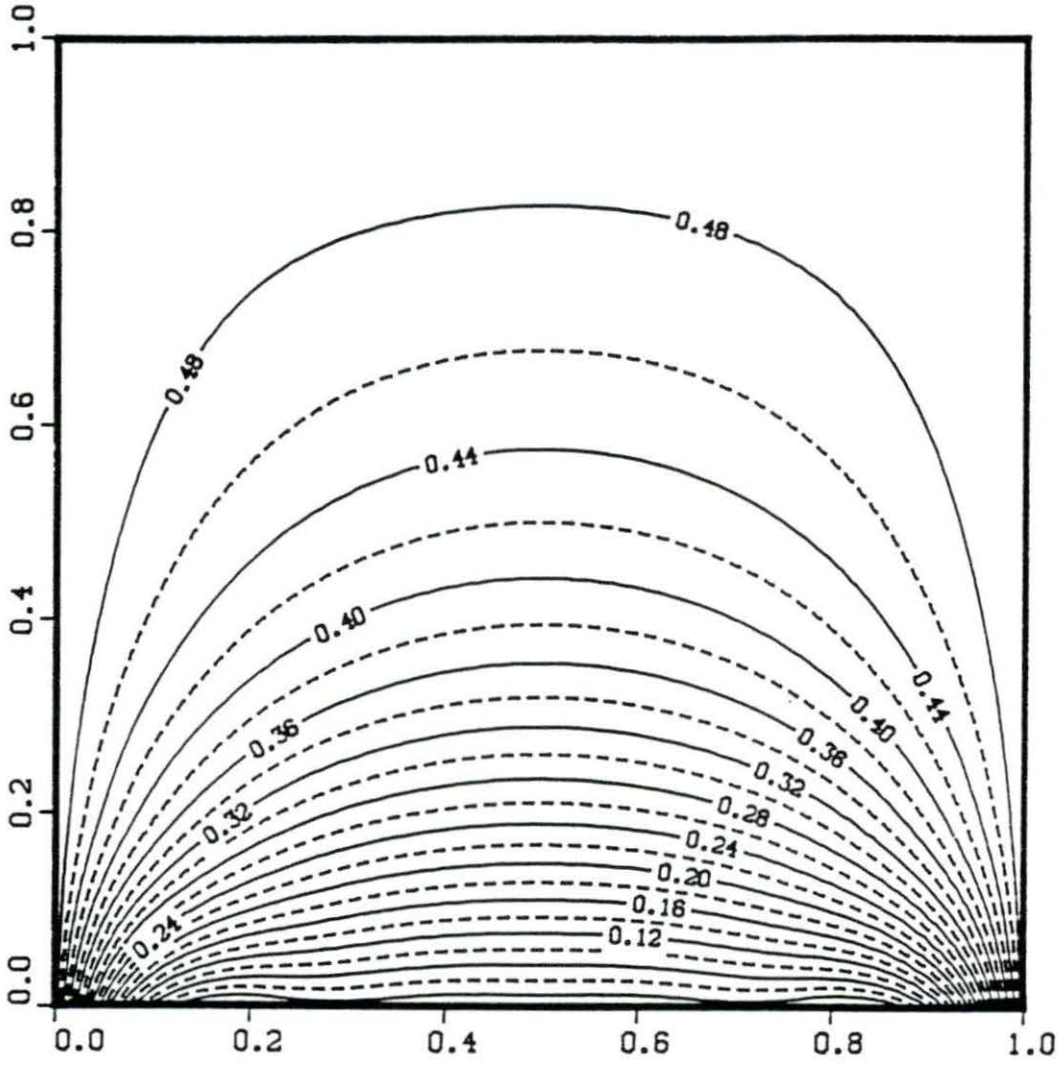

FIGURE 34. Temperature distribution in a black square enclosure with N=0.01 for scattering albedo equal to 0.5 and Bi=100.0

TABLE 16. Temperature distribution and wall net heat flux values in a black square enclosure with N=0.01 for scattering albedo equal to 1.0 and Bi=100.0

Stark Number = 0.01 Scattering Albedo = 1.0
Wall Emissivity : Bottom = 1.0 Top = 1.0 Side = 1.0
Wall Temperature : Top = 0.5 Side = 0.5

Temperature Distribution

Z \ Y	0.000	0.100	0.200	0.300	0.400	0.500
0.0	0.500	0.076	0.013	0.031	0.022	0.022
0.1	0.500	0.274	0.181	0.145	0.126	0.121
0.2	0.500	0.369	0.286	0.238	0.215	0.207
0.3	0.500	0.414	0.351	0.310	0.287	0.280
0.4	0.500	0.443	0.396	0.363	0.343	0.337
0.5	0.500	0.460	0.427	0.402	0.387	0.381
0.6	0.500	0.473	0.449	0.431	0.420	0.416
0.7	0.500	0.482	0.466	0.453	0.446	0.443
0.8	0.500	0.489	0.479	0.471	0.466	0.465
0.9	0.500	0.495	0.490	0.486	0.484	0.483
1.0	0.500	0.500	0.500	0.500	0.500	0.500

Wall Heat Fluxes

Z OR Y	Bottom Wall	Side Wall	Top Wall
0.1	-0.160	-0.159	-0.014
0.2	-0.133	-0.090	-0.017
0.3	-0.098	-0.061	-0.019
0.4	-0.092	-0.044	-0.021
0.5	-0.089	-0.033	-0.021
0.6	-0.092	-0.025	-0.021
0.7	-0.098	-0.019	-0.019
0.8	-0.133	-0.014	-0.017
0.9	-0.160	-0.009	-0.014
Average	-0.110	0.050	0.018
% Error	-7.707		

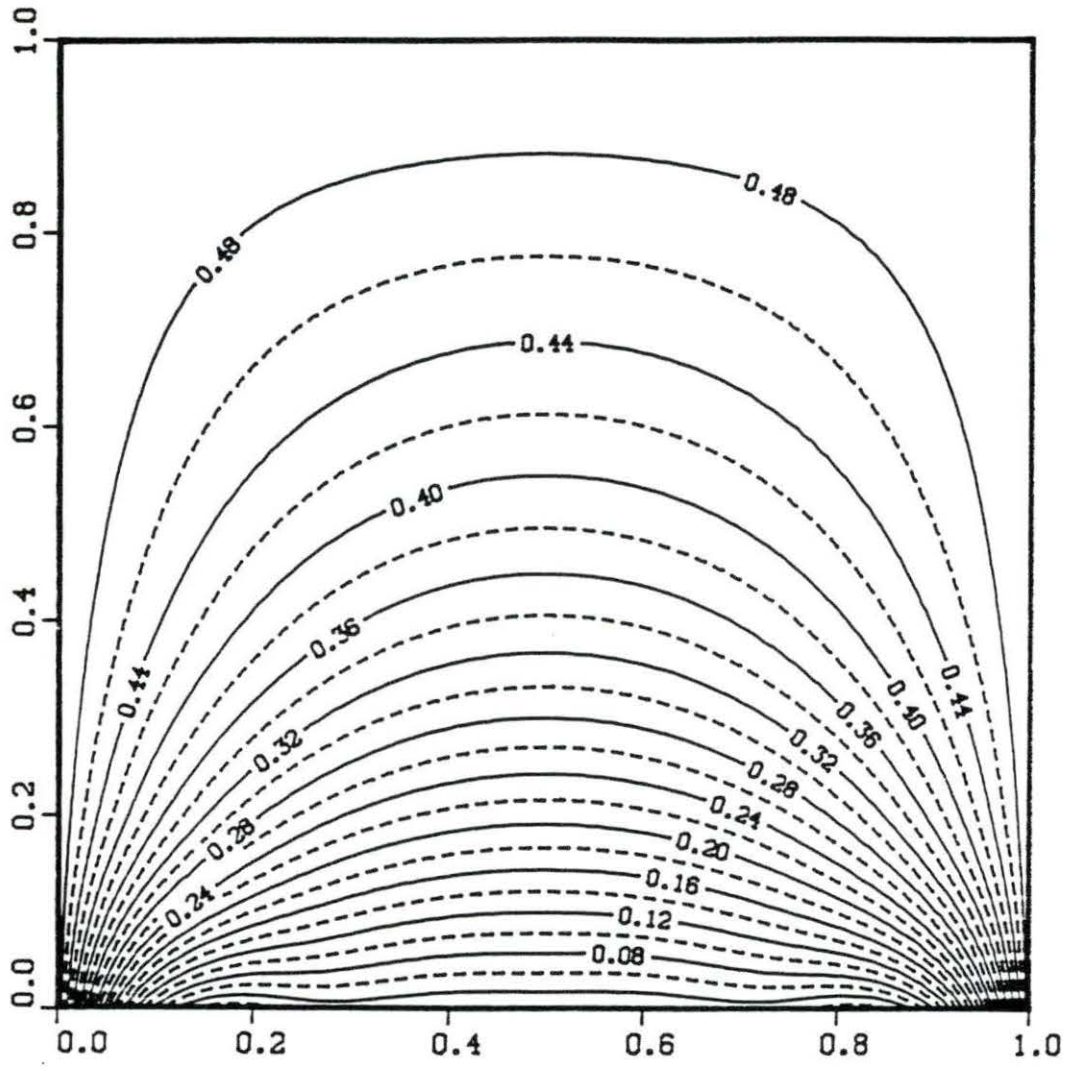

FIGURE 35. Temperature distribution in a black square enclosure with N=0.01 for scattering albedo equal to 1.0 and Bi=100.0

TABLE 17. Temperature distribution and wall net heat flux values in a gray square enclosure with N=0.01 for wall emissivity equal to 0.5 and Bi=10.0

Stark Number = 0.01 Scattering Albedo = 0.0
Wall Emissivity : Bottom = 1.0 Top = 1.0 Side = 1.0
Wall Temperature : Top = 0.5 Side = 0.5

Temperature Distribution

Z \ Y	0.000	0.100	0.200	0.300	0.400	0.500
0.0	0.500	0.241	0.181	0.175	0.164	0.162
0.1	0.500	0.370	0.311	0.285	0.271	0.267
0.2	0.500	0.429	0.384	0.359	0.346	0.341
0.3	0.500	0.455	0.424	0.405	0.395	0.391
0.4	0.500	0.469	0.448	0.434	0.426	0.423
0.5	0.500	0.477	0.462	0.452	0.446	0.444
0.6	0.500	0.483	0.471	0.464	0.460	0.458
0.7	0.500	0.486	0.478	0.473	0.470	0.469
0.8	0.500	0.490	0.484	0.480	0.478	0.477
0.9	0.500	0.494	0.490	0.488	0.487	0.487
1.0	0.500	0.500	0.500	0.500	0.500	0.500

Wall Heat Fluxes

Z OR Y	Bottom Wall	Side Wall	Top Wall
0.2	-0.085	-0.049	-0.012
0.3	-0.070	-0.034	-0.014
0.4	-0.068	-0.025	-0.014
0.5	-0.066	-0.020	-0.015
0.6	-0.068	-0.016	-0.014
0.7	-0.070	-0.013	-0.014
0.8	-0.085	-0.011	-0.012
0.9	-0.089	-0.008	-0.010
Average	-0.070	0.029	0.013
% Error	-0.891		

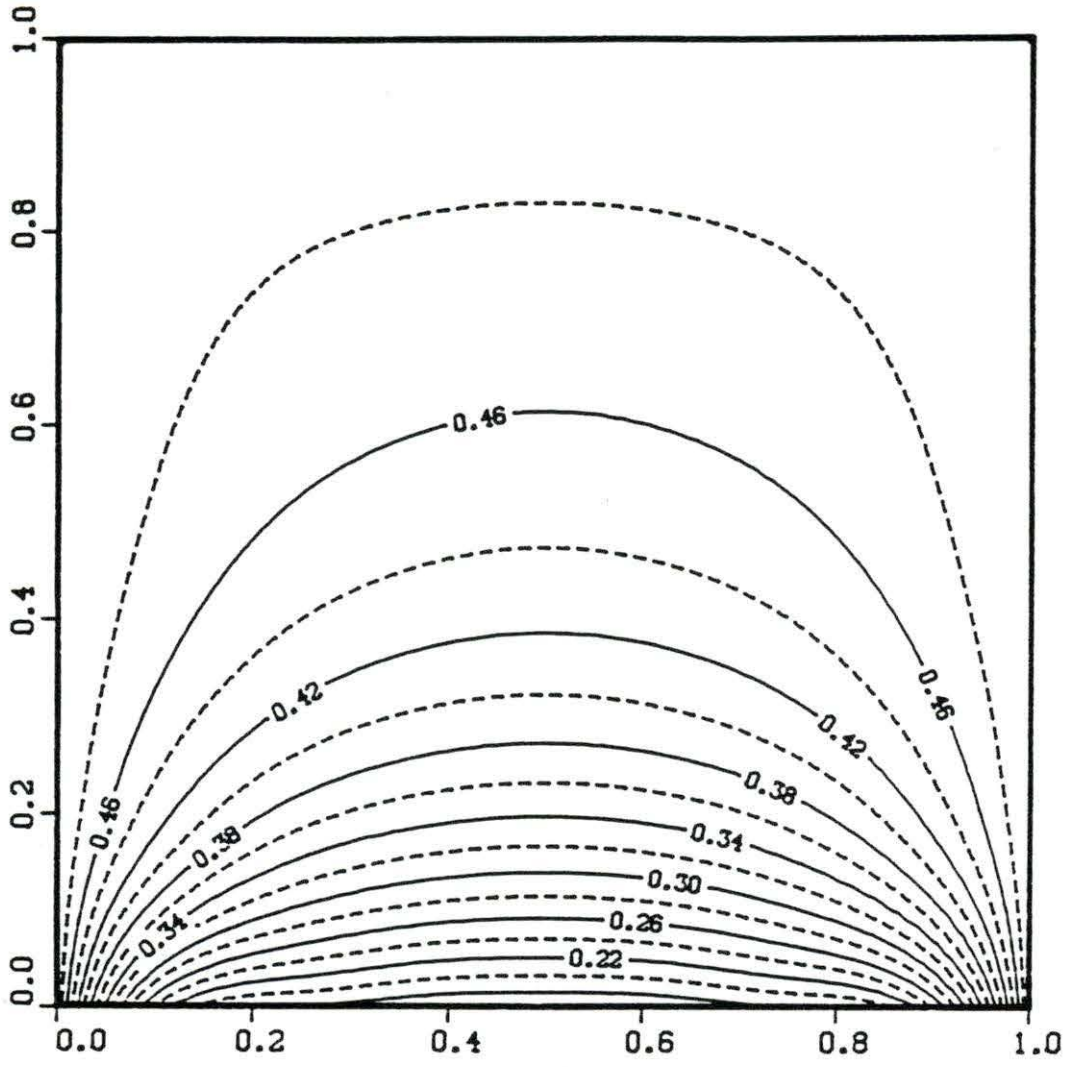

FIGURE 36. Temperature distribution in a gray square enclosure with N=0.01 for wall emissivity equal to 0.5 and Bi=10.0

VIII. ACKNOWLEDGEMENTS

I would like to express my sincere thanks and appreciation to my major professor, Dr. M. M. Razzaque for his valuable guidance, suggestions, and help in the accomplishment of this thesis.